SUSTAINABLE URBAN DEVELOPMENT UNDER A COUPLED HUMAN-LAND-ATMOSPHERIC MODELING FRAMEWORK: THE CASE STUDY OF URUMQI, CHINA

By

Xue Li

A DISSERTATION

Submitted to
Michigan State University
in partial fulfillment of the requirements
for the degree of

Geography – Doctor of Philosophy

2017

ABSTRACT

SUSTAINABLE URBAN DEVELOPMENT UNDER A COUPLED HUMAN-LAND-ATMOSPHERIC MODELING FRAMEWORK: THE CASE STUDY OF URUMQI, CHINA

By

Xue Li

Sustainability is the contemporary philosophy for urban development which requires holistic consideration of the environmental, economic, and social dimensions. Global climate change is an important factor that affects sustainable urban development. On the one hand, climate change is posing various risks for the urban system and its supporting natural environment. On the other hand, different urban development plans have the potential to mitigate or amplify the adverse climate impacts. However, climate concerns often have a low impact on urban planning practice, due to the complexity of the system interactions. Therefore, a generic computational modeling framework is needed to address the causes and consequences of urban development plans, sustainability, and associated regional climate.

The goal of this study is to build a coupled Human-Land-Atmospheric (HLA) modeling framework that supports urban sustainability assessment. The specific aims include (1) developing midterm urban change scenarios and simulating their trajectories, (2) testing the sensitivity of regional climate to urban change trajectories, (3) assessing the impact of land cover data uncertainty on regional climate simulation, and (4) evaluating development strategies for sustainability from the climatic perspective. The city of Urumqi, China is selected as the case area for this study. Rapid economic and population growth are envisioned for the future of Urumqi, but its oasis environment is particularly vulnerable to future climate change and local disruptions.

The coupled HLA modeling framework was constructed by combining statistical models for population, GDP, and urban area predictions, the Dyna-CLUE model which simulate land use change spatially, and the RAMS model which dynamically down-scales general circulation according to local land surface characteristics. Three urban development scenarios were developed

based on different urban land demand models, yielding urban area increase of 20%, 70%, and 120%, respectively, from 2010 to 2030. Their spatial configurations were simulated using Dyna-CLUE. Local afforestation plans were later incorporated into the urban change scenarios. The land use prediction maps were then passed into RAMS to simulate their climatic consequences. The regional climate simulations were forced by the NASA-GISS-E2H General Circulation Model for the IPCC RCP 4.5 scenario in several hot years around 2030. The results were compared first among urban change scenarios and then with the RAMS simulations for the recent climate. The regional climate simulation results revealed interesting spatial patterns that associated to urban change scenarios, but the overall simulation quality was less than desirable. Finally, Urumqi's water supply/demand, agroclimatic resources, and agrometeorological risks were discussed based on literature, local statistics and simulated urban and climate change in an exploratory fashion.

In conclusion, this study presented a coupled HLA modeling framework and an effort of evaluating sustainability-related topics using such framework. Although several research limitations prevent the specific results from supporting real-world decision-making, it made a constructive step towards a more comprehensive and scientifically founded sustainability assessment, especially for alternative urban development decisions. This framework can be expanded in the future to include more sustainability-related subsystems.

ACKNOWLEDGMENTS

First, I would like to thank my advisor Dr. Joseph Messina for his encouragement, patience and continued support throughout my time as his student. I would never have been able to finish this work without his guidance and support. I would also like to thank the rest of my committee, Dr. Ashton Shortridge, Dr. Nathan Moore, Dr. Peilei Fan, and Dr. Jiaguo Qi, for their insightful comments. Thanks to my fellow geography graduate students and colleagues in the Center for Global Change and Earth Observations for the wonderful times we spent together both for work and for fun.

Thanks to the funding agencies National Aeronautics and Space Administration (NNX09AI32G: China's urbanization and its sustainability under future climate change) and National Geospatial-Intelligence Agency (HM02101310002: Managing elevation data uncertainty for global geointelligence) for financially support my research. And thanks again to Dr. Peilei Fan and Dr. Ashton Shortridge for involving me in these interesting but challenging studies.

Special thanks to the Chinese Academy of Sciences Xinjiang Ecology And Geography Institute for hosting me during the field trips in Urumqi area and also for providing valuable local knowledge.

Finally, thanks to my parents, Zhao Li and Xiaozhen Zhang, and my husband, Yuxing Wang, for your love and support, and to my dear child Ivy, for making me stronger and better than ever before.

TABLE OF CONTENTS

LIST OF TABLES

LIST OF FIGURES

CHAPTER 1

GENERAL INTRODUCTION

1.1 Research motivations

Sustainable development is a key concern for global, regional and local societies in this new millennium. Two centuries of industrial development have greatly improved our capability to exploit resources from and output waste to the natural environment in order to support more population and higher living standards. While we historically conceived human-environment relationships as one of humanity's triumph over nature, we have reached the point where the environment can no longer absorb the impacts and our society in turn is facing the negative consequences brought by unfettered development. Borrowed from the field of ecology, the concept of sustainability builds a completely different development philosophy, which demands a holistic view that links our economy, society and environment organically.

Global climate change, in terms of change in temperature, precipitation, and frequency of extreme-weather events, has profound impacts on human society and our living environment. Anthropogenic Green House Gas (GHG) emission since the industrial revolution is the principle cause of accelerated warming because more energy from solar irradiation is trapped in the earth system (IPCC, 2013). We are approaching, if not already surpassed, the "point of no return", meaning even cutting back the current GHG emission would not reverse the warming trend which could eventually end the relatively stable climate of the Holocene (Hansen et al., 2008; Ridley et al., 2010; Noël et al., 2017). Various studies have pointed out the vulnerability of ecosystems, water resources, food security, human health as well as settlements and society to current and future climate change (Cramer et al., 2001; Vörösmarty et al., 2000; Schmidhuber and Tubiello, 2007; Patz et al., 2005; McGranahan et al., 2007; IPCC, 2013). Climate change presents great challenges to sustainable development and thus has drawn substantial amount of research attentions in recent years.

Urban areas are where the most intensive human activities take place. They are the hot spots of human dwelling as well as material and energy exchange between human and the environment, therefore are focal points for problems concerning sustainability (Maclaren, 1996). In 2007, global urbanization rate passed 50% for the first time in human history, and is predicted to reach 60% in 2030 (United Nations, Department of Economic and Social Affairs Population Division, 2015). Industrial civilization draws peasants away from rural areas into urban areas and keeps expanding this most artificial environment on earth. As the majority of current urbanization is occurring in less developed countries, where effective planning and management are usually lacking (Cohen, 2006), rapid urban growth is posing serious pressures on both the natural environment and human society.

From a top-down perspective, global climate change varies over space and time, impacting different regions in different ways. From a bottom-up perspective, local strategies can mitigate and help adapt to climate change. Urban planners are devoting more efforts on understanding the impacts of climate change on urban system and developing mitigation and adaptation strategies for different case cities (Bulkeley and Kern, 2006; Füssel, 2007; Hamin and Gurran, 2009). However in practice, climate concerns often have low impact on urban planning, largely due to the complexity of the problem and lack of accessible tools to support decision making (Eliasson, 2000). The climatic impacts of local development strategies cannot be easily predicted. Humans, land, and the atmosphere interact in complex ways making it very difficult to intuitively predict outcomes. Thus, it is necessary to develop a generic computational modeling framework to address the causes and consequences of urban development plans, sustainability, and associated regional climate.

Urumqi, the study area, is the capital city of Xinjiang Uyghur Autonomous Region (XUAR), northwest China. It is the economic, political and transportation center of XUAR, which constitutes about one-sixth of the entire country in terms of area. With 339 km^2 of urban built-up area, Urumqi holds a population of 2.41 million, of which 1.77 million are urban residents (Statistics Bureau of Urumqi, 2010). The city is situated on an oasis with desert to its north and mountains to the south and east. Rapid economic and population growth are envisioned for the future of Urumqi, but the sensitive environment of this oasis city makes it particularly vulnerable to future climate change.

1.2 Conceptual framework

A coupled human-land-atmosphere (HLA) system is required to understand the drivers and consequences of urban development and regional climate. At global scales, human activities substantially influence the levels of greenhouse gas emissions, the most important factor of global climate change. At the local scale, human activities modify the physical condition of the land surface, thus impacting energy and moisture flows between land and atmosphere, altering the regional climate. In turn, changes in climate, both global and local, affect land cover by, for example, influencing vegetation growth. Perceptions of climate change are also altering human activities. Mitigation and adaptation strategies are being developed aimed at minimizing the adverse impacts of climate change. The coupled HLA system is thus a complex system, in which no element can be understood without considering the whole system.

Figure 1.1 illustrates the concepts, relationships, and methods in the HLA system that will be considered in this study. Each subsystem in HLA is considered in both process and pattern/state. Regional climate is affected by atmospheric forces across scales. At the global scale, the regional climate regime is determined by the general circulation. At regional scales, land surface conditions drive local circulation and create spatial heterogeneities inside regional climate regimes. Land Use and Cover Change (LUCC) is an important manifestation of the interactions between human beings and the earth surface. LUCC is primarily driven by the ever-growing population and economic needs, but its spatial pattern is usually constrained by physical suitability. Human society is the ultimate driver as well as the major sufferer, at least for human's concern, of climate and land use land cover change. The consequences of human behavior in the climate and land systems, as well as the impact of changing climate and land conditions on the sustainability of human society, are not intuitively predictable.

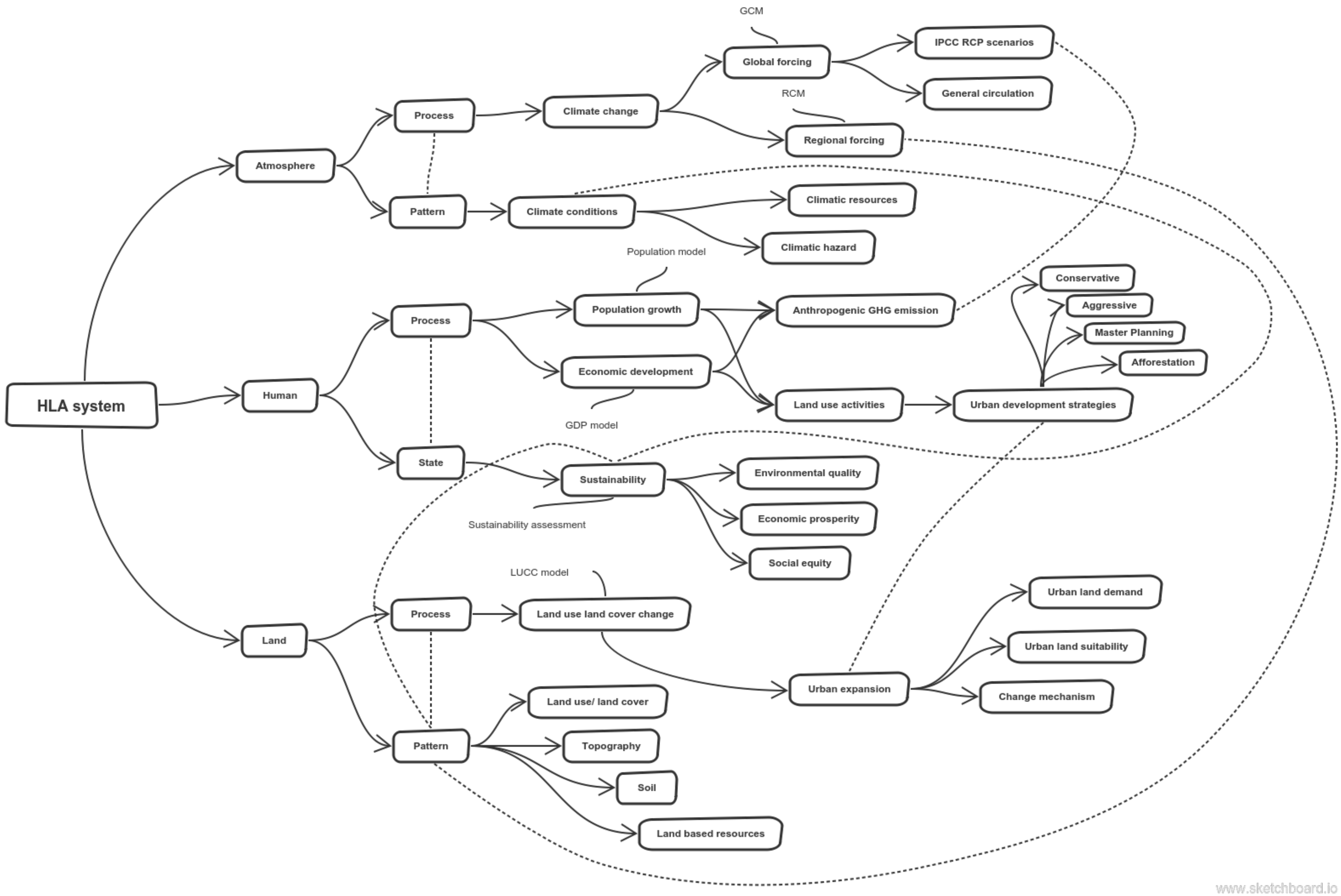

Figure 1.1 Conceptual framework

1.3 Research objectives

The primary objective of this study is to build a systematic modeling framework that can be adopted to different cases in studying causes and consequences in coupled HLA systems with a focus on urban sustainability. Using the city of Urumqi, China as the study area, this modeling framework is going to be tested by assessing different urban development strategies concerning how they contribute to local sustainability. In order to complete this comprehensive assessment, a couple of specific goals need to be attained.

Goal 1: simulate mid-term (2030) urban development trajectories.

Various development strategies can yield substantially different urban development outcomes in both aggregated area and spatial pattern. Many factors drive the change of urban lands. Non-spatial factors, e.g., economic and population growth, determine the total demand for urban lands; spatial factors, e.g., accessibility and topography, determine the the location of new urban lands. The process of urban change can be simulated using LUCC models. Different development strategies produce different land demand and modify driving factors thus altering the trajectory and spatial patterns of future urban morphologies. The potential impacts of development strategies can be simulated by parameterizations of LUCC models. A set of land use maps corresponding to various urban change scenarios will be developed. These spatial products will be used to identify likely development patterns.

Goal 2: test the sensitivity of regional climate to urbanization trajectories and selected IPCC scenario using regional climate model.

Key climate indicators (temperature, precipitation and wind speed) will be modeled in Urumqi's semi-arid oasis environment. Local land cover change impacts how global climate change manifests at the local level. When combined with global climate change scenarios, local changes will either amplify or mitigate the impact of global trends on regional climate. In regional climate modeling, land cover is a key component. By passing the outcomes of goal 1 to a regional climate model, future climate scenarios driven by synergistic effects can be simulated. The expected outcome will be regional climate simulation results from different urban change scenarios based on selected IPCC scenarios. These simulations will suggest likely directions and levels of regional climate change and identify most impacted areas under synergistic effects.

Goal 3: examine the propagation of uncertainty from input land cover data to regional climate modeling results.

Uncertainty inherited in the input land cover data may have a non-trivial impact on regional climate modeling. Land cover maps used as inputs to regional climate models often contain high levels of uncertainty, and this uncertainty may propagate through the applications and affect the results of any climate simulations. Land cover uncertainty can be quantified with an uncertainty model, and its propagation effects then assessed. To evaluate the uncertainty impact, "confidence envelopes" will be generated for the key climate indicators simulated in goal 2. Confidence ranges for each pixel as well as confidence regions across the landscape will be identified.

Goal 4: evaluate development strategies for sustainability from the climate perspective.

Within the context of global climate change, local sustainability can be evaluated with regard to development strategies. Different development strategies will affect certain critical issues that determine Urumqi's sustainability under future climate change. These critical issues, especially those related to climate conditions, will be identified and assessed within the coupled HLA system. Each selected issue will be examined regarding current vulnerability and future conditions based on simulations of urban and climate changes (outcomes of goal 1&2). General discussions and quantitative/spatial assessments on each topic will be the primary outputs from the evaluations.

1.4 Dissertation outline

Chapter 2 reviews a wide range of literature concerning each element, and their relationships within the HLA system. Starting from core theories and methods adopted in previous studies of urban sustainability, land use change, and climate change, substantial efforts were devoted to papers which present connections to different sub-systems.

Chapter 3 gives an overview of the study area, Urumqi, China. First, a broader background of urbanization in China and the primary driving factors are discussed. The role of urban planning is elaborated separately because of its distinct situation in China. Second, natural and social conditions of Urumqi city are illustrated together with the key issues related to the city's sustainability.

In chapter 4, story-lines of three different urban change scenarios for Urumqi 2030 are designed, “conservative scenario”, “planning scenario”, and “aggressive scenario”. Each plan is translated into a set of parameters used in determining total demand and spatial priority for certain land use types. The future land use change trajectories of these scenarios for the year 2030 are then simulated using the Dyna-CLUE model. Additionally, the "afforestation plan", derived from local green space system planning, was added on top of the urbanization scenarios. Together with the baseline scenario, which is the unchanged land use map in 2011, there are seven scenarios (baseline + 3 urbanization scenarios + 3 afforested urbanization scenarios) to pass into regional climate model in chapter 5.

In chapter 5, the year 2030 regional climate is simulated based on different future urban land maps produced in chapter 4 and selected IPCC scenario. The sensitivity of future regional climate simulations to different urban change scenarios are tested. Before looking at future climate change, the uncertainty propagation from MODIS land cover maps is examined. Finally, the magnitude and spatial patterns of climate change are analyzed by comparing the future projections to the baseline regional climate simulations fed by current global forcing and land surface conditions.

In chapter 6, results from previous chapters, urban change and climate change projections, are re-organized and interpreted regarding sustainability-related issues. The potential usage of the HLA modeling framework is explored, using water resources and agriculture productivity as case examples.

Chapter 7 concludes the main findings of this study and discusses the limitations of current work and prospects for future work.

CHAPTER 2

THEORIES AND METHODS IN HUMAN-LAND-ATMOSPHERIC SYSTEM

2.1 Urban sustainability

Urban areas, as the concentrations of diverse consumptive and productive activities, are hot spots for problems concerning sustainability. The physical expansion of cities impacts not only the natural landscapes but also the agricultural capacity of the human system (Jepson Jr, 2001). Urban land use market mechanisms, if left unrestrained, have the potential for producing significantly negative environmental damage. From a policy-making point of view, the fundamental concepts that compose sustainability are considered to be most applicable at local levels, at which most urban planning occurs (Campbell, 1996). Thus urban sustainability and sustainable urban development are becoming dominant concepts in urban planning practices.

One of the most popular definitions of sustainability is "meeting the needs of the present without compromising the ability of future generations to meet their own needs" (Brundtland and Khalid, 1987). This statement has been criticized as imprecise and vague, but it does reveal one of the most important ideas underlying the concept of sustainability, that sustainability concerns long-term well-being instead of immediate needs. Two terms, sustainability and sustainable development are often used interchangeably. One way to distinguish them is to consider sustainability as a desirable state, while sustainable development is the process by which sustainability can be attained. However, these two terms both are concered with the health of dynamic complex systems, thus are better considered in a common framework.

The concept of sustainability emerged from ecology (Callicott and Mumford, 1997), but it goes far beyond protecting the natural environment. The other concerns are the development and well-being of human race, which brings economic growth and social justice into the realm of sustainability (Barbier, 1987; Pearce, 1988). The contemporary understanding of sustainability often constitutes three different dimensions which are Environmental protection, Economic development, and social Equity (Campbell, 1996). According to Jepson Jr (2001), the environmental dimension looks at conservation and protection of our natural environment; the economic dimension focuses on the improvements in living conditions, as a result of economic development; while the equity dimension takes into consideration intrageneration equity in addition to the more environmental-oriented intergeneration side.

Given the rising concern on sustainability issues, it is important to assess the degree of sustainability quantitatively, thus provide a baseline for comparing sustainability across different places or times. There have been many efforts devoted to developing and evaluating indicators for sustainability (Maclaren, 1996; Alberti, 1996; Shen et al., 2011; Mori and Christodoulou, 2012). However, the concept of sustainability itself is diverse and complicated (Tanguay et al., 2010), making it nearly impossible to come up with a universal agreement on the definition, let alone indicators for sustainability.

The most common approach to measure sustainability is to develop a set of indicators that account for many aspects of this concept. Maclaren (1996) suggested that the selection of indicators should be integrating, forward-looking, distributional, and from multiple stakeholders, to distinguish them from other simple indicators. From a more practical point of view, they should also be policy relevant, scientifically founded, readily implemented, and usable for decision-making (Alberti, 1996). The indicators selected are often grouped into categories that represent at least the three pillars of sustainability. Environmental indicators often include environment quality (air, water, soil), use of pesticides and fertilizers, and emission of greenhouse gases. Economic indicators may include GDP, FDI, CPI, and median household income. Equity indicators may include unemployment rates, income distribution, household below poverty, adult literacy rate, and crime rates.

Besides selecting an extensive collection of indicators, there are also some efforts in developing a composite indicator to evaluate the overall status of sustainability. Some scholars and global organizations have developed several aggregated indicators, including Living Planet Index (Loh et al., 2005), Ecological Footprint (Rees, 1992), City Development Index (Programme), 2001), and Human Development Index (Klugman, 2009). This composite indicators reduced the amount of information, which makes them easier to use in comparing and supporting policy-making. However, they are more often criticized. The rules for selecting variables, normalization, and weighting are ambiguous and subjective. Böhringer and Jochem (2007) argued that the use of these indicators might be "useless if not misleading."

Most of the above-mentioned indicators function at different administrative levels. There is also spatial indicators which can quantitatively represent the spatial distribution of some key element in assessing sustainability. Borrowed from ecology, landscape pattern analysis is used to evaluate the performance of different land use patterns (Leitao and Ahern, 2002). Ideas from landscape ecology, such as abundance, diversity, shape, and connectivity, can be adopted to evaluate processes in the urban ecological system. They are particularly valuable for comparing different land use configurations in land use/cover change, prediction, or alternative scenario analyses.

Another important concept is the contradiction between weak and strong sustainability. The essential difference of the two models, according to Neumayer (2003), is whether natural capital is considered substitutable by human-made capital. In practice, weak sustainability allows advances in the economic and social aspects to offset adverse impacts on the environment, while strong sustainability aims at preserving environmental functions and defining ecological limits to growth (Nourry, 2008). As cities, at most times, have negative impacts on natural capital, and such impacts are often not limited to urban area and hard to measure, it is safer to take the stronger view of sustainability to avoid underestimating environmental problems. One way of doing that is evaluating different aspects independently without trade-offs (Mori and Christodoulou, 2012).

2.2 Human-induced land use/cover change

Land use/cover change (LUCC) is one of the most direct forms of human-environmental interactions led to various environmental problems locally and globally (Foley et al., 2005). Land use and land cover are a pair of related terms that describe the state of the land (Fisher et al., 2005). Land use focuses on the type of human activities (agricultural, urban, etc.) conducted on that land while land cover concerns its physical material (grass, forest, asphalt, etc.). Land cover can reflect land use, and land use change is a major cause for the conversion of land cover. As a result, these two terms are usually used interchangeably when studying human impact on land surface. LUCC alters land surface in the type and intensity of human activity (farming, mining, manufacturing, etc.) as well as in physical characteristics (albedo, vegetation coverage, imperviousness, etc.), which lead to further changes in climate (Pielke et al., 2002; Kalnay and Cai, 2003; Brovkin et al., 2013), hydrology (Harbor, 1994; DeFries and Eshleman, 2004; Li et al., 2009), biodiversity (Poschlod et al., 2005; Jetz et al., 2007; Newbold et al., 2015), environmental quality (Mattikalli and Richards, 1996; Tong and Chen, 2002; Heald and Spracklen, 2015), and more.

LUCC studies may be grouped into three main categories: observation, mechanism, and implication. As implications usually weigh more in other fields, the core of LUCC studies lies in identifying the places and types of changes, and factors and processes that drive those changes, in other words, LUCC detection and modeling. Reliable observation is the starting point of understanding the underlying mechanisms. Each topic has its own origin and specific set of methods and research questions.

Remote sensing images have enabled land surface observation to cover almost every corner of the world since the 1970s (Aldrich, 1975; Todd, 1977; Bauer et al., 1979). Advancements in image resolution (spatial, spectral, and temporal), processing techniques, and data availability have made it possible to detect LUCC at a range of spatial scales, temporal frequencies, and on various thematic foci (Borak et al., 2000; Brink and Eva, 2009; Hansen et al., 2013). As a result, remote sensing images, instead of land use maps from land surveys, became the dominant data source in LUCC studies. There are generally two branches of methods in detecting LUCC from remote sensing images, depending on whether the images have been classified into land use/cover maps first.

Post-classification LUCC detection requires remote sensing images to be classified into land use/cover maps in advance. Change is then derived from differencing land use/cover maps of different dates. The core methodology in this type of change detection is image classification, which is primarily based on the spectral signatures of remote sensing images. Contemporary classification methods include pattern recognition, Artificial Neural Networks, Support Vector Machines, Fuzzy Set Theory, Decision Trees (Mather and Tso, 2016). Post-classification differencing is straightforward and allows convenient incorporation of existing land use/cover maps from other sources, thus the most popular approach in LUCC analysis. However, its output is especially susceptible to low classification accuracy which may compound from each time-snaps.

Another route for detecting LUCC feeds pre-classified data, e.g., multi-spectral reflectance and vegetation index, from multiple dates directly into change detection algorithms without first classifying pixels into land cover types. Change detection method can be as simple as thresholding or as complicated as image classification, depending on the target land cover classes and the degree of detail required by each study (Singh, 1989; Mas, 1999; Tewkesbury et al., 2015). Pre-classification change detection methods are generally less computationally intensive and less vulnerable to compounded error, compared to post-classification differencing. As the inventory of remote sensing images keeps exploding, pre-classification methods are becoming more popular for large-scale and long-term continuous monitoring of land surface changes (Zhu and Woodcock, 2014).

Analysis of mechanisms of LUCC can be traced back to classical location theories, with focus on urban and agriculture locations. Both land use patterns and underlying processes that create such pattern are studied along this tradition. In the early 19th centure, Von Thunen developed an ideal concentric agricultural land model based on the theory of rent (Sinclair, 1967). Burgess adapted the Thunen model in to an urban context, and developed the concentric urban model about 100 years later (Anderson and Egeland, 1961). The sector urban models were developed to take into account the influence of transportation axes (Sultana, 2007). The multi nuclei model and the hybrid model were developed to account for more factors, e.g., (Harris and Ullman, 1945). With the development of complex system theory, self-organized urban land use models emerged (Batty, 2007).

The methods used in these studies also evolved over time. Von Thunen's agriculture land model predicts the location (distance to market) of different agricultural activities based on mathematical functions of product price, transportation cost and land rent. Influenced by the quantitative movements, statistical approaches were later adopted to describe the relations between land use and various natural and socioeconomic determinants (Serneels and Lambin, 2001; Serra et al., 2008). With the advancement in computer science, more sophisticated models, such as cellular automata (White and Engelen, 1993; Li and Yeh, 2002) and agent-based models (Parker et al., 2003; Matthews et al., 2007), were developed to account for interactions among land use units and different land use agents. Predictions produced by well-developed LUCC models provide important testbeds for researchers to experiment on different land-related policies and changing socio-economic scenarios (Veldkamp and Verburg, 2004; Verburg et al., 2010), which are extremely difficult to experiment with reality.

2.3 Climate change and urban development

Global climate has changed with recorded warming air and ocean, shrinking snow and ice, and rising sea level (Pachauri et al., 2014). The primary cause of global climate change is the vast emission of GHG, including carbon dioxide, methane and nitrous oxide, since industrialization (Stocker, 2014). The increased concentration of GHG trapped more energy in the climate system, causing overall warming in the atmosphere and ocean. Climate change further impacts hydrological systems (water quantity and quality), biological systems (habitat, behavior, abundance, etc.), and human society (food security, health risks, weather-related disasters, etc.) (Field et al., 2014). All these changes are expected to continue even in the most conservative future scenario. Thus mitigation and adaptation strategies are vital to ensure sustainable development.

The relationship between climate change and urban development has many dimensions. From the climate perspective, urbanization, as an inevitable consequence of industrialization and modernization, is an internal driver of the ever increasing consumption of fossil fuel energy. The GHG emission related to urban consumption and lifestyle, but its effects are not spatially limited to the urban areas, accounts for about 80 % of the global sum (Hoornweg et al., 2011). The conversion from natural to urban landscape also alters climate at the local scale. For example, urban heat island effects are found in many metropolitan areas as a result of changing thermal and radiative properties of the surface material, lack of evapotranspiration, and waste heat emission (Oke, 1982; Weng et al., 2004). Urban morphology also affects aerodynamics thus altering wind and precipitation patterns near cities (Martilli, 2002; Collier, 2006). Climate change poses additional challenges to the cities, especially in dealing with more frequent weather extremes, such as heat waves, floods, and tropical cyclones (Revi, 2008; Hamin and Gurran, 2009). Bearing those in mind, mitigation and adaptation strategies in response to climate change became priorities in urban planning and decision-making to make cities more resilient to those changes (Leichenko, 2011; Davoudi et al., 2012).

Quantitative studies on climate change are irreplaceable in supporting policy- and decision-making. Climatological variables have long been measured and recorded at stations all over the world. Many stations have joined global networks (e.g., Global Historical Climatology Network) and made their records available to support historical climate reconstruction (Smith and Reynolds, 2005). Remote sensing satellites now provide the ability to monitor many key climate variables for a greater spatial coverage and finer resolutions, e.g., land surface temperature (Li et al., 2013), sea surface temperature (Wentz et al., 2000; Reynolds et al., 2007), soil moisture (Njoku et al., 2003; Liu et al., 2011b), precipitation (Huffman et al., 2010; Kidd and Levizzani, 2011), etc..

Besides observations, climate change studies are also fueled by climate models, which were developed to quantitatively simulate the physical processes within climate system and predict climate conditions in the future. Dozens of global climate models (GCM) were developed by international research communities and their combined results were used to support comprehensive analysis on climate change (Gates, 1992; Meehl et al., 2000; Taylor et al., 2012). In these models, the planet is divided into a 3-dimensional grid. The atmospheric physics are calculated for each grid point and their interactions with nearby points. The spacing between grid points are typically several latitude/longitude degrees (hundreds of kilometers), with spatial resolution limited by computation power. For studies focusing on a smaller area but requiring greater spatial details, a regional climate model (RCM) is usually the answer. RCM, e.g., the Weather Research and Forecasting

(WRF, Skamarock et al. (2005)) Model and the Regional Atmospheric Modeling System (RAMS, Pielke et al. (1992)), takes coarse GCM results and dynamically downscales them to finer grids, taking into account local characteristics such as topography and land cover.

2.4 Integrated environmental modeling

The complex nature of environmental problems calls for holistic systems thinking to account for various interactions within the complex human-environment system. Integrated environmental modeling (IEM) assimilates knowledge and tools from multiple relevant disciplines to support system understanding, prediction, and scenario exploration (Laniak et al., 2013). Kelly et al. (2013) grouped existing IEM applications into five broad approaches, including systems dynamics, Bayesian networks, coupled component models, agent-based models, and knowledge-based models. The coupled component models (CCM) is the most popular approach that takes advantage of readily available models developed in specific disciplines, usually process-based, thus allowing in-depth representation of corresponding components.

There are abundant models developed in a spectrum of disciplines as a result of ever improving power and accessibility of computation resources. Within the human-land-atmospheric system, various models have been developed to describe processes in different subsystems, and many have been actively evolving by coupling, either loosely or tightly, with additional models to explain some critical sub-processes better. For example, land use change models are using socioeconomic models to describe the internal drivers of changing land use demand (Verburg et al., 2002; Rounsevell et al., 2006; Wu et al., 2015). Climate model performances are gradually improved by coupling land surface sub-models (Walko et al., 2000; Bonan et al., 2002; Niu et al., 2011; Chen et al., 2011). Models for global carbon cycle (DeFries et al., 1999; Jung et al., 2006; Friedlingstein et al., 2006; Cox et al., 2013), hydrological process (Hernandez et al., 2000; Chen and Dudhia, 2001; Cuo et al., 2009), urban transportation system (Waddell, 2002; Suarez et al., 2005; Anas and Liu, 2007), pollutant dispersion (Christensen, 1997; Di Sabatino et al., 2007; Jacob and Winner, 2009), etc., have all been coupled with land use and/or climate models, as these systems by nature interact with each other.

Coupling multiple models for particular research topics is theoretically feasible, but the compounded complexity and uncertainty can prevent the coupled models from being useful (Fulton et al., 2003; Lindenschmidt, 2006). Complexity, in both the models and their underlying systems, requires significant time, computation resources, as well as expertise, to configure, run and understand the models. It usually leads to a vast parameter space that requires modelers to spend substantial time in parameter estimation and model calibration. The standard practice is to perform a sensitivity analysis to identify most influential parameters and then estimate their optimal values to achieve best model fit (Hamby, 1994; Campolongo et al., 2007; Nossent et al., 2011). The inevitable side-effect of this approach is the added computational cost, especially for the models that are already computational intensive.

Uncertainty further complicates the situation, since it may rise from all steps of modeling, from data measurement and representation, to model design, and to model implementation (Barry and Elith, 2006; Chatfield, 2006; Beven, 2007). Uncertainty results from imperfect model representations of the problems/processes in reality. The imperfections come from the limitation of the tools used in observation as well as the state of academic understanding of the system. Therefore, uncertainty is fundamentally irreducible, and its magnitude is determined by the technical, methodological and cognitive gaps. Uncertainty evaluation and management (Rotmans and van Asselt, 2001; Refsgaard et al., 2007; Matott et al., 2009) are thus essential for the effective use of integrated models. However, it can be difficult to characterize and communicate uncertainty (Manning, 2003; Fulton et al., 2011; Renard et al., 2010). Uncertainty analysis also multiplies computational requests. These challenges usually discourage modelers from adequately performing uncertainty analysis, but ignoring uncertainty is dangerous especially when using model outputs to support decision-making.

Nevertheless, coupled component models are still the most compelling approaches to test hypotheses and explore alternative scenarios on system interactions that are usually difficult to experiment physically, and make predictions out of the best understanding of the phenomena. They can provide scientifically based decision-support if complexity is well understood and uncertainty sufficiently acknowledged.

The coupled HLA modeling framework proposed in the previous chapter is in the form of a coupled component model. It aims at addressing urban sustainability problems by linking them with human-induced urban land use/cover change and climate change. This modeling framework will be applied with some considerations of uncertainty. Before running the models, it is important to first learn the characteristics of the study area.

CHAPTER 3

STUDY AREA

3.1 Urban change in Chinese cities

3.1.1 Countrywide urbanization

Urbanization is the corollary of industrialization and modernization. People are drawn from rural to urban areas due to changes in labor demand, economic opportunities and overall prospects of urban lifestyle. China's urbanization in recent decades is unprecedentedly rapid and extensive in the human history (Zhang and Song, 2003; Lu et al., 2006). Started from less than 20% in 1960, China's urbanization rate reached 50% in 2011 and surpassed global average in 2013. It is projected to reach 70% in 2030 and 75% in 2050 (figure 3.1). Both social structures and the natural environment have been profoundly impacted by the process of urbanization (Kalnay and Cai, 2003; Ma and Wu, 2005).

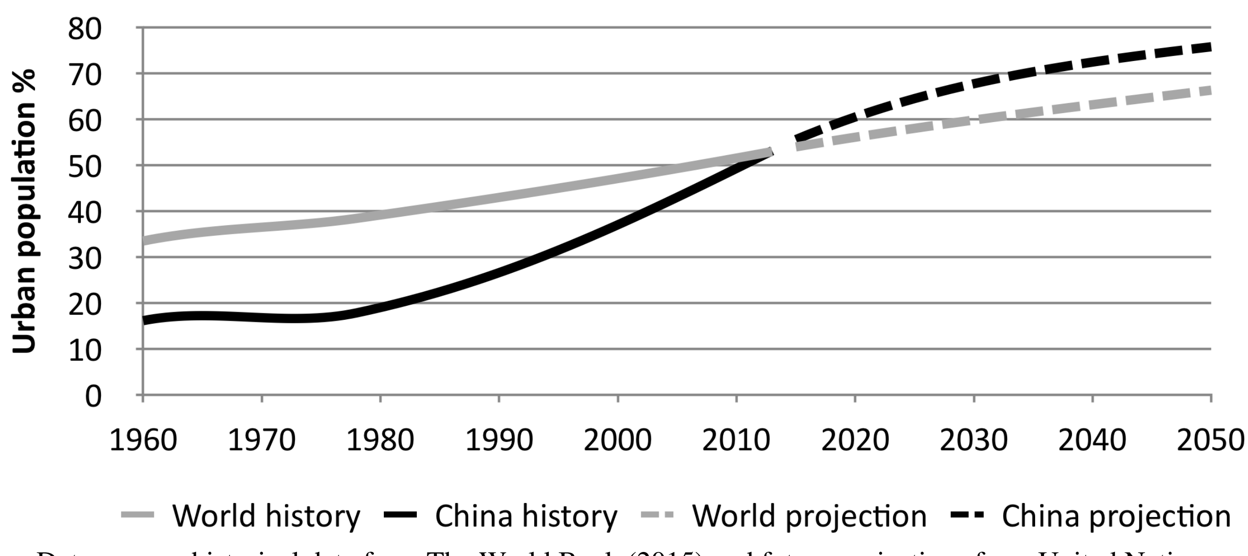

Data source: historical data from The World Bank (2015) and future projections from United Nations, Department of Economic and Social Affairs Population Division (2015)

Figure 3.1 Trend of urbanization rate

While China's urban population has tripled since 1981, urban land area expanded six times during the same period (figure 3.2). The majority of the newly urbanized lands replaced cropland (figure 3.3), creating national concerns about food security (Zhang et al., 2004; Chen, 2007). The Urban Heat Island (UHI) effect has intensified over the recent decades (Ren et al., 2007). The combination of these negative effects forced the government to enact policies regulating land use conversions.

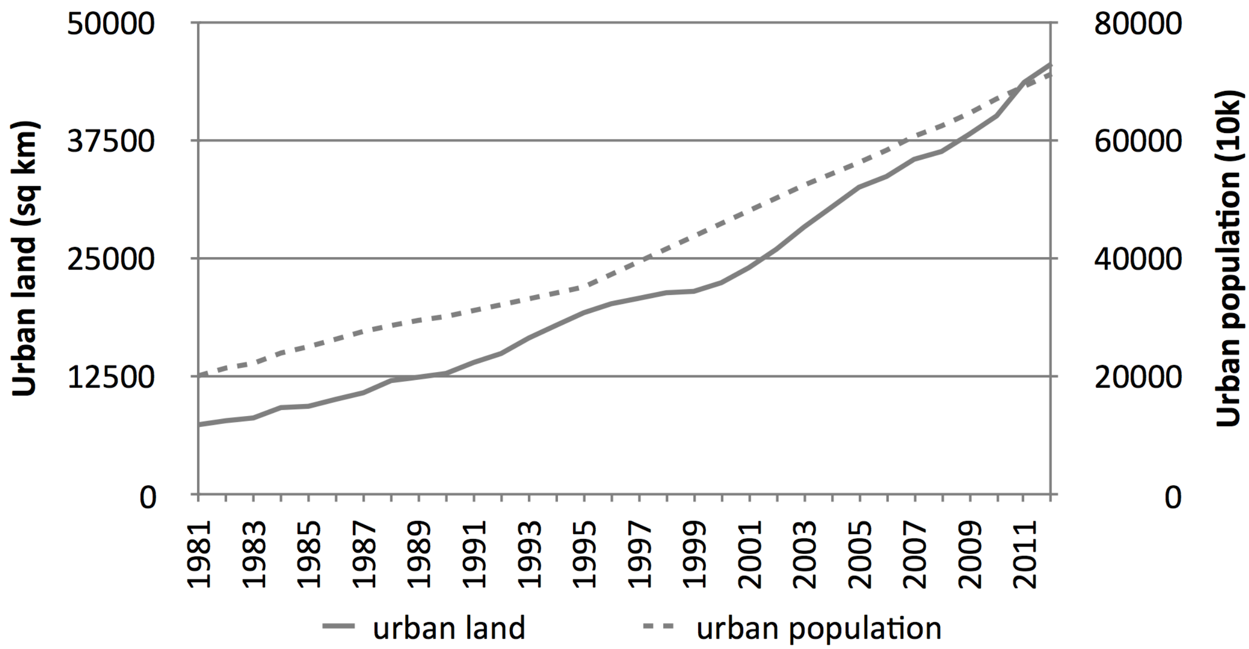

Data source: urban land from "Area of built district" in China Urban Construction Statistical Yearbook 2012 and urban population was from China Statistical Yearbook 2013

Figure 3.2 Historical trend of urban land and population

3.1.2 The role of planning

Modern urban planning started in China in the 1950s, soon after the People's Republic was founded. The majority of country's industry and infrastructure had been destroyed during decades of warfare. Under the socialist ideology and in the hope of rebuilding the economy quickly with limited resources, the post-war Soviet system was adopted, which was characterized by a centrally-planned economy and urban planning as an instrument to achieve such goals (Xie and Costa, 1993). Urban growth and planning practices halted during the 60s and early 70s due to the chaos created by a

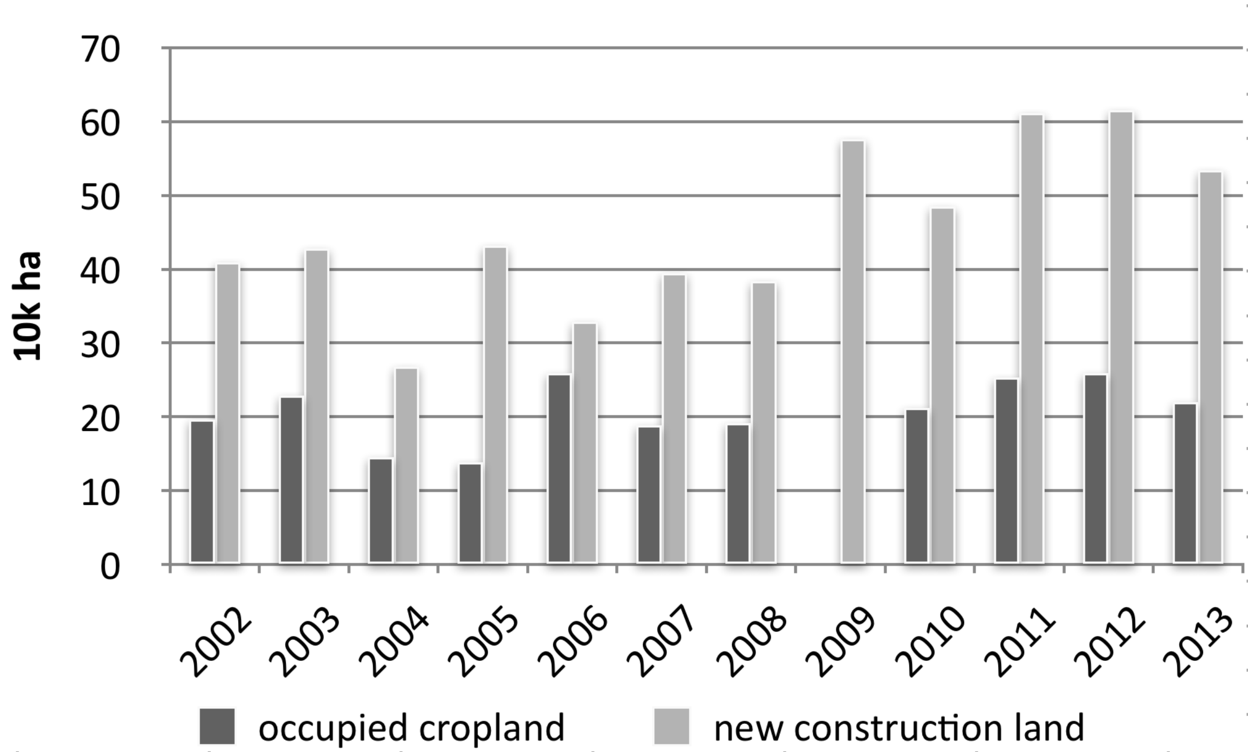

Data source: China Land Resource Report, multiple years
Note: occupied cropland data is not available for year 2009

Figure 3.3 Occupied cropland in new construction land

series of political and environmental disasters. In 1978, the Chinese Economic Reform marked the beginning of market economy and power decentralization, which fueled economic development and urbanization. New demands for urban planning were promoted during this time, leading to the development of China's first City Planning Law in 1989. It was later modified and expanded to coordinate both urban and rural development, becoming the Urban and Rural Planning Law in 2007.

China now has a hierarchical urban planning system corresponding to administrative levels. In the national and provincial levels, the Urban System Planning prioritizes different cities and defines their functions and interrelationships. At the city level and below, both comprehensive and detailed (project-oriented) planning are required. The comprehensive city plan (master plan), which typically covers a time-span of 20 years, is most relevant for this study. It incorporates pre-set sustainable goals and is intended to mitigate the adverse impact of urban sprawl and to manage development (Qian, 2013). The master plan is largely techno-rational (directed by technical experts) and a top-down extension of central economic planning. It usually comprises a detailed spatial arrangement of the population, land use and infrastructure planning, conceptual design, and mega-urban projects (Wu, 2007).

In today's socialist market economy, often cited as state capitalism in western literature, China's urban planning gradually evolved into negotiations among central, local governments and different interest groups (Ng and Tang, 2004). The municipal government plays the leading role in the process of developing and implementing city master plans. The central state expresses its vision but provides room to localities for negotiations over the ceilings in local urban growth that fulfill their development interest (Oi, 1995). Then, local government has a decisive role in local pro-growth coalitions (Zhang and Wu, 2008) because of the state's ownership of land. The tension between planning and market forces creates disparities between master plans and urban development realities. Planning adjustments and revisions then take place at local levels to alleviate such tension.

The land use master plan is another spatial planning tool in China intended to regulate urban growth directly. While city planning is lead by a Municipal Bureau of Planning, land use planning is under the jurisdiction of a Municipal Bureau of Land and Resources (Feng and Su, 2016). The focus of land use planning is to coordinate land resources between construction and agricultural uses by allocating a set of top-down quotas of built-up and cropland areas. Ideally, city planning would be performed inside the spatial extent designated by the land use master plan. In reality, the two planning systems are usually incompatible with each other. They have different time-frames, land use categories, and coverage areas. With different interests and goals, they were developed separately with little connection and reference to each other (Meligrana et al., 2008). The conflict and inconsistencies brought by the "dual-track" planning institution is another reason preventing effective implementation of these plans.

3.2 Urumqi

3.2.1 Overview

Note: red - Urumqi, orange - Xinjiang, yellow - China

Figure 3.4 Location of Urumqi in Xinjiang, China

Urumqi, 43°48'N 87°35'E, is the capital city of Xinjiang Uyghur Autonomous Region (XUAR, Xinjiang hereafter), northwest China (figure 3.4). Urumqi is also known as the world's most inland major city that is furthest away from any ocean on earth. It is an oasis metropolis and serves as the political, economic and cultural center of Xinjiang. The total area of Urumqi is $13,788km^2$, with a built-up area of $339km^2$ (Statistics Bureau of Urumqi, 2010). According to 2010 census, the population of Urumqi is 3.11 million, of which 74% are urban residents. Urumqi has a high urban population percentage, compared to the then national average of 49.68%. The urban density is also high at $2,780.4ppl/km^2$. People from 49 different ethnic groups live in this city, including Han (75%), Uygur (12%), Hui(9%), Kazak (2%), along with many small constituencies.

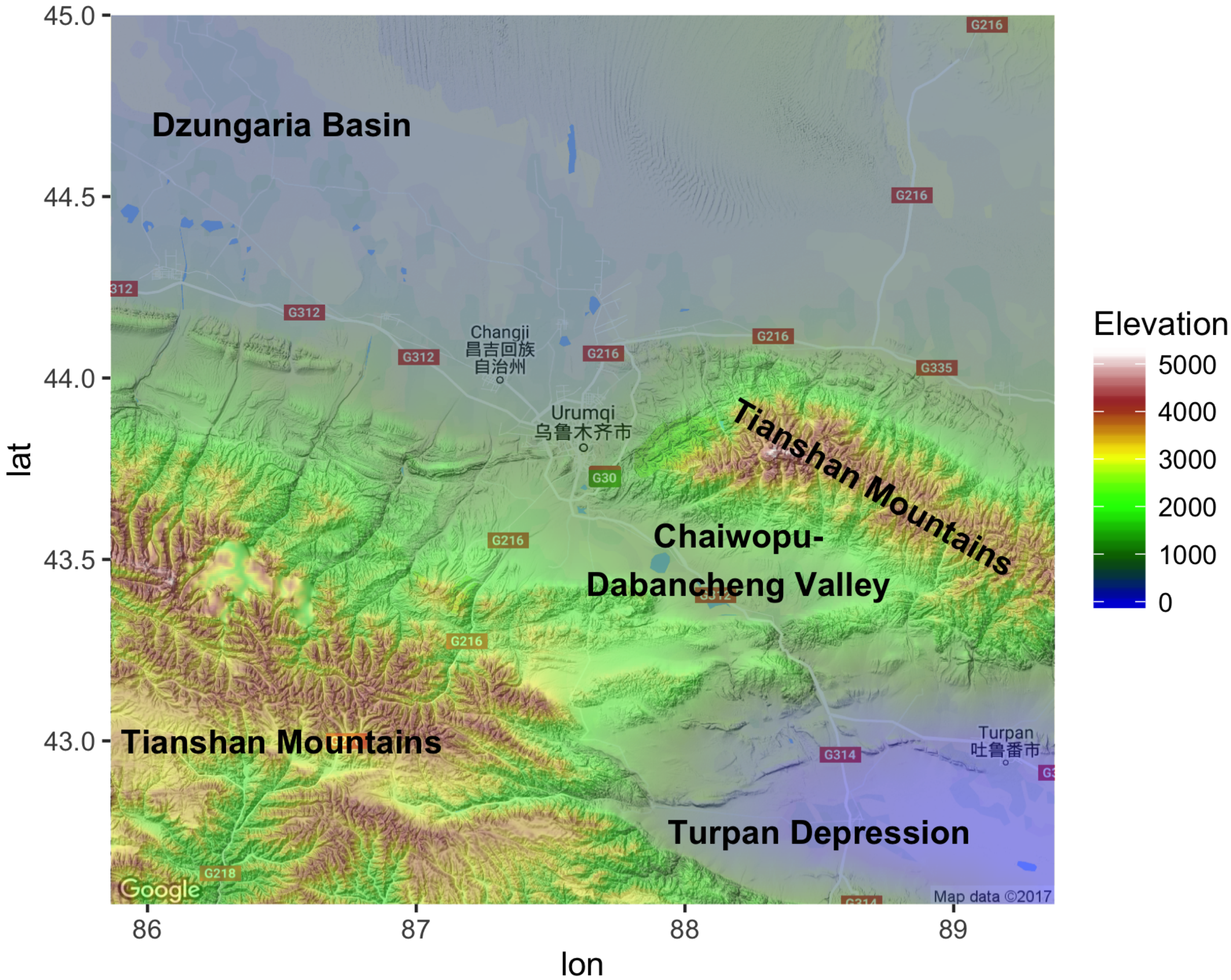

Figure 3.5 Urumqi topography, blending SRTM v4 with Google terrain base map

Urumqi rests on the north slope of the Tianshan Mountains and the southern fringe of the Dzungaria Basin (figure 3.5). Mountains surround Urumqi to the east, south, and west, leaving one opening, the Chaiwopu-Dabancheng Valley in the southeast. North of the city is a broad alluvial plain of the Urumqi River and the Toutun River. The city is uniquely shaped like a "T" due to topographic constraints in the south and open terrain in the north. Urumqi is a semi-arid oasis system. The average yearly temperature is $6.9°C$, and average annual precipitation is $286.3mm$, with summers slightly wetter than winters. The majority of Urumqi's water supply comes from several small rivers originating from mountain glaciers on top of the Tianshan Mountains. Suitable land for human habitat and agriculture is mainly limited to the alluvial plains alongside the foothills of the Tianshan Mountains (Luo et al., 2010).

Urumqi is comprised of eight district/county-level subdivisions (figure 3.6). Tianshan District, Saybargh District, Shuimogou District and Xinshi District constitute the central part of Urumqi. Midong District, Toutunhe District, and Dabanchen District are suburbs, while Urumqi County is a rural agricultural area. The Urumqi High-tech Industry Development Zone (HDZ) and the Urumqi Economic and Technology Development Zone (EDZ) were founded in 1992 and 1994, respectively, to promote economic growth. These two zones sit in Xinshi District but have the same management jurisdiction as other districts.

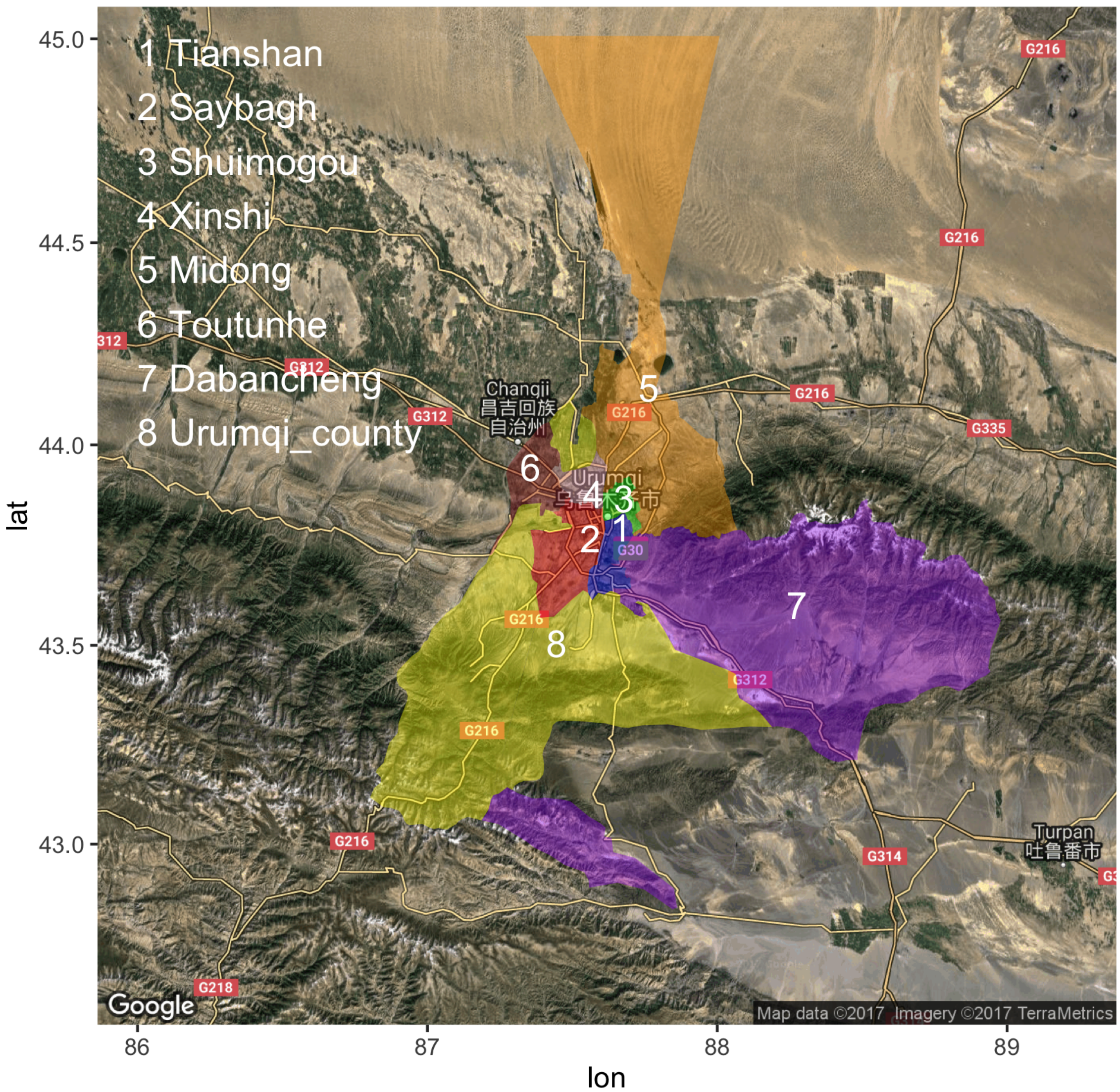

Figure 3.6 Urumqi district/county-level administrative boundaries, with Google hybrid base map

Though situated near the northern route of the Silk Road, Urumqi as a city can be traced back only to the Qing Dynasty (Han and Chen, 2005). In 1755, the Qing ruler defeated the Mongols who controlled this area in the Jungar Basin, then built the city and named it Dihua, meaning “to enlighten”. This established the city as a place to extend eastern culture across the western region (Sines, 2002). Troops were sent there not only for defense but also to work as farmers, herders, and miners. Given its favorable geographical location and economic growth, Dihua became a commercial and traffic center in Xinjiang, especially as the gateway connecting Central Asia and the rest of China. The successive governance from Kuomintang (1911-1949) generally adopted the same administrative division structure as Qing did, which made Dihua the most important city in Xinjiang, but under the governance of Han people.

Following the founding of the People’s Republic of China, on February 1st, 1954, the city was renamed Urumqi, meaning "beautiful pasture" in Mongolian. The built-up area then was only about $8km^2$ with little infrastructure. After the new Chinese government took control, large-scale industrial, traffic, and civil infrastructure constructions started to emerge under a controlled economy (Dong and Zhang, 2011). The 1978 Economic Reform marked the beginning of an era of market economy, but Urumqi fell behind other parts of the country due to its inland location. Starting in 1990, multiple favorable policies, especially the China Western Development Plan (2000), were adopted by the central government to promote economic development in western China, bringing Urumqi a new round of opportunities. With high-quality coal and potentially significant oil and natural gas deposits, the energy sector arose as the new driver of industry in Urumqi and entire Xinjiang (Dorian et al., 1997). Most recently, the One Belt and One Road Initiative (2013) marked Urumqi as a starting point of the new Silk Road Economic Belt that connect resources and economic activities through Central Asia, West Asia, the Middle East, and Europe. Urumqi’s rapid economic growth and urban expansion are expected to continue in the near future.

3.2.2 Key issues for a sustainable Urumqi

Rapid urban growth is a sign of economic prosperity. However, problems emerging from the urbanization process have greatly impacted the sustainability of Urumqi city. These problems hinder the development of Urumqi in every aspect including economic, environmental and social dimensions.

- Resources

In the oasis ecosystem, water supplies are limited. According to Xia et al. (2014), the 2012 water resource per capita in Urumqi is $377.8m^3$, far below the global average of $5829m^3$ (FAO, 2016). Although recent climate change brings to this area more precipitation and higher temperature, thus more snow and glacier melting and increased streamflow (Sun et al., 2013; Li et al., 2010), Urumqi is still under constant water stress. Expansions in farming, industry, and housing all place a significant demand on water resources. According to Du et al. (2006), Urumqi has put almost all its surface water into reservoirs and has been over extracting ground-water. Its primary water source, the Urumqi River, has been turned into the walled Heping Canal inside the city, which since 2011 frequently dries up due to high water usage. Given the limits of local water resources, Urumqi has been seeking solutions including suppressing agricultural use, reusing wastewater, and transporting water from other drainage areas.

Urumqi also lacks suitable land resources for urban expansion. More than 50% of the area is mountains. Alluvial plains that are suitable for farming and housing constitute less than 10%. The rough landform constrains the general shape of the city together with existing farmland, as a result of the strict Basic Farmland Protection Regulation (1994). Basic Farmland is similar to the term Prime Farmland in the US, the protection of which made it extremely difficult to convert high-quality farmland into urban uses. There was not much suitable land left within the city boundary for further expansion. One recent strategy for solving the land shortage is to put Urumqi and neighboring Changji Hui Autonomous Prefecture into a single entity for regional development consideration. The establishment of Wu-Chang (Urumqi-Changji) Economic Region in 2004 supports an integrated development plan. One movement under this strategy was the merging of Miquan city from Changji into Urumqi (forming the new Midong district by combining with Urumqi's old Dongshan district) which indeed stimulated growth in Urumqi.

- Environmental crisis

As an oasis metropolis, Urumqi is especially susceptible to environmental stresses. The water shortage mentioned above brings a series of environmental issues. The excessive use of surface and groundwater has lowered the water table, causing soil salinization in downstream areas, increasing pollutant concentration in lakes and reservoirs, and deteriorating the environment of local plants and animals (Chai et al., 2008; Du et al., 2006).

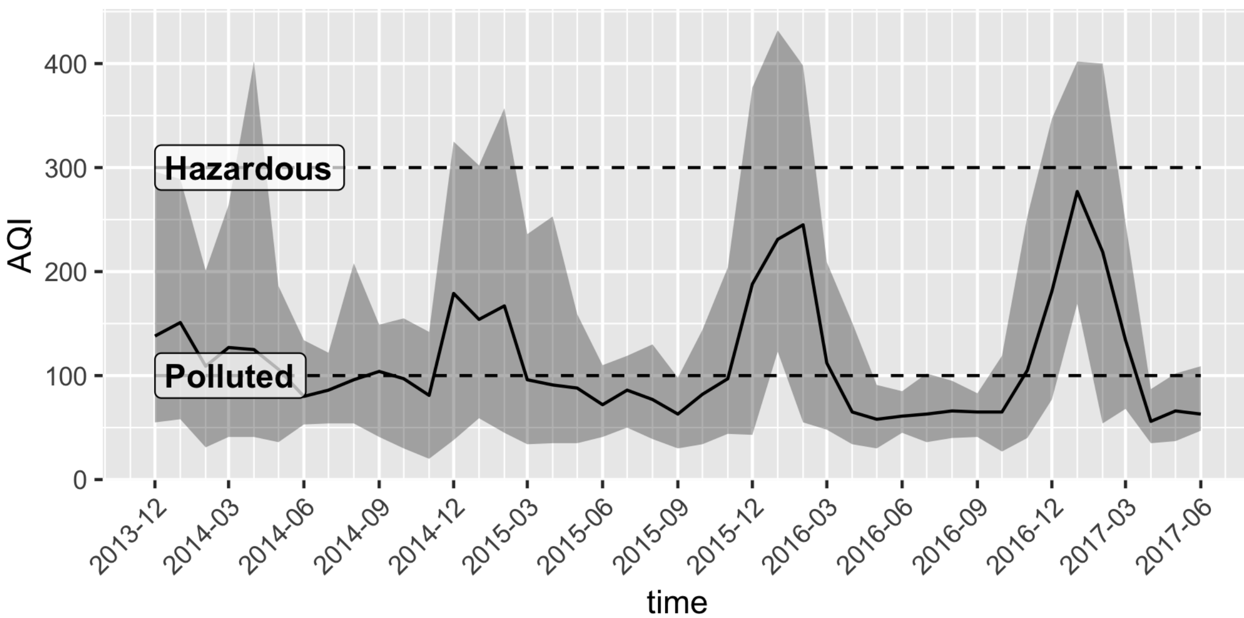

Data source: China Air Quality Index online monitoring and analysis platform (https://www.aqistudy.cn)
Note: The solid line shows the average and the shaded area shows the ranges of variation.

Figure 3.7 Historical average monthly Air Quality Index (AQI) for Urumqi

Urumqi is notorious for its bad air quality, especially in winters (figure 3.7). It was ranked the city with worst air pollution in the first quarter of 2016 among 74 major Chinese cities (China National Environmental Monitoring Centre, 2016). Nearly one-third of the days in 2016 had polluted air (Urumqi Environmental Protection Bureau, 2017). Fossil fuel, particularly coal, based energy production and domestic heating are considered major contributors to the air pollution problem (Mamtimin and Meixner, 2011; Song et al., 2015). Besides, the Tianshan Mountains surround three sides of the city, preventing the wind from effectively dispersing pollutants (Li et al., 2008).

Beyond air, water and soil are also heavily polluted with heavy metals (Wei et al., 2010; Zhang et al., 2013). The city has taken a series of measures to tackle the pollution problems, including more comprehensive environmental planning, more strict regulations and enforcement, and energy upgrading. However, no improvement has been seen in recent years.

- Contentious Uyghur-Han relationship

The Uyghur, with more than 10 million people, is the fourth largest minority group in China which primarily reside in the Xinjiang Uyghur Autonomous Region. As a Turkic ethnic group, the Uyghurs have an entirely different language, religion, and lifestyle compared to the majority Chinese Han people. China's current ethnic policy, the same for the Uyghurs and other major ethnic groups, is regional autonomy together with series of preferential policies in education, family planning, tax, and in political and legal areas (Shan and Chen, 2011). Despite this, the Uyghur-Han relationship continues to deteriorate.

One reason for the contention is the immigration of Han into Xinjiang (Mackerras, 2001; Howell, 2011; Howell and Fan, 2011). The influx of Han into what they regard as Uyghur territory challenges Uyghur for their dominance in Xinjiang. Differences in culture and beliefs make it difficult for both communities to mix. The inequality between east coast and west is another factor (Yee, 2003). The coastal economy benefits from Xinjiang's natural resource export, e.g., coal, oil, and gas. However, Xinjiang hasn't been adequately rewarded for its output. The poor industrial and civil infrastructure made it difficult for local residents to utilize resources in-situ. Moreover, only a tiny portion of the enormous revenue gained in this resource exploitation industry goes back to the local treasury as a result of a dated taxation scheme (Wang and Pu, 2011). One example of this problem was in the price of domestic natural gas, which in early years was higher in Xinjiang than in coastal cities. Additionally, the income inequality between the Hans and the Uyghurs adds to the already contentious relationship (Shan and Chen, 2011).

Terrorist events took place as the most negative manifestation of the Uyghur-Han conflict. Influenced by radical Islamic groups, terrorist attacks were conducted aiming at civilian Han people. Major events happened in Urumqi include bus bombs in 1992 and 1997, the horrific violent riots in 2009, and a suicide bombing at a busy market in 2014. Together they took hundreds of lives and left thousands injured (Wikipedia, nd). The tragedies and their aftermath deepened the distrust between Han and Uyghur, which led to more intensive segregation (Jiang and Gao, 2003).

The current national policy on inter-ethnic issues follows a Marxist framework (Dorian et al., 1997), which regards economic development as the cure for almost every issue and state apparatus as a necessary tool. Efforts were put on increased security and economic aid. More police forces were moved to Urumqi area to promote stability. At the same time, city-level cooperation among coastal developed cities and Xinjiang cities were intensified to accelerate economic activity.

In summary, Urumqi shares many problems with other rapid growing inland cities, but its oasis environment and ethnic background make it unique from other major Chinese cities. Various research efforts have been devoted into this area but rarely encompass the integrated human-land-atmosphere system which is the goal of this dissertation.

CHAPTER 4

URBAN CHANGE SCENARIOS

4.1 Introduction

Our ability to look into the future is based on our understanding of what has happened in the past and what is going on right now. In the field of urban change prediction, researchers have built various models trying to explain how urban area changes in response to its physical, economic and social environment. However, different models and their inherent assumptions may yield different explanations of the past and thus different projections into the future. Instead of producing one single prediction, we can explore several possible urban change scenarios based on different models and assumptions.

Urban change can be modeled using two different approaches: aggregated area and spatial pattern. The overall urban land demand is usually driven by population and economic activities. Future demand for urban land thus can be estimated from projected population and economic acticity. The spatial pattern of a city is often constrained by its physical landscape and accessibility to existing urban infrastructures. It may also be influenced by local policies on land use restrictions or incentives.

In this chapter, I will discuss the urban change in Urumqi from recent history to near future projections. Changes in urban land demand will be modeled primarily using time-series analyses. All the statistical analyses conducted in this research was implemented in the statistical package R. The spatial patterns of urban changes will be simulated using the Dyna-CLUE model (Verburg and Overmars, 2009). Three different scenarios of urban change will be developed. Another set of scenarios will add Urumqi's aggressive afforestation plan on top of the urban change scenarios. The consequences of those scenarios, regarding urban sustainability, will be explored in later chapters.

4.2 Near future urban land demand under different stories

4.2.1 Driving forces of increasing urban land demand

Population and economic growth are two major driving factors of urban expansion in China (Tan and Ma, 2003; Tan et al., 2003; Tian et al., 2005). The area of urban built-up area can be potentially explained by population and economic indices, such as Gross Domestic Product (GDP). Their statistical relationships can be explored through Urumqi's historical development trajectory as well as the general pattern of Chinese cities. Once the relationship is established, the future urban area can be estimated based on projections of population and GDP as an indicator of economic development.

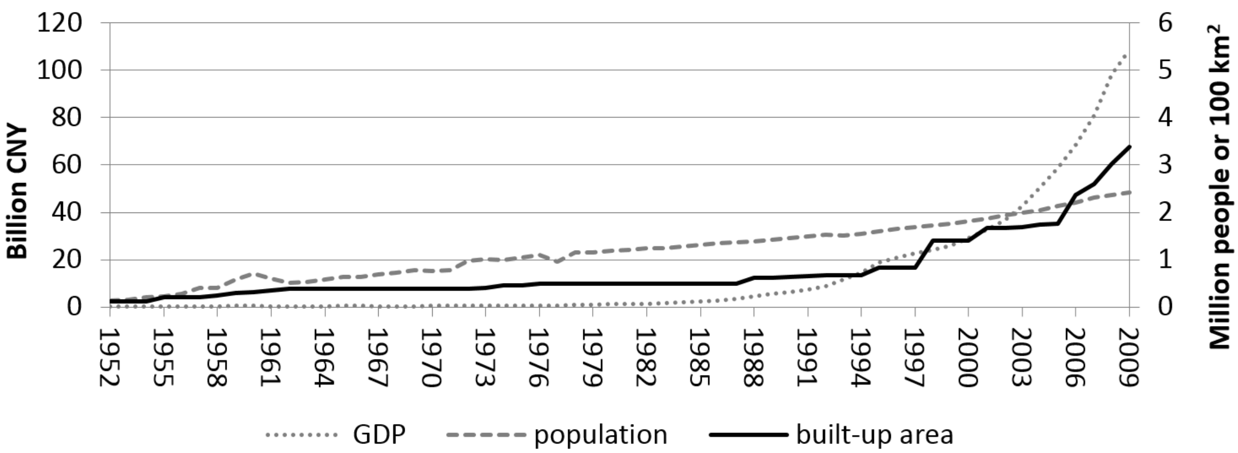

Data source: Urumqi Statistic Yearbooks

Note: Data for 2007-2009 were adjusted because Miquan was merged into Urumqi in 2007. For data consistency, Miquan's numbers in 2007 were subtracted from Urumqi's total numbers in subsequent years.

Figure 4.1 Historical trend of GDP, population, and urban area in Urumqi

- Urumqi, 1952-2009

Urumqi's historical data are first explored to establish a statistical model for urban built-up area based on population and GDP at the city level. Figure 4.1 illustrates the growing trend of Urumqi's population, GDP and urban area from year 1952 to 2009. The population increased steadily during the whole period. GDP grew slowly for the first three decades and then took off since the late 1980s. The Urban area grew steadily until the 1990s when a few leaps took place and eventually accelerated around 2005.

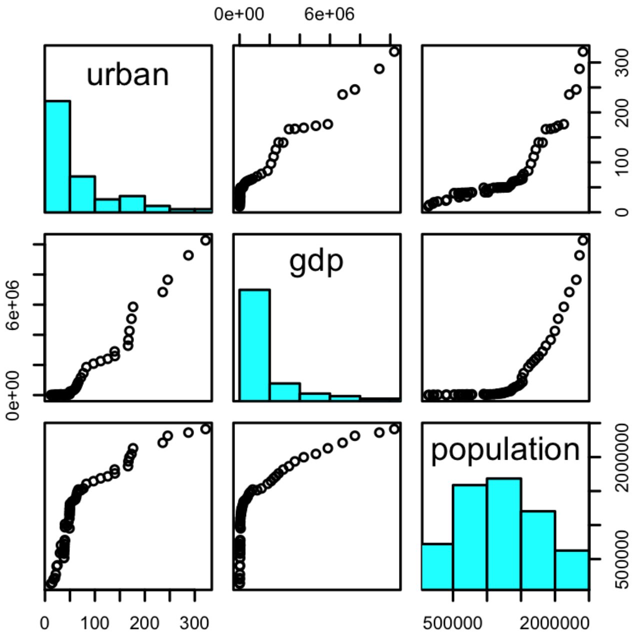

(a) Original data

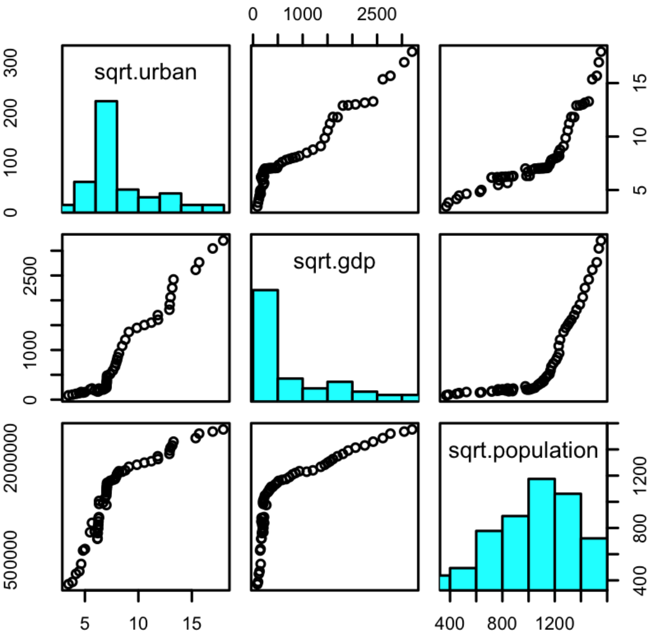

(b) SQRT-transformed data

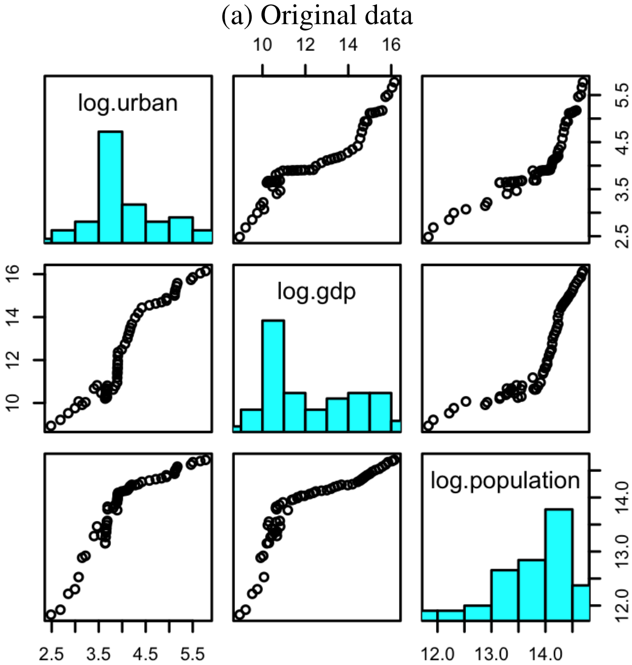

(c) LOG-transformed data

Figure 4.2 Distribution of the original and transformed Urumqi historical data

The histograms of the original data showed that urban area and GDP are right-skewed (figure 4.2a), which suggests transformation is needed before fitting them to regression models. Square root (SQRT) transformation (figure 4.2b) and natural LOG transformation (figure 4.2c) were performed.

First, data were fed into the Ordinary least squares (OLS) model, in the form of eq. 4.1, where βs are the regression coefficients and ε is the error term. It is not a surprise that ε is auto-correlated for both the SQRT- (figure 4.3a) and the LOG-transformed datasets (figure 4.3b). The gradual decay of Auto-Correlation Function (ACF) suggests and Auto-Regressive (AR) function instead of Moving-average (MA), and the Partial ACF (PACF) suggests the order of AR function to be 1.

$$Urban = \beta_0 + GDP\beta_1 + Population\beta_2 + \varepsilon \tag{4.1}$$

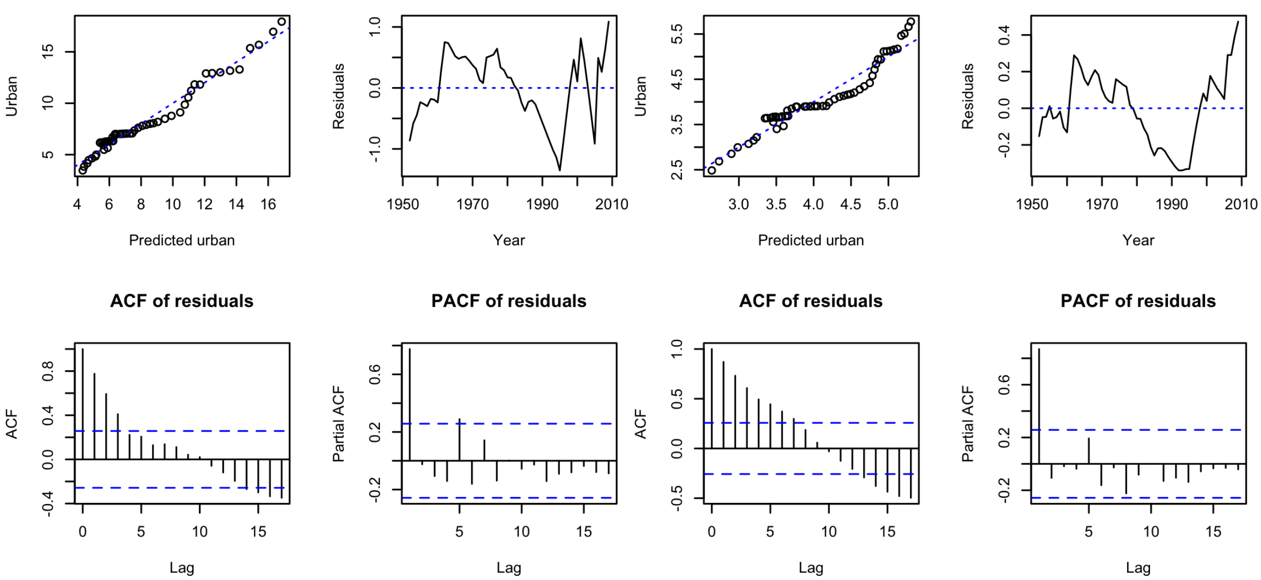

(a) SQRT-transformed data (b) LOG-transformed data

Figure 4.3 Structure of OLS residual auto-correlation for transformed Urumqi historical data

The model coefficients were re-estimated using the generalized least squares (GLS) model and the results are presented in table 4.1. GDP and population are significant from both transformations. Model performance was further evaluated using Pseudo R^2, which is the ratio of the sum of squared errors (SSE) to the total sum of squares (SST). Model fits are excellent, accounting for 99.5% and 95.9% of the variance in the urban area for the SQRT- and LOG-transformed datasets, respectively. This confirms that the data transformations, the selected model, and the coefficient

Table 4.1 GLS model results for Urumqi historical data

Transformation	Coefficients			Goodness-of-fit		
	β_0	β_1	β_2	SSE	SST	Pseudo R^2
SQRT	3.478(***)	0.004(***)	0.002(.)	21.300	4507.339	0.995
LOG	-0.831	0.195(***)	0.188(.)	4.722	116.402	0.959

Signif. codes: 0 ‘***’ 0.001 ‘**’ 0.01 ‘*’ 0.05 ‘.’ 0.1 ‘ ’ 1

estimations are capable of predicting urban area using GDP and population as independent variables. They will be used as candidate models to predict future urban land demand in the next section.

- Chinese cities, 2010

Another way to look at urban built-up area, GDP, and population is to relate them in the context of other Chinese cities. A collection of population and GDP of other Chinese cities are also expected to explain well the urban built-up area. Compared to the time-series model based on Urumqi's historical data, this regression model will reflect the "norm" of such relationship for Chinese cities in general. Figure 4.4a shows where Urumqi stands among all 286 of the Chinese cities in major socio-economic indices. In general, Urumqi has a vast urban area with a small population and above-average GDP. Consequently, its urban population density and GDP density, in terms of the number of people and GDP production per km^2 of urban land, respectively, are both in the lowest quartile. Considering that Urumqi is a capital city with multiple functions, it may be more appropriate to compare it with cities of similar features. Provincial capitals and the direct-controlled municipalities (e.g., Beijing, Shanghai, Tianjin, etc.) were selected, making a different data subset for coefficient estimation. As shown in figure 4.4b, Urumqi now has an average urban area, but both population and GDP are in the lowest quartile, making the densities almost the lowest among the capital cities.

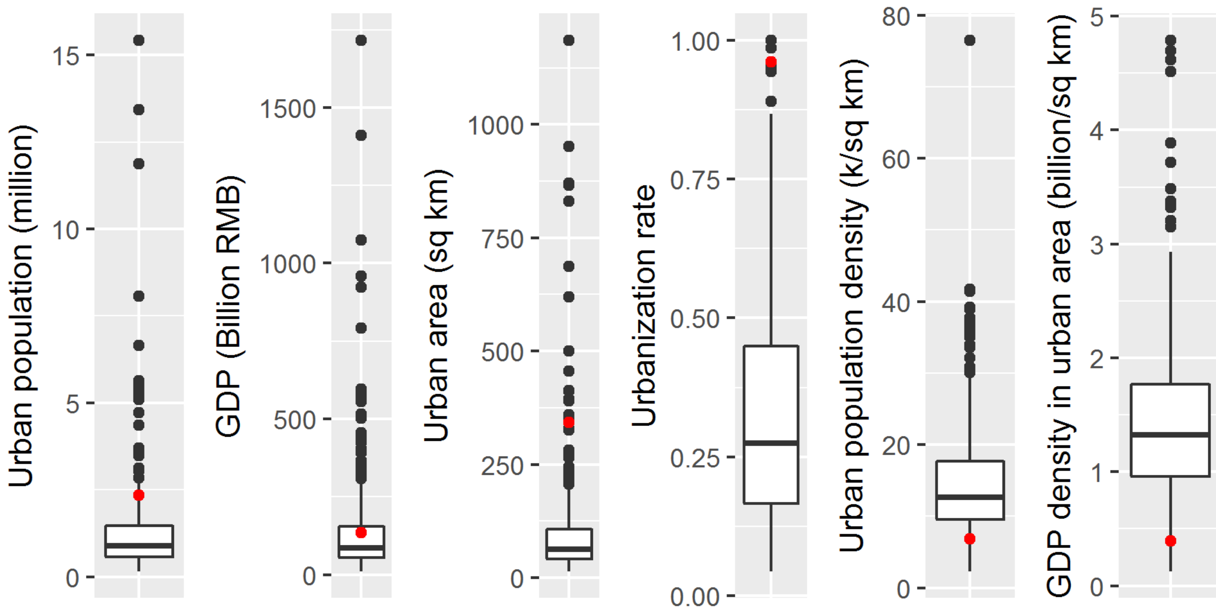

(a) All cities

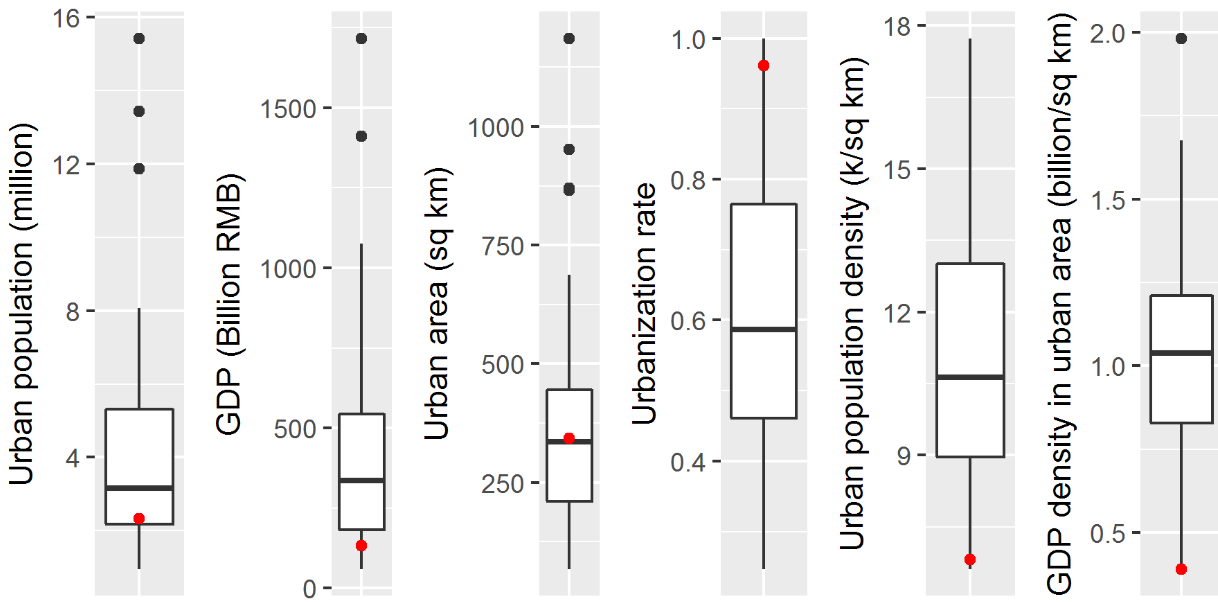

(b) Captial cities
Data source: China City Statistical Yearbook 2011
Note: Urumqi in red dots

Figure 4.4 Urumqi compared to other Chinese cities

Table 4.2 OLS model results for Chinese city dataset and capital city subset

Datasets		Coefficients			Adjusted R^2	Fitted value
		β_0	β_1	β_2		
All	SQRT	2.0327(***)	0.0018(***)	0.0029(***)	0.8766	171.7604
	LOG	-7.0215(***)	0.5240(***)	0.2449(***)	0.8356	174.3109
Capital	SQRT	4.6757(***)	0.0014(***)	0.0034(**)	0.9094	221.6638
	LOG	-6.6938(***)	0.4856(***)	0.2804(*)	0.9262	217.3056

Signif. codes: 0 '***' 0.001 '**' 0.01 '*' 0.05 '.' 0.1 ' ' 1

Figure 4.4 also indicates a far above average urbanization rate[1] for Urumqi. As a result, it is more appropriate to regress urban area against urban population and GDP in urban districts to avoid any bias introduced by including rural population. Both the all-city (figure 4.5) and capital-city (figure 4.6) datasets are right-skewed, requiring data transformation. Again, SQRT- and LOG-transformations were applied.

The OLS regression results are shown in table 4.2. Again, GDP and population are significant in all models. Regarding model performance, all models fit excellently, with the capital models perform slightly better, as expected, than the all-cities models. Urumqi is largely underestimated in all models, compared to the observed area of $343km^2$. Again, they suggest that Urumqi's current urban land use intensity is far below national average.

• GDP and population projections

To project future urban area based on the regression models developed above, we need to produce future projections for GDP and population first. Time series analysis (Box and Jenkins, 1976; Land, 1986; Clements and Hendry, 1998) was used here to study the historical trend in Urumqi and then extrapolate that trend into the future.

Here, two families of time series models were tested, exponential smoothing (ETS) and autoregressive integrated moving average (ARIMA), using the "forecast" package in R. The ETS models use a three-letter string identify the particular framework, with the first one as error type,

[1] Due to data availability in the China City Statistical Yearbook 2001, urbanization rate is calculated as the ratio of population living in urban districts, which may contain a small portion of rural residents, to the total population. Thus it is inconsistent with the number (74%) listed in section 3.2.1, which was based on the number of urban residents.

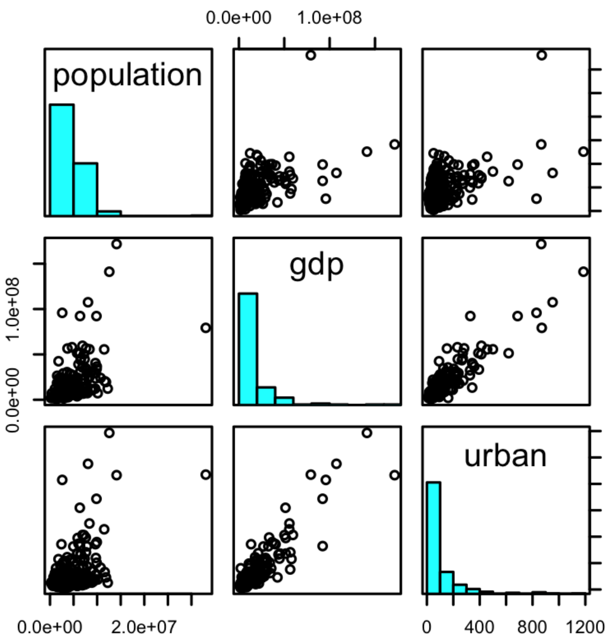

(a) Original data

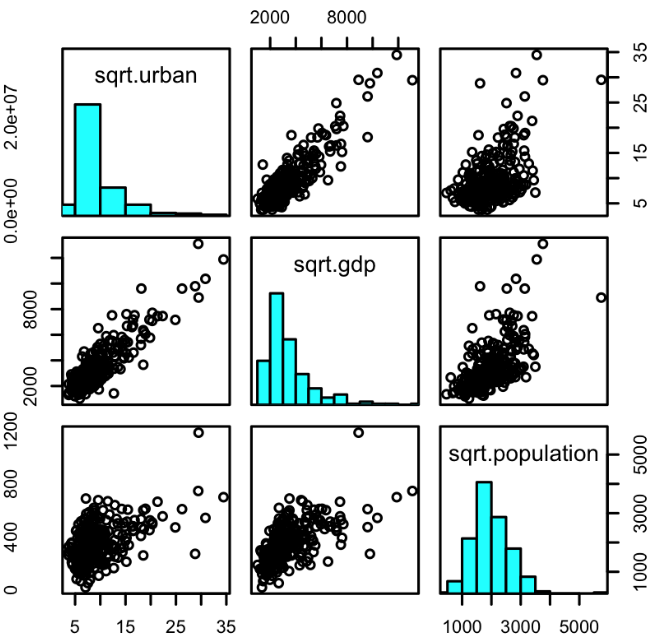

(b) SQRT-transformed data

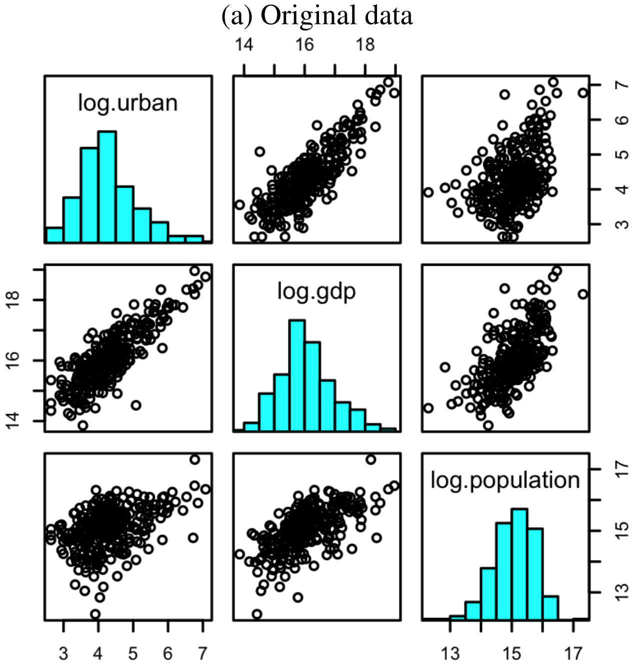

(c) LOG-transformed data

Figure 4.5 Distribution of the original and transformed Chinese city data

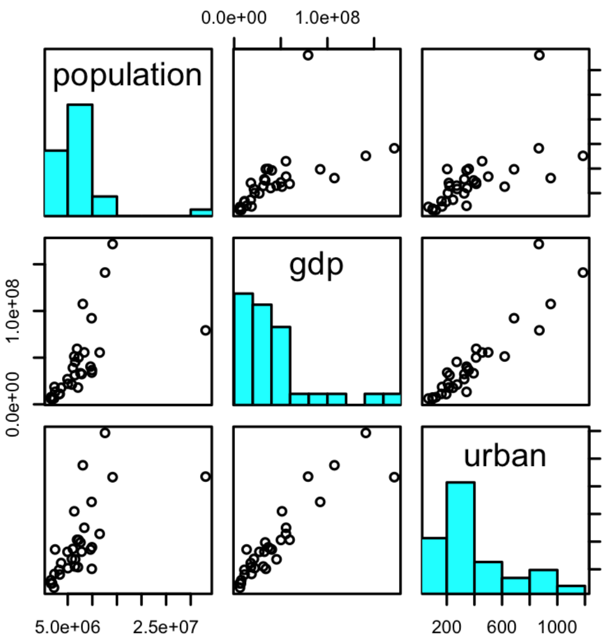

(a) Original data

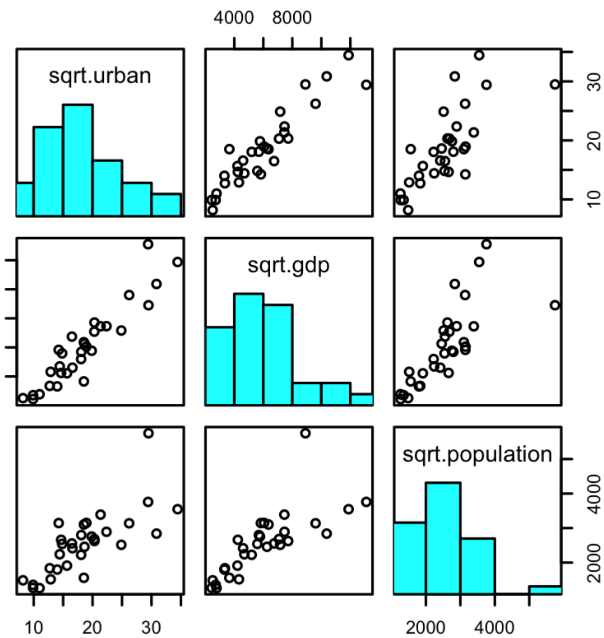

(b) SQRT-transformed data

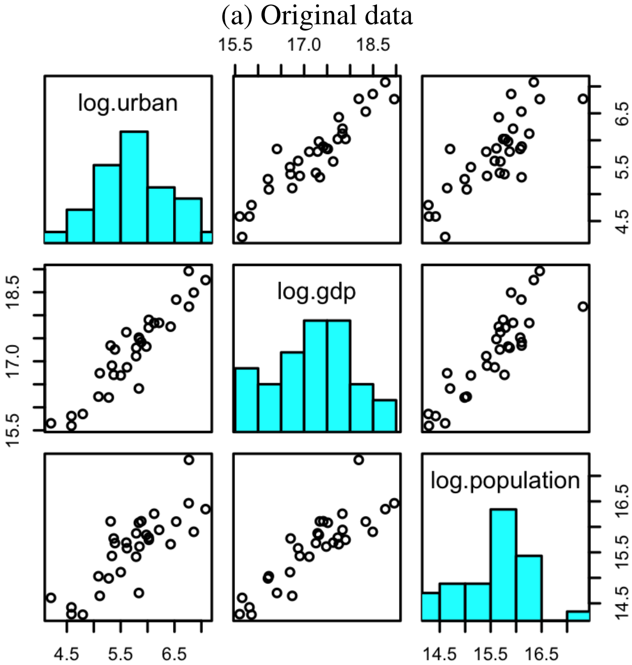

(c) LOG-transformed data

Figure 4.6 Distribution of the original and transformed Chinese capital city data

Table 4.3 Time series model performances on GDP and population

		GDP (10k CNY)		Population	
Model		ETS(M,A,N)	ARIMA(1,2,0)	ETS(A,A,N)	ARIMA(0,1,0) with drift
Parameter		alpha = 0.99991 beta = 0.1631 l = 1860.7518 b = 4170.3151	ar1 = -0.6706 s.e. = 0.1262	alpha = 0.8853 beta = 0.0624 l = 19865.7762 b = 64499.7081	drift = 39901.842 s.e. = 7448.075
	sigma	0.1694	124378.45	58242.51	56231.66
	AIC	1455.64	1477.4	1516.30	1412.6
Goodness-of-fit	AICc	1456.39	1477.62	1517.06	1412.83
	BIC	1463.88	1481.45	1524.54	1416.69
Projection 2030		26954656	36522720	3476870	3249877
Confidence	low	-76026819.4	27889516	2630493	2744822
intervals 95%	high	129936131	45155925	4323247	3754932

the second as trend type, and the third as season type. The letters are selected from N (none), A (additive), and M (multiplicative). By setting them to "Z", the $ets()$ function automatically test different model setups and return the one with the lowest Akaike Information Criterion (AIC). Similarly, the $auto.arima()$ function returns the best ARIMA model setup by specifying a three-integer code for the AR order, the degree of differencing, and the MA order. In addition, "drift" can be included to represent an underlying trend. Candidates from both families were then compared regarding model fitting and projection results[2] (table 4.3).

For the GDP models, the ETS(M,A,N) model has slightly lower AIC and almost zero sigma, but the problem is that it allows a much greater level of uncertainty, as a result of the multiplicative error term. It can easily be seen from the model's wide confidence interval for the future projections that spans from -760 billion to 1300 billion (figure 4.7a). Thus the ARIMA(1,2,0) model was finally chosen, given its decent model fit and constrained future projection (figure 4.7b). For the population model (figure 4.7c & figure 4.7d), the choice was easier. The ARIMA(0,1,0) with drift wins in both AIC and sigma, as well as producing a constrained future projection. As a result, the selected 2030 projection for GDP is 365.23 billion CNY, and for population is 3.25 million.

[2]The adjusted historical dataset, with Miquan taken out, was used in model fitting, while the future projection started with Urumqi's gross GDP and population in 2009.

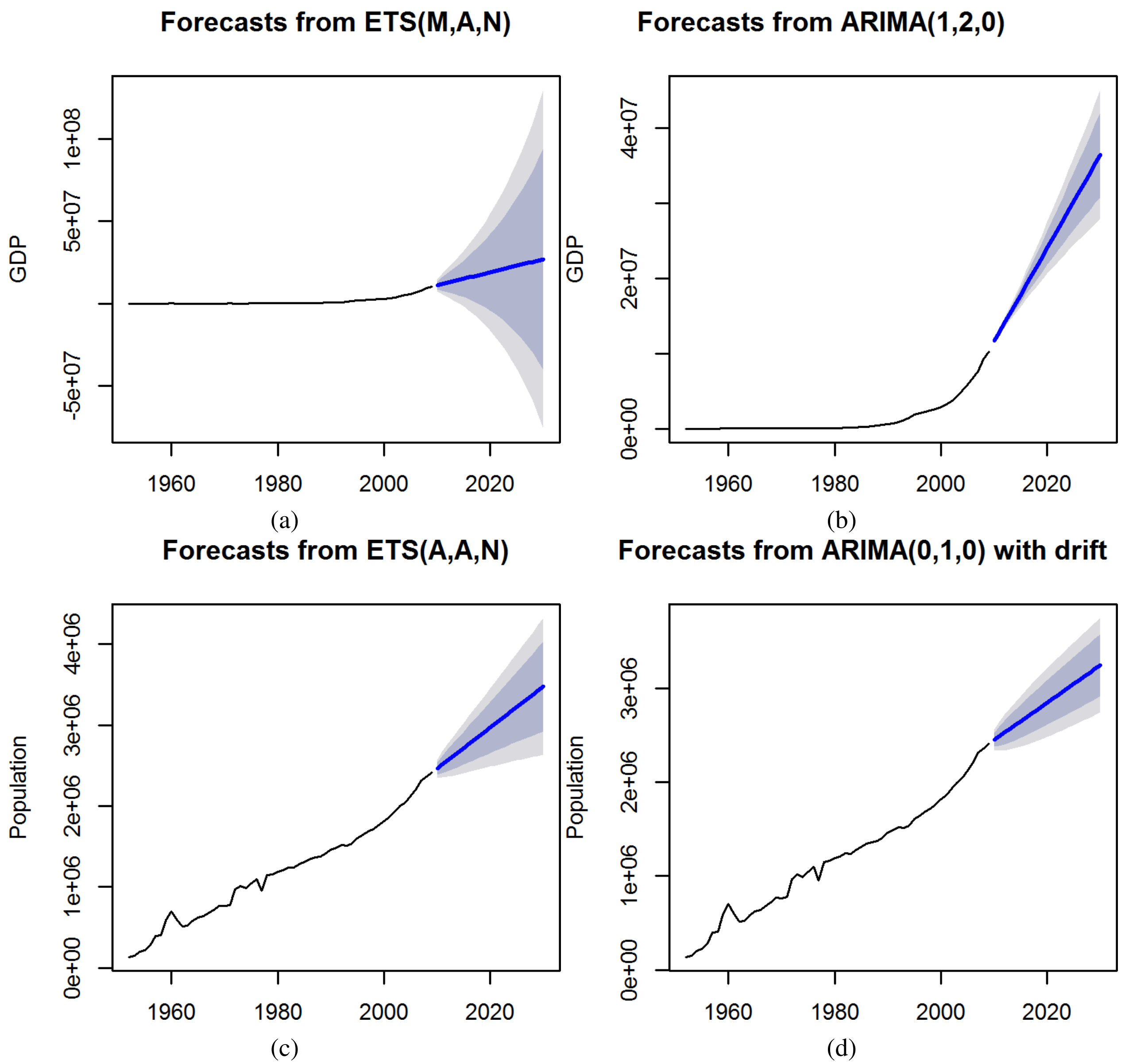

Note: confidence intervals at 80% and 95% levels

Figure 4.7 Model projections on GDP and population

Table 4.4 Urban area projections and references

		Urban area km^2	Urban population density ppl/km^2	Urban GDP density $10kRMB/km^2$
Time series regression	SQRT	787.34	3967.16	46387.45
	LOG	218.06	14323.96	167487.93
Chinese city regression	SQRT	325.46	9597.31	112219.91
	LOG	314.41	9934.62	116164.08
Capital city regression	SQRT	357.61	8734.30	102128.83
	LOG	381.81	8180.79	95656.79
References 2010	Urumqi	343.00	6809.91	38495.64
	Beijing	1186.00	10009.36	117237.88
	Shanghai	866.00	15512.36	195976.33
	Chinese cities	111.08	12234.33	77442.15
	Capital cites	394.93	11292.69	91222.48

4.2.2 Three stories with their supporting models

• Model projections

Urban area projections were produced based on the regression models and GDP and population projections developed in the previous section. For the Chinese city regression models, GDP and population projections were adjusted to urban GDP and population based on their ratios to the total population and GDP, respectively, in the year 2010. The urban area projections are listed in table 4.4.

It is worth noticing that three of these projections are smaller than Urumqi's current urban area, quite impossible as future scenarios. The primary reason is the low urban land use intensity in Urumqi (figure 4.8). All the unrealistically low predictions have intensities more on a par with the biggest metropolitans, such as Beijing and Shanghai.

Projection from SQRT transformed time series regression produced a far too large urban area, 787.34 km^2, more than twice of the current urban extent, and almost as big as Shanghai today. It has a lower population density and higher GDP density compared to what they are today, following the historical trend. This projection may serve as the aggressive urban expansion scenario.

The Chinese city regressions for capital cities produced more conservative projections, which can serve as a scenario encouraging denser development, compared to Urumqi today. It is closer

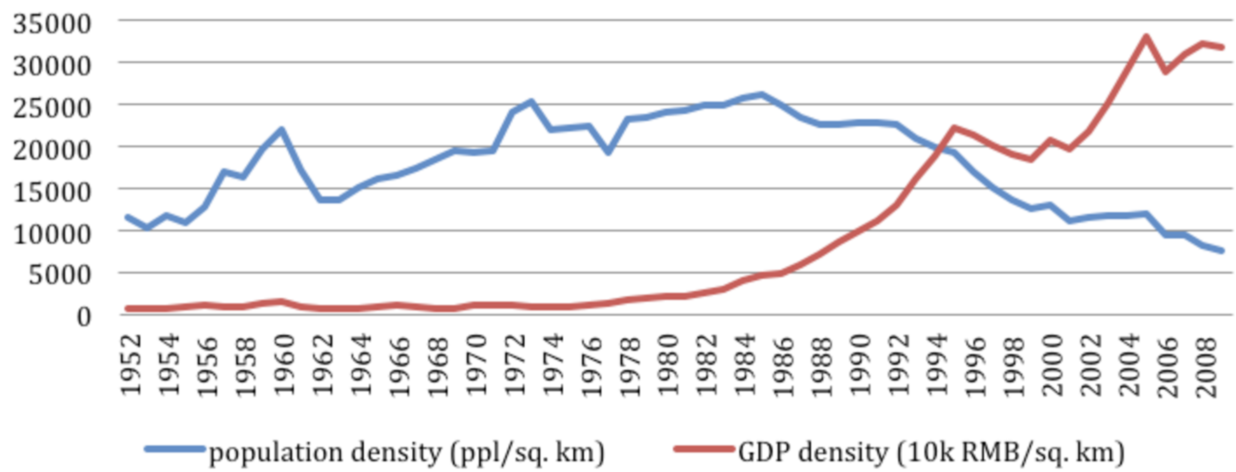

Figure 4.8 Urumqi's urban land use intensity over time

to the average level of the capital cities, most of them from more developed regions in China. However, given the historical trajectory of Urumqi's development, such densification will be very difficult to reach in the near future.

- Other future estimates

The Urumqi Land Use Planning 2006-2020 suggests that in the year 2020, Urumqi will require an urban area of 545.6 km^2 to support a population of 4 million. This plan asks for an aggressive 59% increase in 10 years. No published planning documents describe the year 2030. By linearly extrapolating this trend, urban area in 2030 can be estimated at 748.02 km^2, similar to the time series SQRT model prediction. If we assume the growing speed slows down after 2020 because the city finished its fast expansion phase and attains a more stable stage, a rough estimate of urban area in 2030 is about 600 km^2.

One thing worth mentioning is that their population estimation (5 million in 2020) is much larger than mine (3.25 million in 2030). It is partly because they also consider an estimate of temporary population who are not permanent residents of the city but live in Urumqi. The regression models in this study were built on permanent resident's population, drawn from statistical yearbooks. The actual population living in the city is larger, but since all the models are consistently using this population, there should be no effects for model predictions, especially if we assume

Table 4.5 Summary of 2030 urban area estimations

Methods	Urban area km^2	Percent increased from 2010
Time series SQRT model	787.34	129.55%
Capital city LOG model	381.81	11.31%
Land use planning 2030 (linearly extrapolated)	748.20	118.13%
Land use planning 2030 (slowing down)	600.00	74.93%
Urban planning density standard 120	567.16	65.35%

these two population numbers are proportional.

Another way to estimate future urban area is referencing an established standard for population density in urban planning. It is suggested in China urban planning that urban land per person should not exceed 120 m^2, which also means a population density of no less than 8333 ppl/km^2. In this case, Urumqi's urban area should be no more than $385km^2$ in 2030. However, temporary residents will become a problem because they also demand urban land. According to Urumqi statistical yearbook 2011, temporary residents' population is 1.06 million compared to a permanent population of 2.33 million in urban districts. Assuming their ratio remains the same, the total urban population in 2030 is estimated to be 4.73 million. Then the urban area should be no more than $567.16km^2$.

• Summary - the three stories

It is not easy to select urban area projections for the year 2030 because different models give wildly different results. However, based on both model performance and reality, different estimations (table 4.5) can be fused together to represent different future scenarios. The percentage increase is used to describe future scenarios because it is easier to perceive and can be directly adapted when including the greater Wu-Chang (Urumqi-Changji) area into consideration. Below are the details of the three scenarios:

1. **Conservative scenario**: +20%

   This scenario represents the average urban land intensity of Chinese capital cities. It is a much denser pattern compared to the current Urumqi. The China City Statistical Yearbook 2013 shows that Urumqi's urban area has already reached 384 km^2 in 2012, surpassed the capital city LOG model. Therefore, the number is slightly increased from 11% to 20% to represent a more realistic conservative future.

2. **Planning scenario**: + 70%

   This scenario respects the published land use/urban planning documents. It is based on the 120 $m^2/person$ standard of urban density and a conservative extrapolation from land use planning 2020.

3. **Aggressive scenario**: + 120%

   This scenario is supported by time series SQRT model and the linearly extrapolated land use planning. It represents an extensive growing pattern matching the low-land-use-intensity history of this city.

4.3 Simulating spatial configurations of future urban change

4.3.1 The Dyna-CLUE model

The Dyna-CLUE model is the current version in the CLUE (the Conversion of Land Use and its Effects) model family (Verburg et al., 1999, 2002; Verburg and Overmars, 2009). The models were developed for the spatially explicit simulation of land use change based on location suitability combined with competition and interactions among the spatial and temporal dynamics of land use systems.

The Dyna-CLUE model has two distinct modules, a non-spatial demand module and a spatial allocation module (4.9). The non-spatial module calculates the area change for all land use types at the aggregate level. Area demands of different land use types are inputs to the model which may be produced using simple or advanced methods. The spatial module allocates land use demands to specific locations based on a combination of empirical, spatial analysis and dynamic modeling. Its input parameters can be further divided into three categories, including location and neighborhood characteristics, specific conversion settings, and spatial policies and restrictions. Together

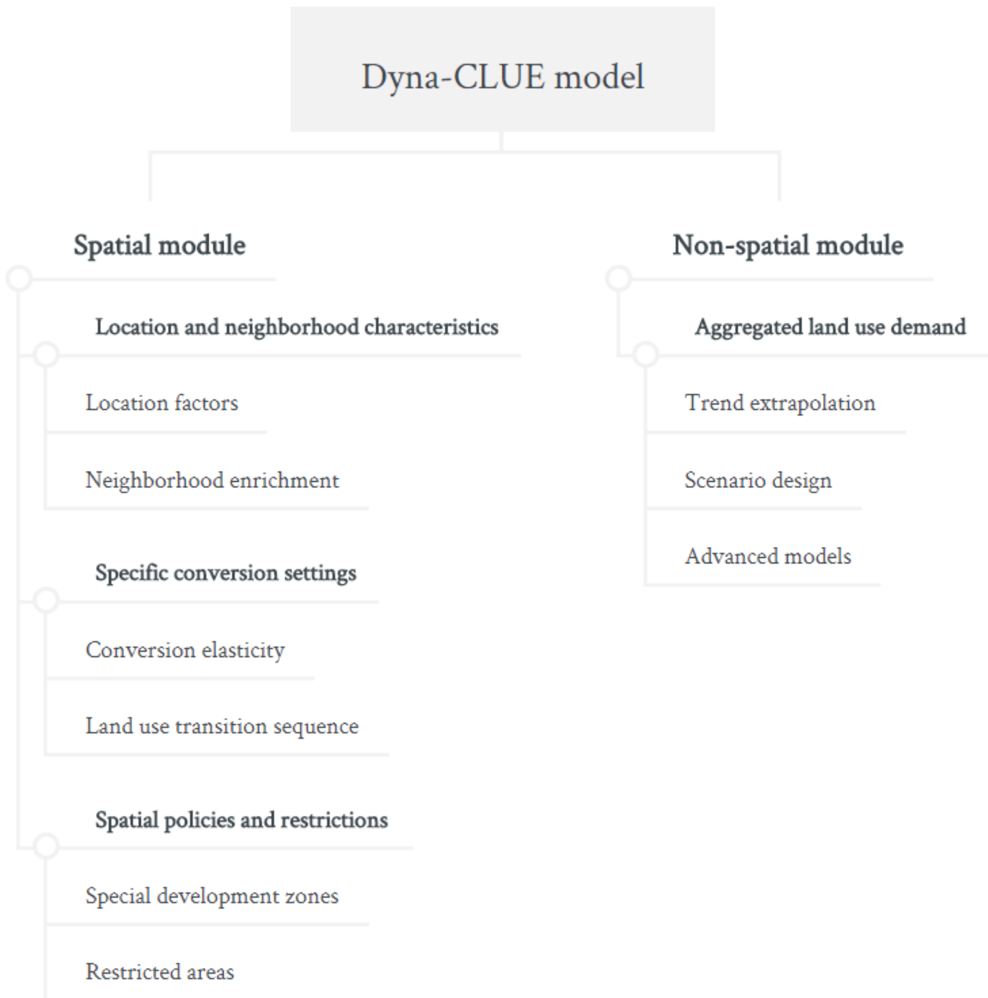

Figure 4.9 Dyna-CLUE model structure

they create a set of conditions and probabilities for which the model iteratively calculates the best solution for each land use type.

The core of the allocation procedure is to calculate the preference map for each land use type. The spatial preference of a land use type is empirically estimated from a set of factors based on the understanding of determinants of land use change. The preference is calculated as in eq. 4.2.

$$R_{ki} = a_k X_{1i} + b_k X_{2i} + \ldots \tag{4.2}$$

Where:

R_{ki} is the preference to devote location i to land use type k

$X_{1i,2i,...}$ are biophysical or socio-economical characteristics of location i

a_k and b_k are the relative impact of the characteristics on the preference for land use type k

The Dyna-CLUE model is also capable of incorporating autonomous developments through bottom-up simulation (Verburg and Overmars, 2009). More specifically, neighborhood characteristics can be taken into consideration when calculating spatial preferences for selected land use types. The neighborhood of a location is characterized using the enrichment factor (F, eq. 4.3). This measure is defined by the abundance of a land use type in the neighborhood of a location relative to the abundance of this land use type in the entire study area.

$$F_{ikd} = \frac{n_{kdi}/n_{di}}{N_k/N} \tag{4.3}$$

Where:

F_{ikd} characterizes the enrichment of neighborhood d of location i with land use type k

n_{kdi} is the number of cells of land use type k in the neighborhood with size d of cell i

n_{di} is the total number of cells in the neighborhood

N_k is the number of cells with land use type k in the whole simulation domain

N is the total number of cells in the simulation domain

The relationship between the probability P of a location i and the enrichment factors for each of the n land use types is expressed in a logit model (eq. 4.4). The β coefficients can be estimated using logistic regression. Finally, R and P are averaged by weight to determine the suitability of each cell for each land use type. The weight needs to be calibrated by model users.

$$log(\frac{P_i}{1-P_i}) = \beta_0 + \beta_1 F_{1i} + \beta_2 F_{2i} + ... + \beta_n F_{ni} \tag{4.4}$$

4.3.2 Preparing model inputs

The Dyna-CLUE model requires many inputs. For non-spatial data, it requires aggregated land use demand as well as other parameters that need to be set specific to the study area. Urban land demand (figure 4.10) was set up by applying the percentage change of different urban change scenarios to the total urban area within the modeling domain, which is an 80 by 80 km area including Urumqi and a major part of Changji. For model parameters, here we only discuss those related to location and neighborhood factors and leave the rest to calibration. For spatial data, Dyna-CLUE needs (1) land cover maps as initial state, (2) location factors and (3) neighborhood factors to calculate land use suitability, and (4) restriction map to apply local constraining policies.

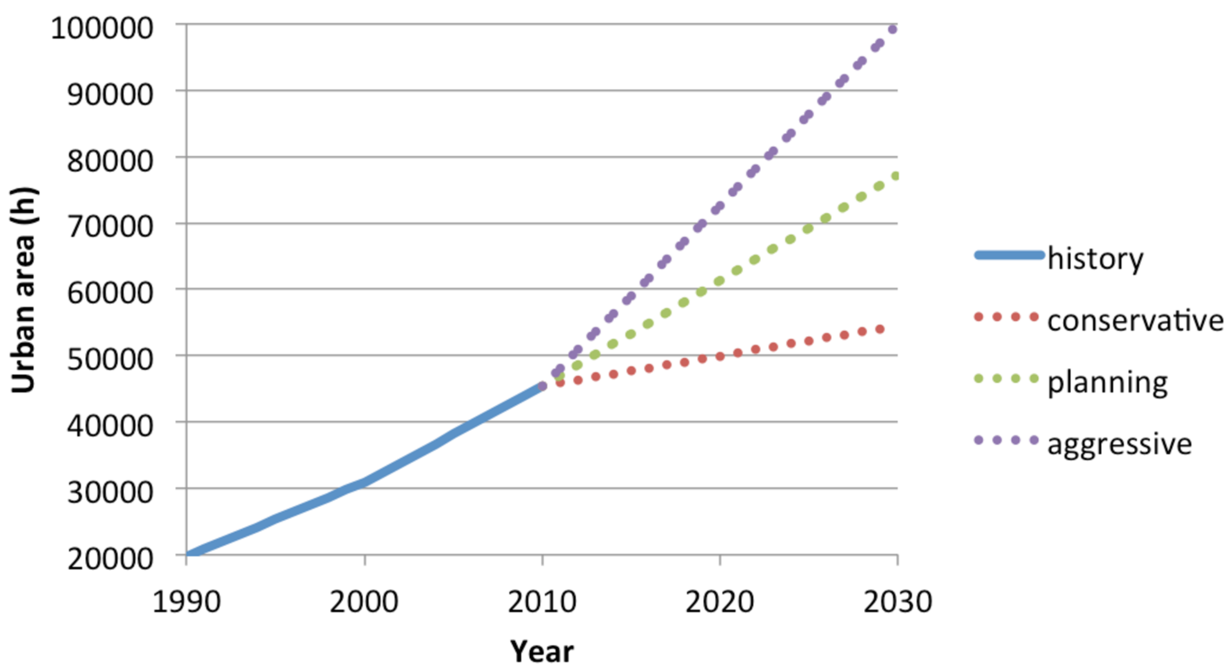

Figure 4.10 Historical and projected urban land area

• Land cover maps 1990, 2000 and 2010

Land cover maps for the three different dates (figure 4.11) were prepared based on Landsat TM and ETM+ images of respective years and a vector reference map of 2000 land use provided by a local collaborator[3]. Supervised classification was first conducted on Landsat images focusing on urban and agricultural lands. Classification outputs then went through post-processing to eliminate small disconnected patches. Finally, manual adjustments were made to correct obvious mismatches based on visual interpretation of the original Landsat images and high-resolution images from Google Earth.

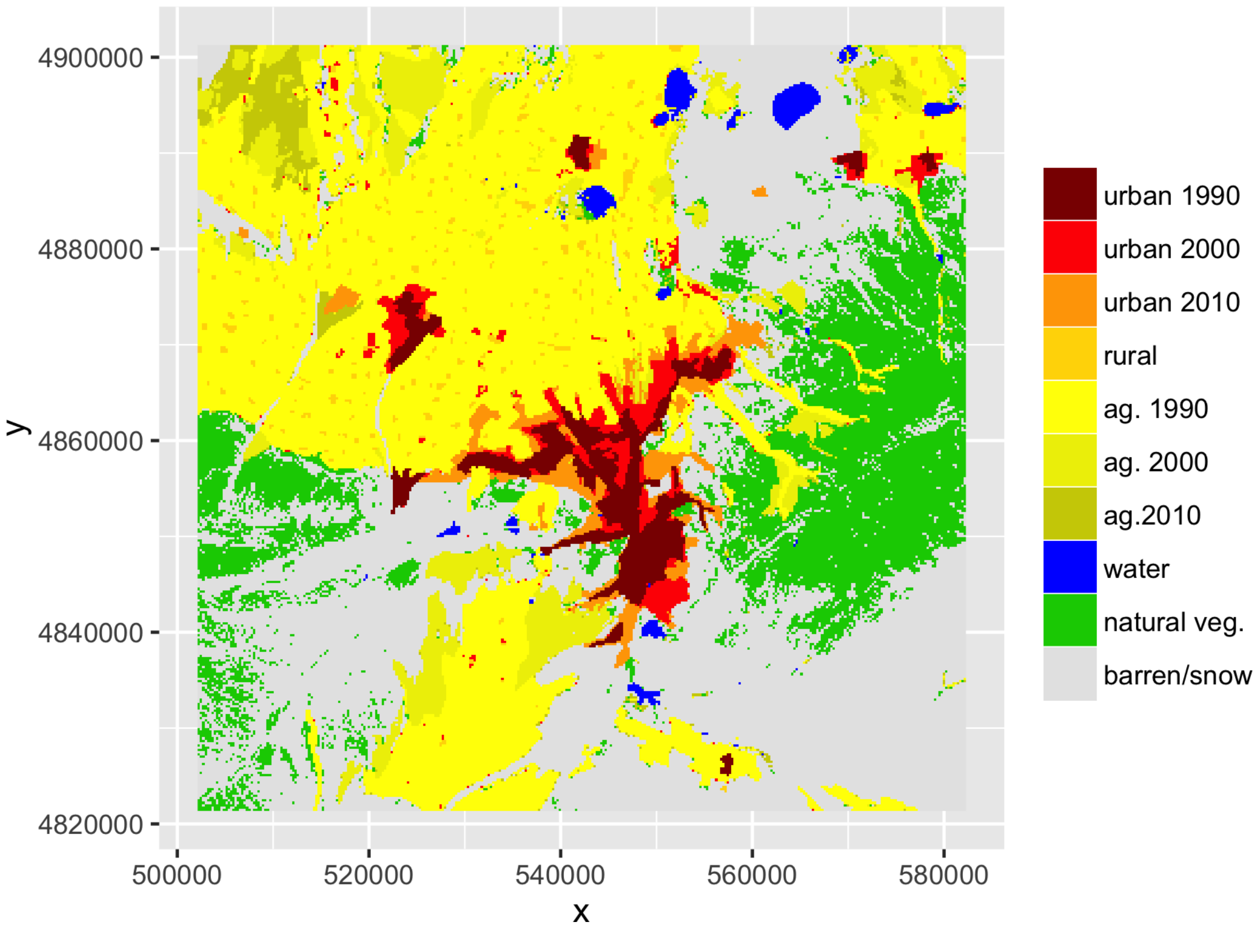

Figure 4.11 Map of land use change in Urumqi: 1990, 2000, to 2010

• Location factors

[3]Xinjiang Institute of Ecology and Geography Chinese Academy of Sciences is a local collaborator of the NASA project NNX09AI32G, "China's urbanization and its sustainability under future climate change", which funded most part of this research

Five variables (figure 4.12) were tested for their explanatory power for determining urban land: (1) elevation, (2) slope, (3) distance to city, (4) distance to road, and (5) distance to water. Distance to different city centers was inversely weighted based on their population (Distance to Urumqi was weighted as 1) and then combined to find the minimum distance to any city centers.

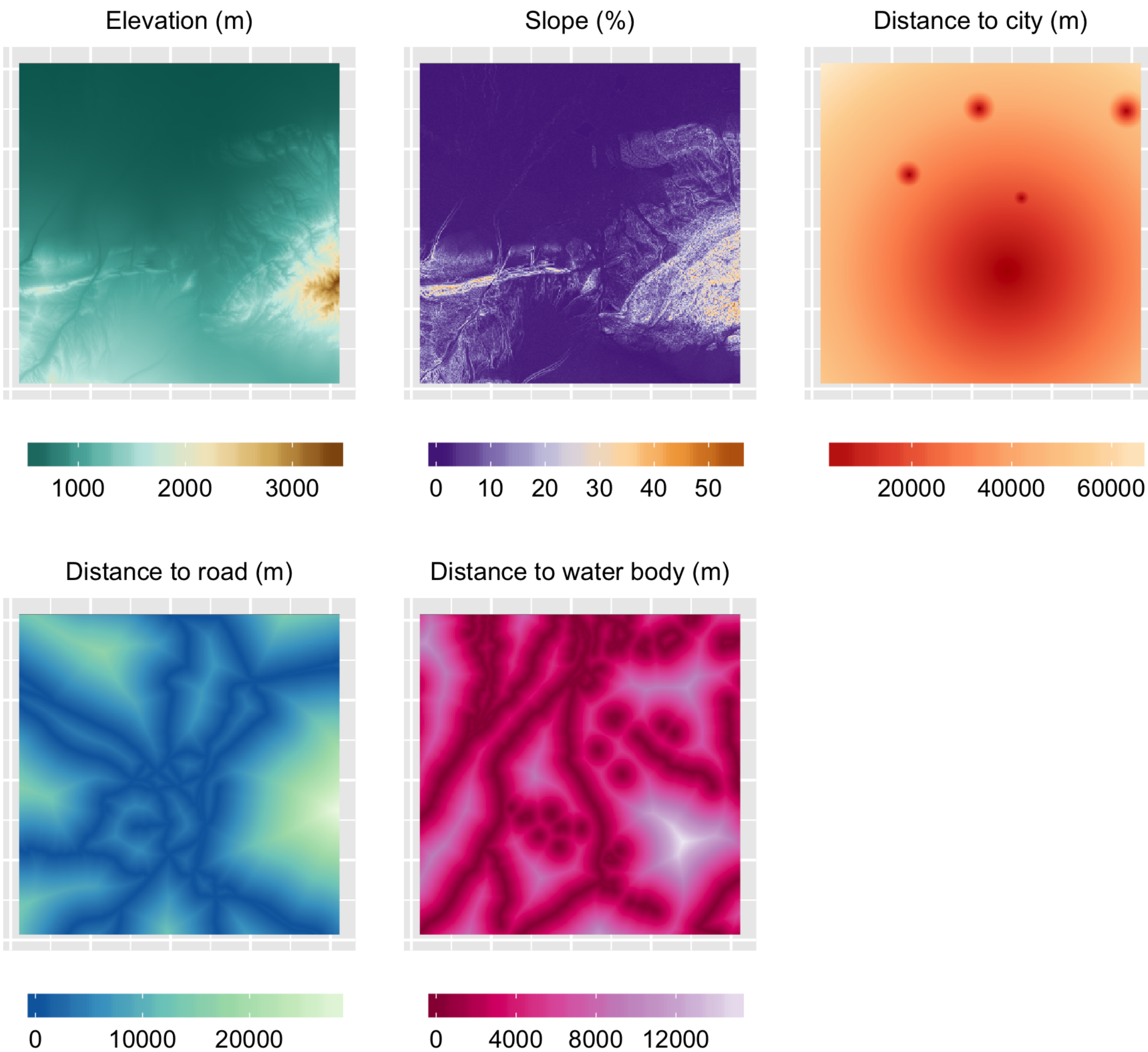

Figure 4.12 Location factors passed into dyna-CLUE model

I tested these variables against the presence of urban land in a logistic regression model (based on eq. 4.2) under a range of different spatial resolutions and on the three different years of land cover maps (table 4.6). Model fits were measured using ROC Area Under Curve (AUC) and all settings show excellent fit. Most variables are significant except distance to river, which is only significant in earlier years and finer spatial resolutions. When variables are significant, their magnitudes are consistent among different resolutions and years, suggesting they are good indicators for predicting urban land. As a balance between computational efficiency and explaining power from independent variables, 240 m was chosen as the final spatial resolution to work with later in Dyna-CLUE simulations.

• Neighborhood factors

The enrichment factor (eq. 4.3) was calculated under different combinations of resolution, year of land cover and neighborhood size (figure 4.13). Experiments were done to test neighborhood model (eq. 4.4) sensitivity under those combinations. Table 4.7 shows a subset of results for resolution 240 m. All settings, except radius 1 in the year 2000, are significant and fit perfectly with observed urban lands. Model performance declines as neighborhood size increases, suggesting a weakening correlation between the pixel and its neighbors as their distance increases.

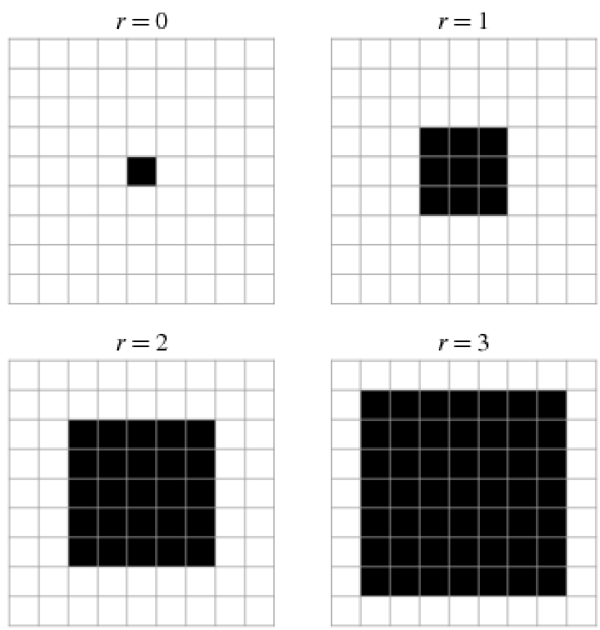

Image source: MathWorld–A Wolfram Web Resource
(http://mathworld.wolfram.com/MooreNeighborhood.html)

Figure 4.13 Moore neighborhood

Table 4.6 Logistic regression results for location factors

resolution	year	intercept	dem	slope	dis2road	dis2water	dis2city	ROC AUC
	1990	7.70E+00(***)	-3.69E-03(***)	-1.55E-01(***)	-5.63E-04(***)	-7.89E-05(***)	-1.50E-04(***)	0.9590
60m	2000	9.04E+00(***)	-4.94E-03(***)	-2.01E-01(***)	-5.09E-04(***)	-2.51E-05(***)	-1.69E-04(***)	0.9617
	2010	9.72E+00(***)	-5.31E-03(***)	-1.34E-01(***)	-5.96E-04(***)	0.00E+00	-1.80E-04(***)	0.9635
	1990	7.83E+00(***)	-3.67E-03(***)	-1.55E-01(***)	-5.63E-04(***)	-8.06E-05(***)	-1.57E-04(***)	0.9614
120m	2000	9.12E+00(***)	-4.90E-03(***)	-2.06E-01(***)	-4.91E-04(***)	-3.69E-05(**)	-1.72E-04(***)	0.9628
	2010	9.86E+00(***)	-5.47E-03(***)	-1.24E-01(***)	-6.11E-04(***)	0.00E+00	-1.80E-04(***)	0.9648
	1990	7.47E+00(***)	-3.80E-03(***)	-1.73E-01(***)	-5.61E-04(***)	0.00E+00	-1.44E-04(***)	0.9555
240m	2000	8.99E+00(***)	-4.76E-03(***)	-2.20E-01(***)	-5.01E-04(***)	-3.77E-05	-1.72E-04(***)	0.9614
	2010	9.91E+00(***)	-5.52E-03(***)	-1.13E-01(***)	-6.10E-04(***)	0.00E+00	-1.80E-04(***)	0.9650
	1990	6.82E+00(***)	-2.98E-03(***)	-1.30E-01(**)	-4.37E-04(***)	-8.24E-05	-1.42E-04(***)	0.9486
480m	2000	8.73E+00(***)	-4.37E-03(***)	-1.85E-01(***)	-5.14E-04(***)	0.00E+00	-1.80E-04(***)	0.9626
	2010	9.99E+00(***)	-5.46E-03(***)	-1.05E-01(**)	-6.02E-04(***)	0.00E+00	-1.85E-04(***)	0.9662
	1990	6.37E+00(***)	-2.38E-03(.)	0.00E+00	-5.43E-04(**)	-1.91E-04	-1.52E-04(***)	0.9497
960m	2000	1.19E+00(***)	-7.47E-03(***)	-1.96E-01(*)	-5.99E-04(***)	0.00E+00	-2.21E-04(***)	0.9751
	2010	9.34E+00(***)	-5.17E-03(***)	-1.68E-01(*)	-5.37E-04(***)	0.00E+00	-1.65E-04(***)	0.9559

Signif. codes: 0 ‘***’ 0.001 ‘**’ 0.01 ‘*’ 0.05 ‘.’ 0.1 ‘ ’ 1

Table 4.7 Logistic regression results for enrichment factors

year	radius	intercept	β	ROC AUC
	1	-6.367(***)	0.497(***)	0.9993
1990	2	-5.419(***)	0.471(***)	0.9977
	3	-4.948(***)	0.462(***)	0.9960
	1	-60.009	7.748	0.9999
2000	2	-7.228(***)	1.033(***)	0.9997
	3	-6.562(***)	0.986(***)	0.9994
	1	-7.538(***)	1.198(***)	0.9998
2010	2	-7.062(***)	1.165(***)	0.9996
	3	-6.921(***)	1.194(***)	0.9995

Signif. codes: 0 '***' 0.001 '**' 0.01 '*' 0.05 '.' 0.1 ' ' 1

• Land use restrictions

Urumqi is rich in coal. After decades of unorganized underground mining, several places in Urumqi, which could be suitable for urban land, are now at high risk of surface subsidence (figure 4.14, hazard zones extracted from Sun et al. (1998)). Urban development at such locations is thus prohibited and need to be addressed in land use change simulations.

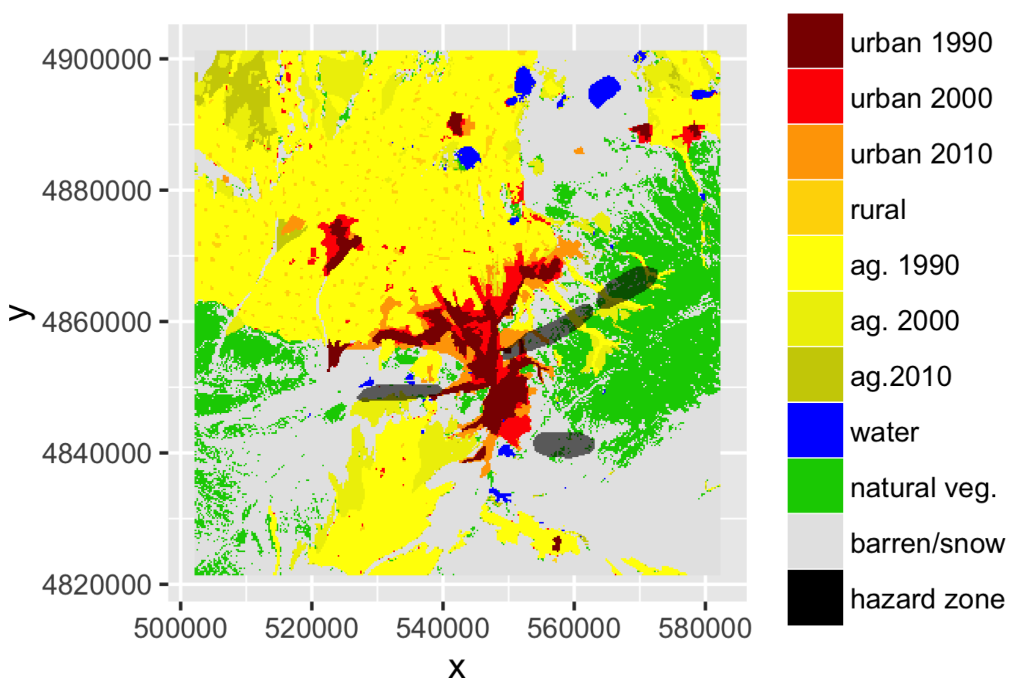

Figure 4.14 Geological hazard zones in Urumqi

4.3.3 Calibration and validation using a new measure of goodness-of-fit

In this section, I will first introduce a novel approach to measure the performance of land use change models, given original year, actual target year and simulated target year land use maps. This measure is then applied to evaluate different model setups, supporting the optimal choice for simulating future land use change.

• Adjusted multi-resolution kappa index

The proposed method is a combination of multi-resolution measure (Costanza, 1989) and adjusted kappa to account for land use persistence (van Vliet et al., 2011). The multi-resolution measure gives credit to "near-hits", thus awarding matches on general shapes instead of exact pixels. The adjusted kappa method uses observed no-change areas, instead of the traditional chance agreement, to condition the "expected agreement" in Cohen's kappa coefficient. It prevents over estimating model performance by focusing on the "changed" areas instead of the entire landscape.

The model fit in a particular resolution (window size) is defined as follows (eq. 4.5). For window size w, k_w is the adjusted kappa, p_{wo} the observed agreement between reference scene and simulated scene (eq. 4.6), p_{we} the expected agreement conditioned with the original scene (eq. 4.7).

$$k_w = \frac{p_{wo} - p_{we}}{1 - p_{we}} \tag{4.5}$$

$$p_{wo} = \frac{\sum_{t=1}^{t_w} \left[1 - \frac{\sum_{i=1}^{c} |n_{ai} - n_{si}|}{2w^2} \right]_t}{t_w} \tag{4.6}$$

Where:

n_{ai} is the number of cells of land use type i in actual scene in the sampling windows

n_{si} is the number of cells of land use type i in the simulated scene

c is the number of different land use types in the sampling windows

t is the sampling window of dimension w by w which slides through the scene one cell at a time

t_w is the total number of sampling windows in the scene for window size w.

$$p_{we} = \sum_{j=1}^{c} p(o=j) \cdot \sum_{i=1}^{c} p_w(a=i|o=j) \cdot p_w(s=i|o=j) \tag{4.7}$$

I define $p_w(a=i|o=j)$ as the probability of cells changing from land use type j in the original scene to i in the actual scene for window size w (eq. 4.8). Again, this measure is not based on exact pixels but general match within each window. $p_w(s=i|o=j)$ is similarly defined, by replacing the actual scene with the simulated scene.

$$p_w(a=i|o=j) = \frac{\sum_{t=1}^{t_w} \left[\frac{n_{ai} \cdot n_{oj}}{w^4}\right]_t}{t_w} \tag{4.8}$$

Multi-resolution synthesis can be achieved by average k_w across different window size $w(1,2,...,m)$, weighted by a distance-decay function (eq. 4.9). The value of l determines how much weight is to be given to small versus large sampling windows. In this study, the l is set to be 0.1.

$$k_{multi\_res} = \frac{\sum_{w=1}^{m} k_w e^{-l(w-1)}}{\sum_{w=1}^{m} e^{-l(w-1)}} \tag{4.9}$$

• Sensitivity test on different model setups

A range of different setups and parameter combinations were tested using k_{multi_res} (eq. 4.9) for urban/non-urban accuracy. First, two alternative location factors were introduced (figure 4.15): distance to 1990 urban land and cost distance to roads[4]. Second, regression coefficients from different years were tested. Logistic regressions were re-run for each model setup using selected

[4]The cost distance was calculated using corresponding ArcGIS function, with the cost layer generated from the 1990 land use map. The costs were arbitrarily set as 0 for urban, 3 for rural, 7 agricultural land, 10 for water, 5 for natural vegetation, and 5 for barren/snow without any reference.

Table 4.8 Dyna-CLUE model setups

Setup #	City layer a. Weighted distance to city/town b. Distance to 1990 urban land	Road layer a. Distance to roads b. Cost distance to roads	Regression coefficients a. 1990 b. 2000* c. 2010
M1	a	a	a
M2	a	b	a
M3	b	a	b
M4	a	a	b
M5	a	a	c
M6	b	a	c

* Moore neighborhood with r=2 was used for year 2000 coefficients, since r=1 was not significant.

location factors and land use map of the selected year. A summary of model setups are listed in table 4.8.

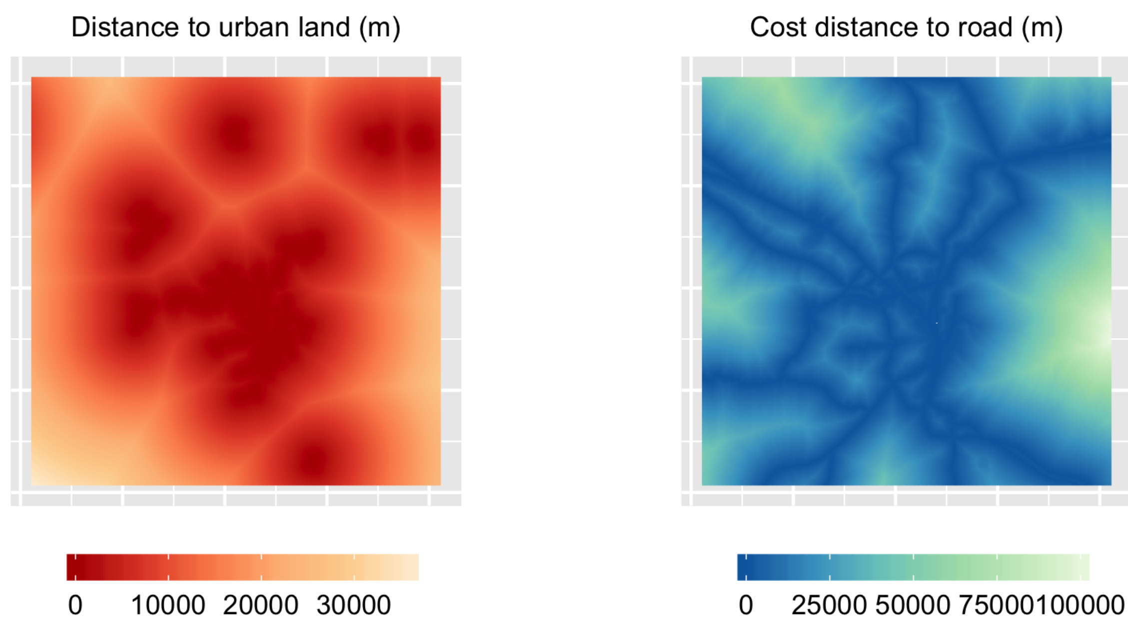

Figure 4.15 Alternative location factors

For each model setup, I further tested model sensitivity on combinations of agriculture land elasticity and neighborhood weight. The elasticity coefficient indicate the additional cost for converting agricultural land while the weight determines the importance of neighborhood enrichment in total suitability. Both of these parameters range from 0 to 1 and were tested at 0.1 increments from 0 to 0.9. Therefore 100 experiments were done for each model. All experiments were run from the year 1990 to 2010, using 1990-2000 as calibration phase and 2000-2010 as validation phase. The distribution of model fits for each model setup and simulation phase were plotted to show respective model performances (figure 4.16).

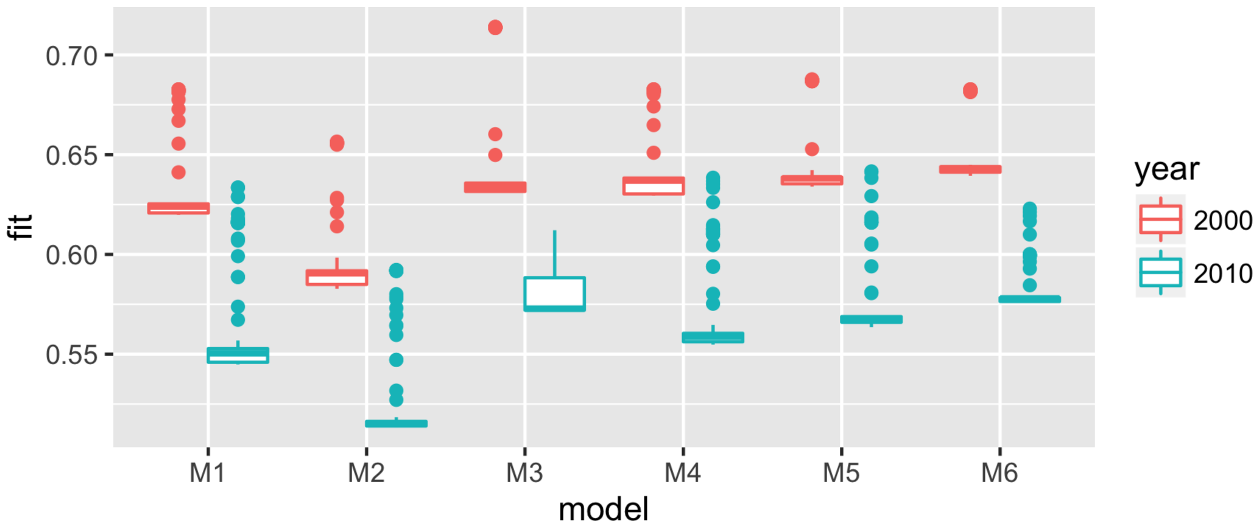

Figure 4.16 Sensitivity test for dyna-CLUE model setups

For the year 2000, all models performed similarly well except M2, which was based on the cost distance to roads. It suggests this newly introduced location factor does not improve model performance thus will not be considered in further evaluations. The absolute best fit and best average fit were achieved by M3 and M6, respectively. Both used the distance to 1990 urban land. For the year 2010, the overall fit was substantially lower than 2000. M3 and M6 still performed well in average fit, though M1, M4, and M5 (all based on weighted distance to city/town) produced better results regarding maximum fit.

Given its overall good performance, model setup M6 was chosen as the final one to be used to project future urban land. Within this setup, agriculture elasticity and neighborhood weights were selected based on the average model fit of both calibration and validation phase (figure 4.17). Elasticity on agriculture land did not benefit model performance at all. The global maximum was found where neighborhood weight equals to 0.2 and agriculture elasticity equals to 0 (easy conversion from agriculture to urban land). Simulated urban change under this setting is shown in figure 4.18.

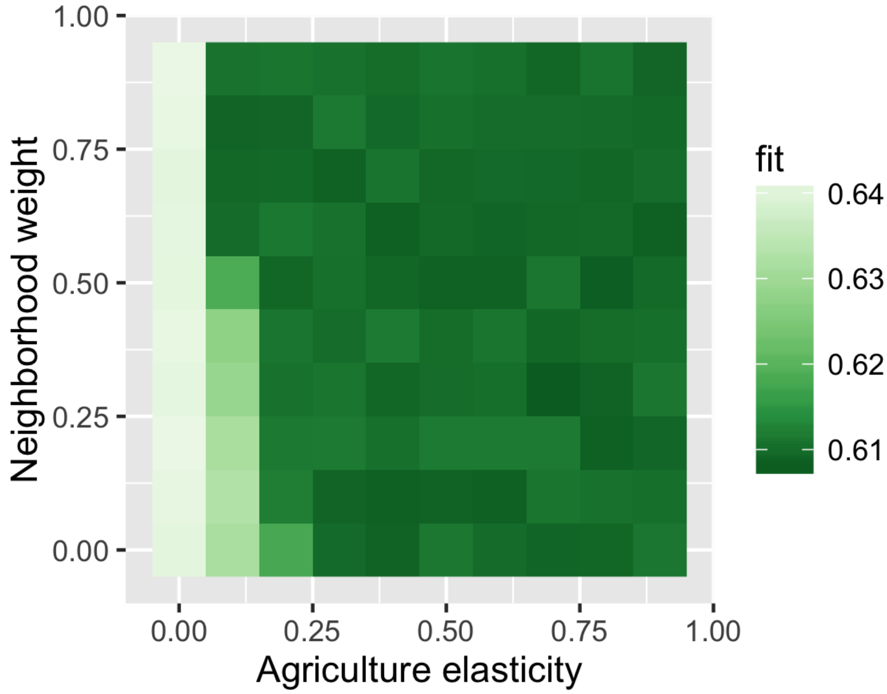

Figure 4.17 Sensitivity test for M6

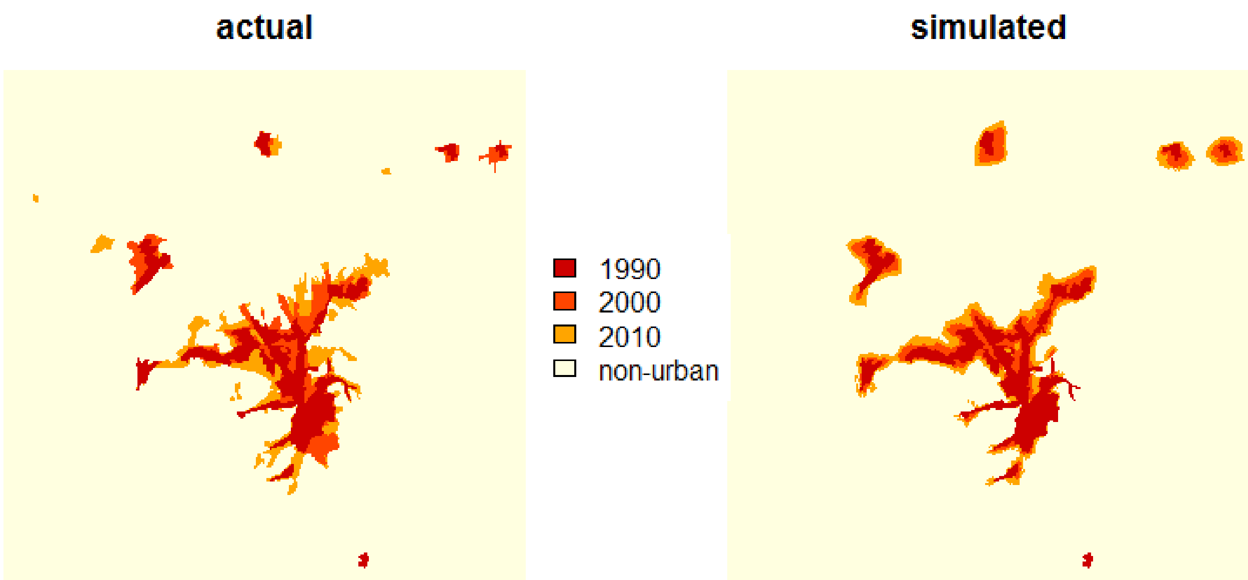

Figure 4.18 Simulated urban change from 1990 to 2010

4.3.4 Urban spatial patterns of the three stories

Before applying the chosen model to simulate future urban land, small modifications were made to accommodate changes in future conditions (figure 4.19). First, distance to 1990 urban land was replaced by that of the 2010 urban land. Second, newly planned urban agglomeration zones (based on Urumqi Urban planning 2011-2020) were added and given higher preference of converting to urban land (location specific preference = 0.2).

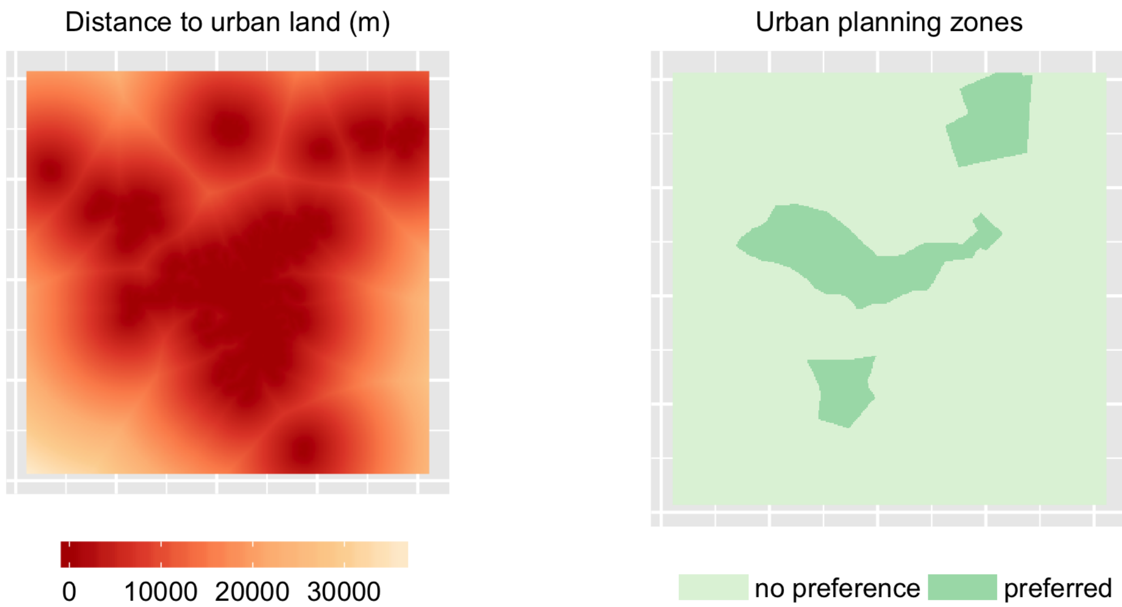

Figure 4.19 Alternative location factors for future simulation

Based on model calibration and validation in the previous section and modified inputs listed above, the future urban land change was simulated using Dyna-CLUE model for the three scenarios described in 4.2.2 (figure 4.20).

• Conservative scenario

New urban lands are primarily located on the northern fringe of Urumqi and along major roads from Changji City. The Ganquanpu industrial park, in between Urumqi and Fukang, also see great expansion.

• Planning scenario

More expansions were found around the highlighted regions discussed in the conservative scenario. Beyond those, Urumqi starts to expand to its West Mount region. All the small cities and towns to the north of Urumqi experience some expansion.

• Aggressive scenario

Urumqi becomes connected to Changji City; Ganquanpu and Fukang City also become connected along major transportation axis. More expansions were found around all urban areas except

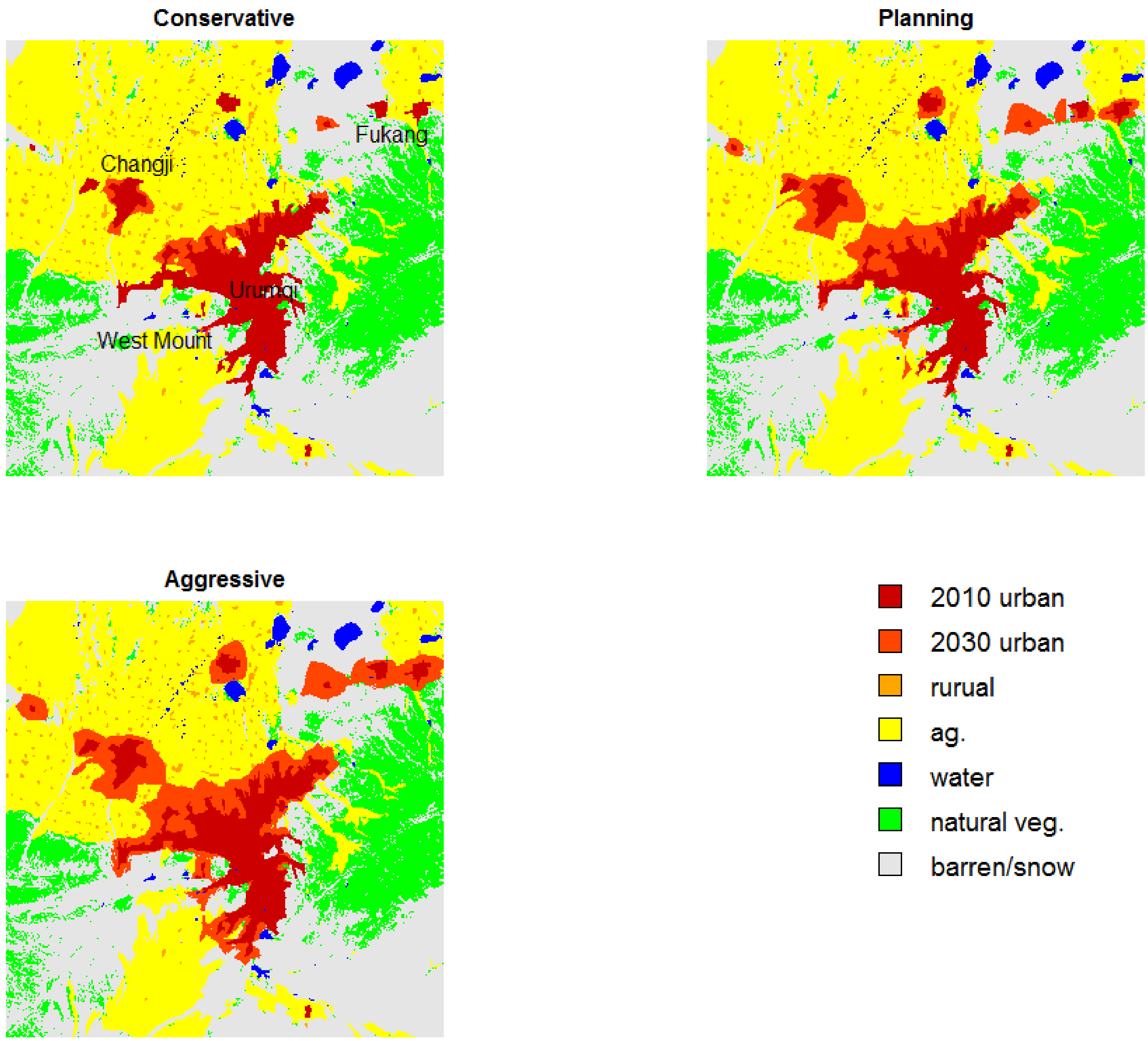

Figure 4.20 Simulated urban land change for year 2030 under three scenarios

Dabancheng to the south of Urumqi.

4.4 Incorporating Urumqi's afforestation plans

Urumqi's afforestation began in the 1950s. Some major city parks, including Hongshan, Yamalikeshan, Hongguanshan, are all fruits of decades of afforestation on otherwise barren lands. Starting from government-funded and civilian volunteered projects, the city encouraged business entities to lead afforestation endeavors using preferential policies, including tax-cuts and discounts in land purchases. However, the policies did not last long due to corruption emergent in their inherent power-land-money chain and the lack of maintenance for newly planted areas (Chang and Zhu, 2012).

Here I am not going to discuss the resolution to successful afforestation, but will rather examine the potential impact on local climate if those plans had succeeded. The planned afforestation areas (fig. 4.21) were extracted from Urumqi's Master Planning (2014-2020) - Urban Green Space System Planning. Those areas were updated to 2030 scenarios as deciduous broadleaf forests based on major species used in afforestation projects (Zhu, 2013).

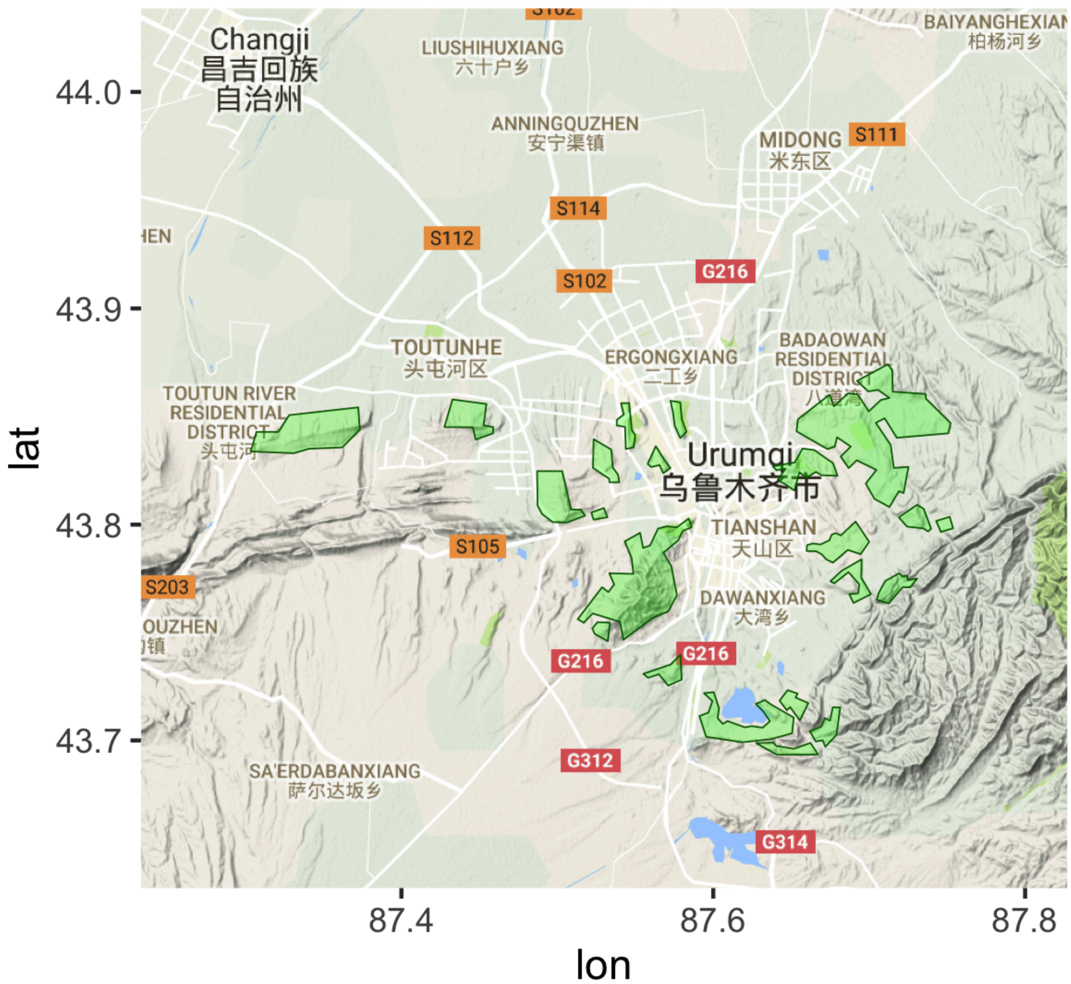

Figure 4.21 Planned afforestation areas with Google terrain base map

4.5 Discussion and conclusions

In this chapter, three future stories of urban change have been developed for both aggregated area and spatial configuration. First, future urban land demands for different scenarios were estimated from different models based on future population and GDP. Using the ARIMA model, population and GDP were projected at 3.25 million and 365.23 billion RMB, respectively, for the year 2030. Second, urban land demands were allocated spatially using Dyna-CLUE model. Model parameters were calibrated using land use maps from 1990 to 2000 and validated using the 2010 map. A multi-resolution adjusted kappa index was developed to measure the goodness-of-fit for urban change simulations. Below are the summaries on urban change for the three future stories:

1. The conservative scenario has a 20% increase of urban land. It was developed based on the relationship between urban land and population/GDP in Chinese capital cities. This is a much denser pattern than what Urumqi has today. The new urban land will occur primarily along the northern fringe of Urumqi city and along the transportation axis between Urumqi and Changji city.

2. The planning scenario has a 70% increase of urban land. It was developed to correspond with the published land use/urban planning documents. All urban and industrial establishments to the north of Tianshan Mountain will grow significantly, including north Urumqi, Changji, Wujiaqu, Ganquanpu, and Fukang. In addition, Urumqi expands into its West Mount region.

3. The aggressive scenario has a 120% increase of urban land. It was developed following the low-intensity past of Urumqi's historical urban land use pattern. In this scenario, two clusters are formed from initially disconnected urban patches, which are Urumqi-Changji and Ganquanpu-Fukang.

In addition, Urumqi's aggressive afforestation plans were incorporated into the three future scenarios, making another three aforestated urban change scenarios. Also, the no-change 2010 urban extent was added as a baseline scenario. In total seven different land cover inputs were then passed into a regional climate model in the next chapter.

CHAPTER 5

REGIONAL CLIMATE SCENARIOS

5.1 Introduction

Urumqi has become warmer and wetter in the last several decades (figure 5.1). Temperature rises 0.03 °C/year while monthly precipitation increases 0.137 mm/year. How is the climate going to change in the future? Will different urban change scenarios impact differently on the regional climate? What are the factors that support/limit the predictability of climate models? These are the questions I am trying to answer in this chapter.

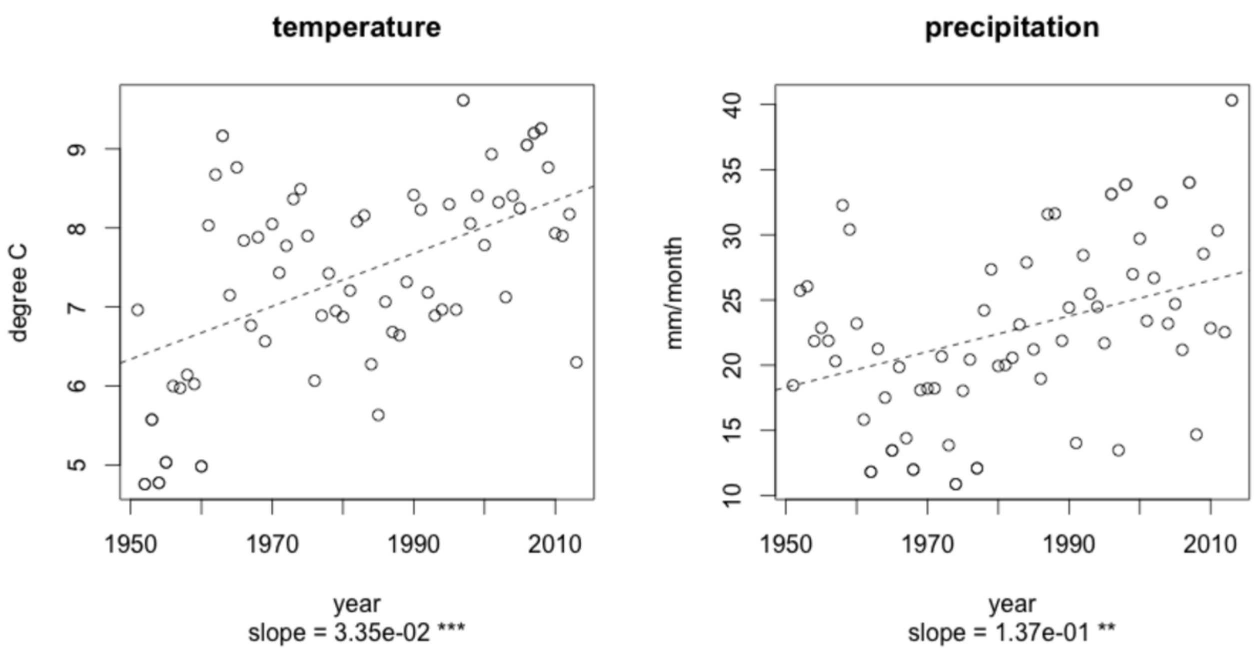

Data source: GHCN
Signif. codes: 0 ‘***’ 0.001 ‘**’ 0.01 ‘*’ 0.05 ‘.’ 0.1 ‘ ’ 1

Figure 5.1 Historical trend of temperature and precipitation in Urumqi

Regional climate is affected by atmospheric forces across scales (Giorgi and Mearns, 1991). At the global scale, the regional climate regime is determined by the general circulation. At regional scales, land surface conditions drive local circulations and create spatial heterogeneities inside regional climate regimes. Therefore, the basic idea of simulating future regional climate through a Regional Climate Model (RCM) is to take the projection from a General Circulation Model (GCM) and dynamically downscale it based on local surface characteristics, e.g. terrain, land cover (Pitman, 2003; Lo et al., 2008).

In this chapter, I will first introduce the framework of GCM projections based on the IPCC Fifth Assessment Report (AR5). Near-term GCM projections for Urumqi will be specifically discussed. The NASA-GISS-E2-H GCM was chosen based on data quality and availability, and its outputs will be dynamically downscaled using Regional Atmospheric Modeling System (RAMS), with regard to the three urban change scenarios and corresponding afforestation scenarios. Moreover, a set of experiments was conducted on testing land cover uncertainty propagation through RAMS. They will provide a "confidence envelope" when interpreting the RAMS simulation outputs for future urban change scenarios.

5.2 Global forcing

5.2.1 IPCC Representative Concentration Pathways

Despite criticisms from various sources, the scientific community has the consensus that global climate has been and will continue to be affected by anthropogenic disturbances in the earth system (Oreskes, 2004; Doran and Zimmerman, 2009). The international climate modeling community has been working together to advance the reliability of climate models. Dozens of GCMs have been developed around the world, through the Coupled Model Intercomparison Project (CMIP, currently in Phase 5), to support projections into the future. The Intergovernmental Panel on Climate Change (IPCC) has been publishing comprehensive assessment reports reviewing the latest progress on climate change related scientific fields. In the most recent version (IPCC AR5, 2014), ensembles of future climate projections, supported by CMIP 5, were presented under different Representative Concentration Pathways (RCP).

The RCPs represent different greenhouse gases concentration pathways and levels by 2100, in terms of added total radiative forcing (W/m^2) compared to pre-industrial levels (figure 5.2). RCPs have replaced the Special Report on Emissions Scenarios (SRES) from the AR4 and provide a new common foundation to explore climate consequences under different future scenarios. Each RCP is based on an internally consistent set of socioeconomic assumptions and could result from different combinations of economic, technological, demographic, policy, and institutional futures.

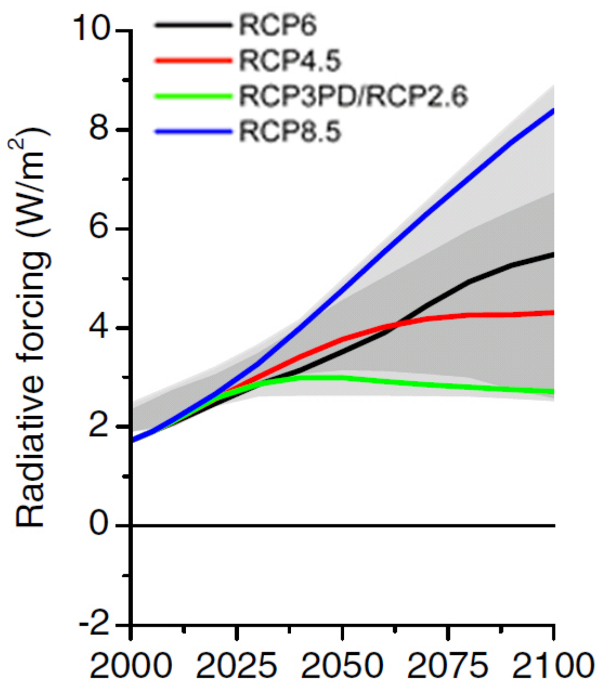

Source: van Vuuren et al. (2011)

Figure 5.2 Trends in radiative forcing

Globally, land is projected to be warmer and wetter under all RCPs (figure 5.3). For temperature, the magnitude of increase among different RCPs starts to diverge after about 2025. Higher radiative forcings result in more substantial temperature increase, ranging from 1.5 to 6 °C by 2100. Increase in winter temperature is slightly larger than that in summer temperature. For precipitation, the average model projections suggest an increase for all RCPs, but the trend is less significant due to the large rainfall variability in model predictions.

The regional trend of Tibetan Plateau[1], which includes the Urumqi area, is showing similar patterns as in the global trend (figure 5.4). Temperature is projected to increase slightly larger than

[1]Urumqi is within the Tibetan Plateau statistical sub-area in IPCC AR5, which is from 30°N to 50°N, 75°E to 100°E. However, in terms of physical extent, Urumqi is in the Tianshan Mountain Range, hundreds of kilometers north from the Tibetan Plateau, separated by the Tarim Basin.

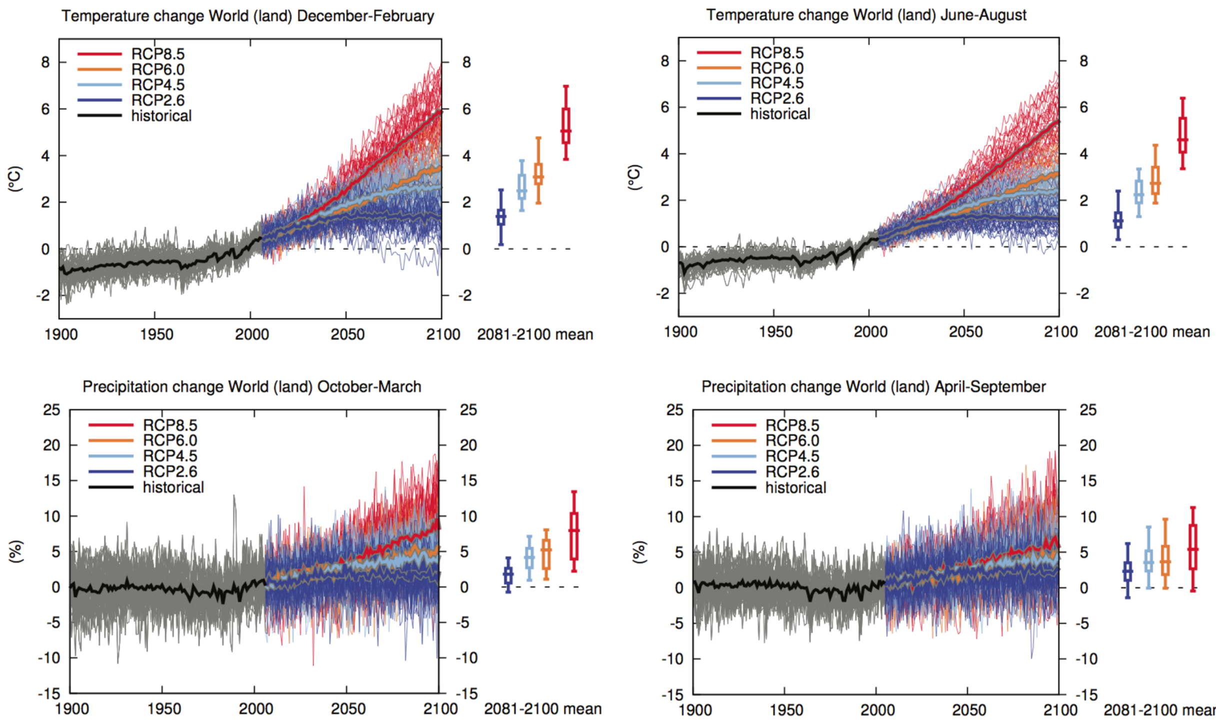

Source: IPCC (2013)

Figure 5.3 Global trends of temperature and precipitation

the global trend, and the variances of both historical observations and GCM simulations are also larger. Precipitation is projected to increase about twice the global rate but varies at four-times of the global range. Again, the increasing trend of precipitation is much less significant than the temperature trend.

5.2.2 Urumqi 2030 from GCMs

Climate is the long-term pattern of weather, and selecting a GCM output of the year 2030 cannot adequately represent the climate regime. Instead of looking into just one year, the temporal profiles of temperature and precipitation change were examined from 2006 to 2045 for several GCM models, including NASA-GISS-E2 models (Schmidt et al., 2014), the MPI-ESM-LR model (Giorgetta et al., 2013), the NCAR-CESM1-BGC (Gent et al., 2011) and the CMCC-CM model (Scoccimarro et al., 2011). The model grid closest to Urumqi was selected from each model outputs for further examination. However, given different grid configurations, the selected grids from different models

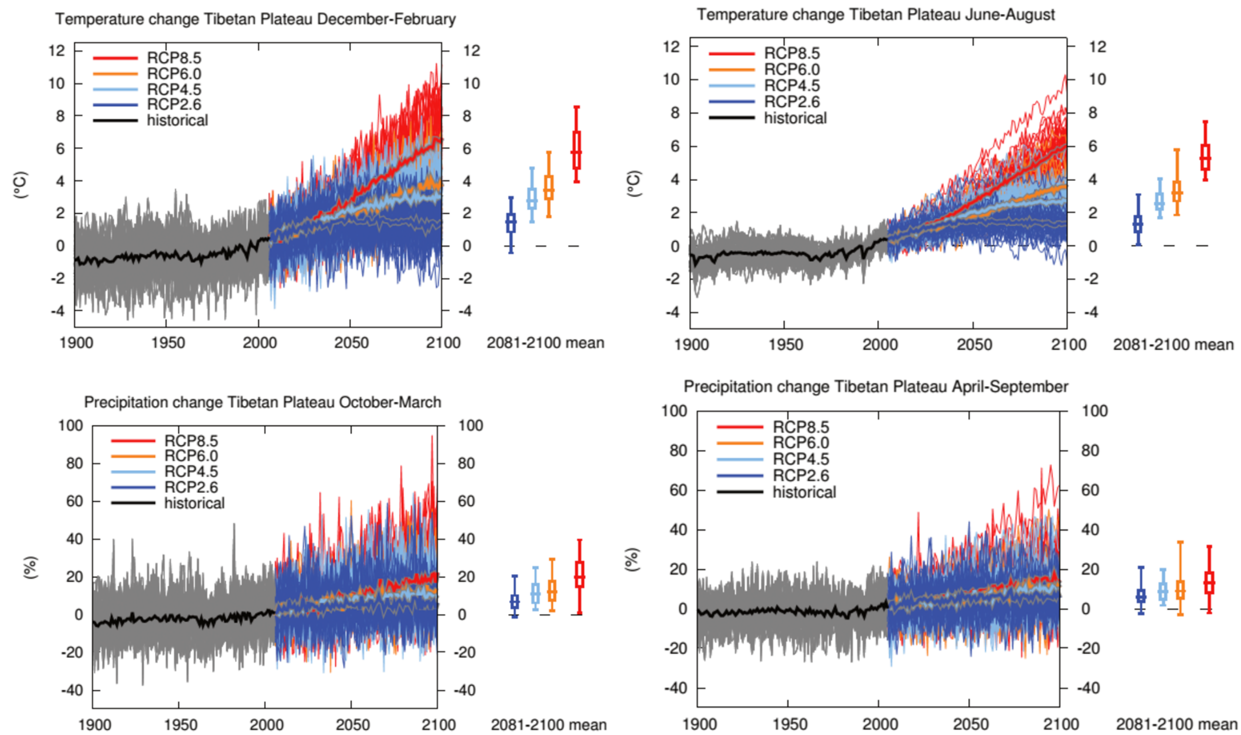

Source: IPCC (2013)

Figure 5.4 Regional trends of temperature and precipitation in the Tibetan Plateau region

cover different areas near Urumqi, and thus their values are not directly comparable.

In table 5.1, the changing slopes and their levels of significance are listed as an indicator of the changing climate for the GCM simulation period of 2006-2045. For temperature, summer maximum (TMAX) and winter minimum (TMIN) are selected instead of respective mean temperatures. For precipitation (PRCP), total precipitation, including resolved and convective precipitation, are summarized. This table is consistent with the global and regional trends as shown in the previous section. Among all variables, summer TMAX is found significantly increased in all models, an average 0.05°C/year. Winter TMIN increases faster (0.06°C/year) but less significantly. PRCP in both summer and winter are rarely significant, and there is even disagreement on the direction of change. Given data availability, only RCP 4.5 and 8.5 were compared. The difference between the two RCPs is however not significant.

Table 5.1 GCM trend for Urumqi in the period 2006-2045

Variable	RCP	NASA-GISS-E2R	NASA-GISS-E2H	MPI-ESM-LR	CMCC-CM	CESM1-BGC
summer TMAX	4.5	$5.78e^{-2}$ (***)	$5.86e^{-2}$(***)	$4.82e^{-2}$(***)	$3.46e^{-2}$(***)	$4.98e^{-2}$(***)
	8.5	$4.83e^{-2}$(***)	$8.02e^{-2}$(***)	$5.36e^{-2}$(**)	$5.71e^{-2}$(***)	$3.94e^{-2}$(***)
winter TMIN	4.5	$7.78e^{-3}$	$6.77e^{-2}$(***)	$8.60e^{-2}$(**)	$4.21e^{-2}$	$5.04e^{-2}$(.)
	8.5	$6.61e^{-2}$(***)	$8.81e^{-2}$(***)	$7.51e^{-2}$(**)	$6.19e^{-2}$(.)	$6.67e^{-2}$(*)
summer PRCP	4.5	$-2.52e^{-3}$	$2.24e^{-3}$	$-6.26e^{-5}$	$1.27e^{-4}$	$-3.23e^{-5}$
	8.5	$-3.42e^{-3}$(*)	$-3.27e^{-3}$(*)	$4.09e^{-5}$	$-3.34e^{-4}$	$6.42e^{-4}$
winter PRCP	4.5	$3.47e^{-4}$	$3.58e^{-5}$	$2.21e^{-4}$	$6.27e^{-4}$(**)	$8.21e^{-5}$
	8.5	$-3.31e^{-4}$	$1.10e^{-3}$(*)	$1.74e^{-4}$	$2.18e^{-4}$	$3.35e^{-4}$(.)

Signif. codes: 0 '***' 0.001 '**' 0.01 '*' 0.05 '.' 0.1 ' ' 1

5.3 Regional climate simulations under urban change scenarios

5.3.1 The RAMS model

RAMS (Pielke et al., 1992; Cotton et al., 2003) is a state-of-the-art limited area model that numerically integrates the fully compressible nonhydrostatic equations of motion, and it solves the equations of radiative transfer; water, heat and momentum exchange between the surface and air, turbulent boundary layer transport, convection; and cloud microphysics. It was first developed at Colorado State University in the 1980's and combines three previously parallel efforts of a non-hydrostatic cloud model (Tripoli, 1982) and two hydrostatic mesoscale models (Tremback et al., 1985; Mahrer and Pielke, 1977). Subsequent development and maintenance were conducted by Drs. Robert L. Walko and Craig J. Tremback at ATMET LLC.

The major components of RAMS are: (1) an atmospheric model which performs the actual simulations, (2) a data analysis package which prepares initial data for the atmospheric model from observed meteorological data, and (3) a post-processing model visualization and analysis package which interfaces atmospheric model output with a variety of visualization software utilities (RAMS, nd).

The surface-atmosphere process is modeled by LEAF-3 (Walko et al., 2000), the newest version of the Land Ecosystem-Atmosphere Feedback model. LEAF-3 includes progressive equations for the temperature and water content of soil, snow cover, vegetation, and canopy air, and includes turbulent and radiative exchanges among these components and with the atmosphere. LEAF-3 allows subgrid structure of different land cover types, called patches, and each patch interacts with other components and the atmosphere with a weight proportional to its fractional coverage (figure 5.5).

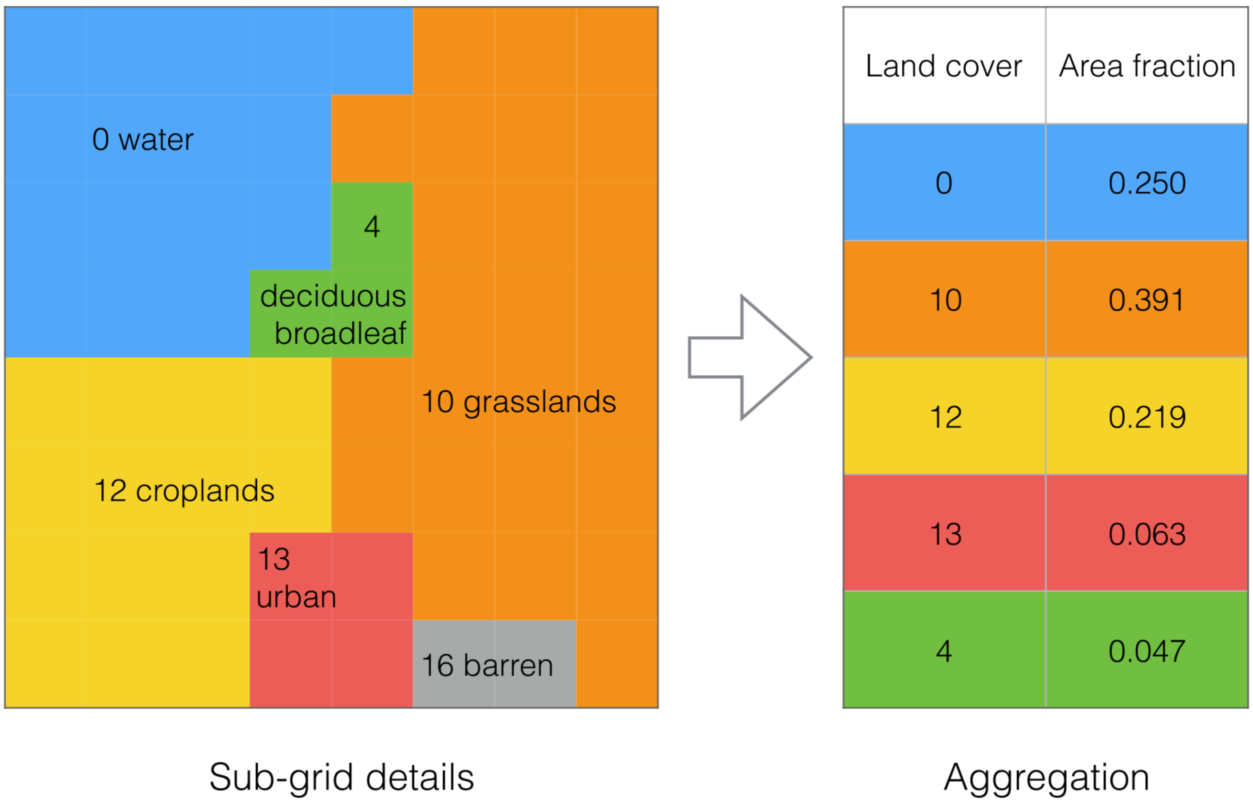

Figure 5.5 A graphic illustration of land cover aggregation in LEAF-3

The RAMS simulations require substantial computation resources. The experiments conducted in this study were run on the Michigan State University High-Performance Computing Center (MSU-HPCC) facilities. Each simulation (scenario) were run on a single node and typically took one month to finish.

5.3.2 Preparing model inputs

- GCM based boundary conditions

RAMS requires large-scale time-varying lateral and surface conditions, in this case from GCM outputs, to drive model simulations. The input data include five 3-D variables: eastward wind, northward wind, temperature, geopotential height and relative humidity; and five 2-D surface variables: sea-level pressure, surface pressure, temperature, snow cover and water surface temperature.

Given data quality and availability, 6-hour outputs from the NASA-GISS-E2H model were selected as the driving dataset and downloaded from Earth System Grid Federation (ESGF). Year 2028, 2029, 2031 and 2032 of RCP 4.5 were chosen to represent a hot 2030 scenario (figure 5.6). Available output data include eastward wind, northward wind, air temperature and specific humidity in 3-D, and sea-level pressure and surface pressure in 2-D.

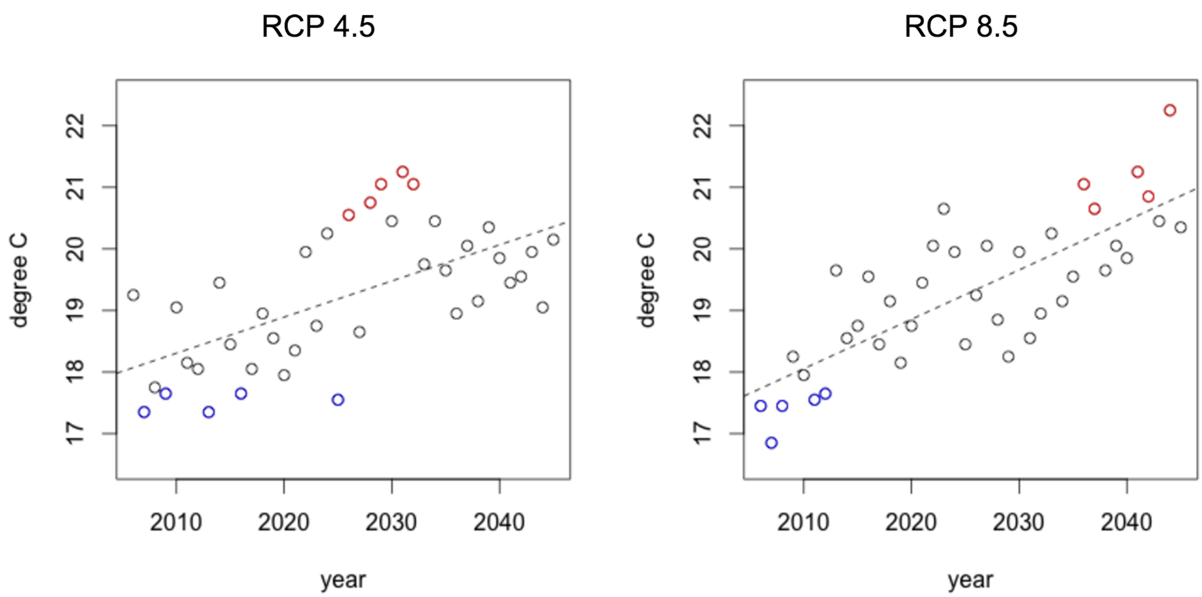

Note: The red and blue color indicate the five hottest and coldest years, respectively.

Figure 5.6 Average JJA maximum temperature from NASA-GISS-E2H model

Not all required variables are ready as GCM standard outputs, and thus need to be calculated from available ones. All calculations were implemented using NCAR Command Language (NCL). Snow cover and water surface temperature were not prepared and initialized as 0. Relative humidity was calculated using the *relhum* function. Geopotential height was calculated using the *cz2ccm* function. To use this function, two additional variables were calculated, which are virtual temperature (eq 5.1) and surface geopotential (eq 5.2). Results were then interpolated from hybrid coordinate system to pressure levels using the *vinth2p* function.

$$T_v = T(1+0.61w) \tag{5.1}$$

Where T_v is virtual temperature (K), T is air temperature (K), w is the mixing ratio (kg/kg) which is approximated by specific humidity.

$$\Phi_s = \frac{p_{sl} - p_s}{\rho} = \frac{(p_{sl} - p_s) R_d T_{vs}}{p_s} \tag{5.2}$$

Where Φ_s is surface geopotential, p_{sl} is sea-level pressure (pa), p_s is surface pressure (pa), ρ is air density, $R_d = 287.058 J/kgK$, is specific gas content for dry air, T_{vs} is surface air virtual temperature (K).

- Surface data

RAMS comes with default datasets that include global terrain height, land cover, soil type, sea surface temperature, etc. In this study, I customized the land cover dataset to represent the three urban change scenarios and corresponding afforestation scenarios (figure 5.7). The base land cover was the modal land cover type for each pixel from the 12-year MODIS land cover type (MCD12Q1, 2001-2012, see section 5.4.1 for more detail) product and converted into the LEAF-3 land cover scheme. The urban and forest patches from the urban and afforestation scenarios were updated on top of the base land cover.

- Namelist specifications

RAMS uses a namelist file to specify model configurations. Some particular settings are listed below:

1. The simulation period was set to be from Jan. 1 to Dec. 31 of selected years.

2. Two nested grids (fig. 5.8) were set both centered at 43.8°N, 87.58 °E. The coarser grid was 16 by 20 (easting by northing) with 32 km resolution, while the finer grid was 30 by 38 with 8 km resolution.

3. The out-most five points are set to be the nudged boundary.

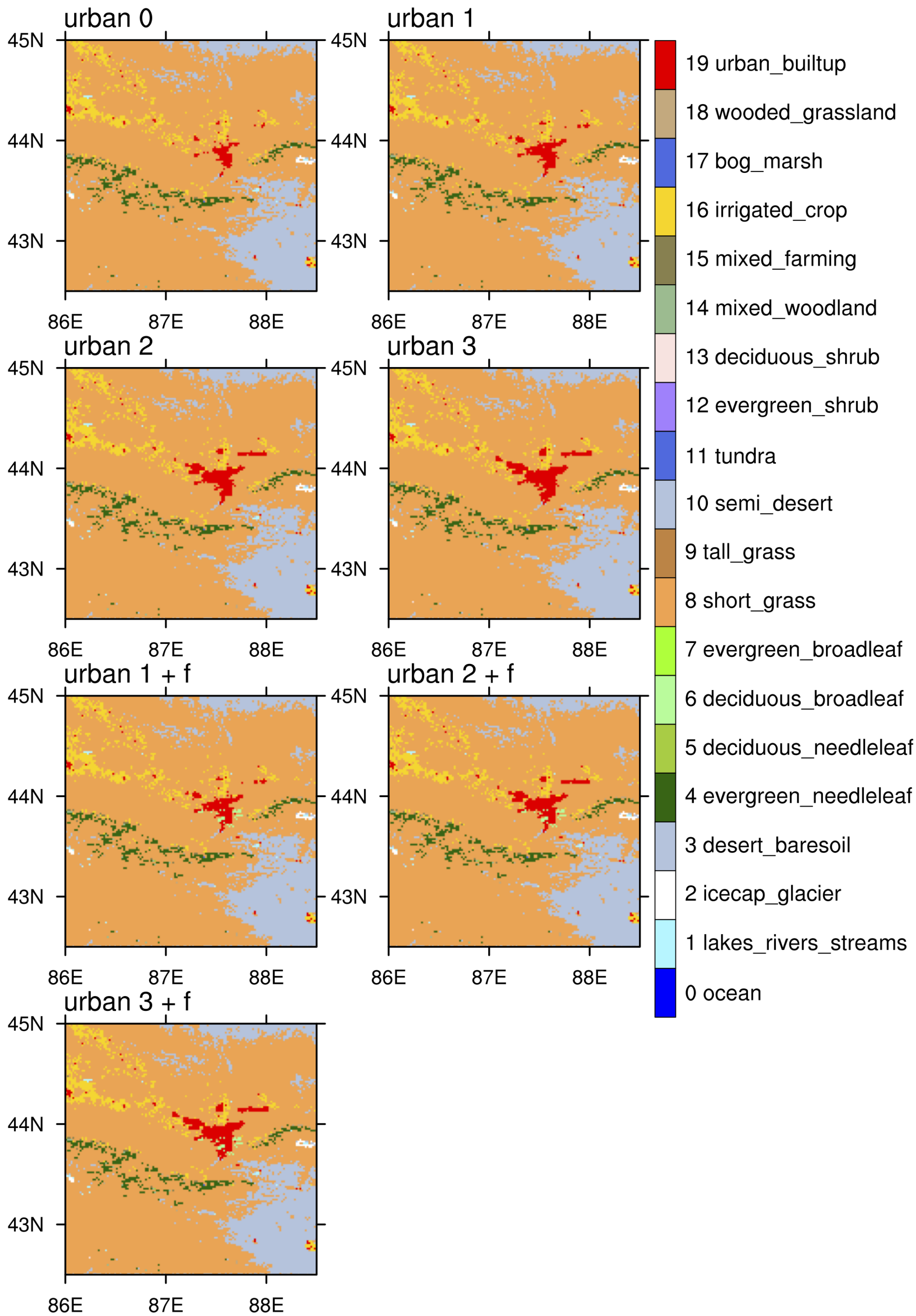

Note: includ the modal MCD12Q1 (urban 0), 3 urban scenarios, and afforestation scenarios (+f)

Figure 5.7 Land cover inputs from different urban scenarios

4. The vertical grid has 30 levels with the spacing started from 100 m at the bottom and stretched at a ratio of 1.15 (100 m, 115 m, 132.25 m, 152.09 m ...).

5. For the land surface grid, each contains five sub-grid patches, including water and its top 4 abundant vegetation classes, with their fractions of area within the grid.

6. The Klemp/Wilhelmson scheme (Klemp and Wilhelmson, 1978) was chosen as the lateral boundary condition.

7. The radiation parameter was set to use the Chen and cotton scheme (Chen and Cotton, 1983).

8. The cumulus parameterization was set to use the Kain-Fritsch scheme (Kain and Fritsch, 1993).

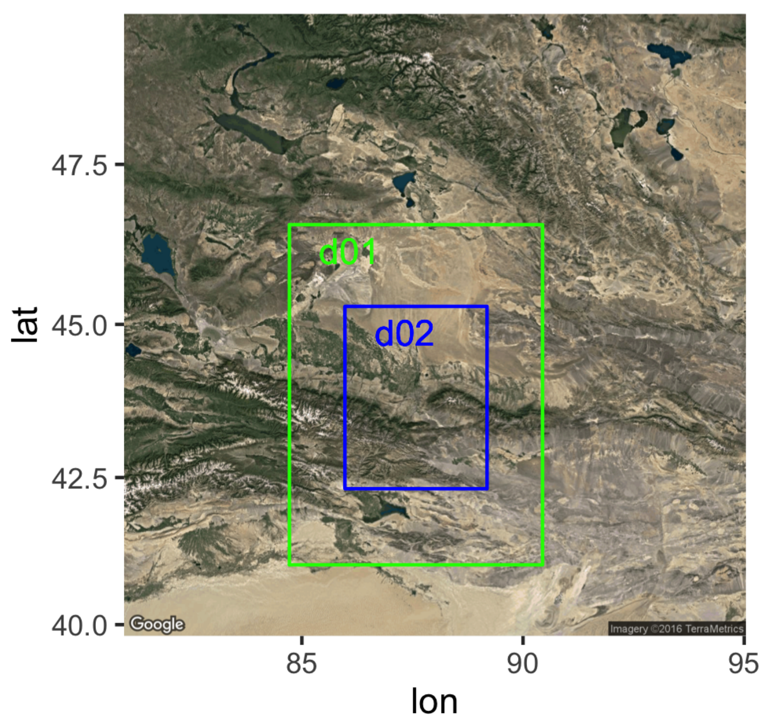

Map data: Google, TerraMetrics

Figure 5.8 Simulation domains

5.3.3 Climate sensitivity of the three stories

Land cover change could affect local climate by altering the physiological and morphological conditions of the land surface. In the case of urban expansion in Urumqi, urban built-up lands will replace irrigated croplands and natural grasslands in various degrees according to the aggressiveness of the associated scenarios. Changes in vegetation cover will affect the amount of evapotranspiration, thus the energy and water balance in the atmosphere. Converting irrigated croplands to urban will significantly reduce evapotranspiration, decreasing water content in the air and increasing the sensible heat by reducing the amount of energy that goes into latent heat. This may not be the case for grasslands because of the low soil moisture in the natural semi-arid environment. Besides, urban expansion will increase land surface roughness which will drag upon the winds, compared to both croplands and grasslands. It will further affect the wind's ability to disperse heat and moisture which in turn affect plant evapotranspiration. Afforestation, in sparsely vegetated areas, is supposed to increase both evapotranspiration (primarily due to irrigation) and surface roughness. However, the specific outcome of these impacts, in terms of magnitude and spatial pattern, needs to be uncovered through climate simulation.

Three RAMS output variables, temperature at 2 m (°C), hourly precipitation (mm/hr), and wind speed at 10 m (m/s), were selected to represent the climate sensitivity on urban change scenarios. The first two months of simulation were discarded as the spin-up period, allowing climate simulation to stabilize from its imperfect initial and boundary conditions. Thus only outputs from March to November were used in the following analysis. For each pixel, T-test and F-test, adjusted for temporal autocorrelation (Zwiers and von Storch, 1995), were performed to test whether the scenario-induced changes in these variables are statistically significant. The T-test plots show the difference in mean, and F-test plots show the difference in variance, in the form of $\sigma(scenario)/\sigma(base)$, and with the dotted pattern denoting the significant areas at 0.05 level.

For temperature (figure 5.9), some warming effect can be found at places immediately north of Urumqi where most of the simulated urban expansion occurs. Such effect is especially apparent for the basic urban expansion scenarios. The magnitude and spatial extent of warming are positively

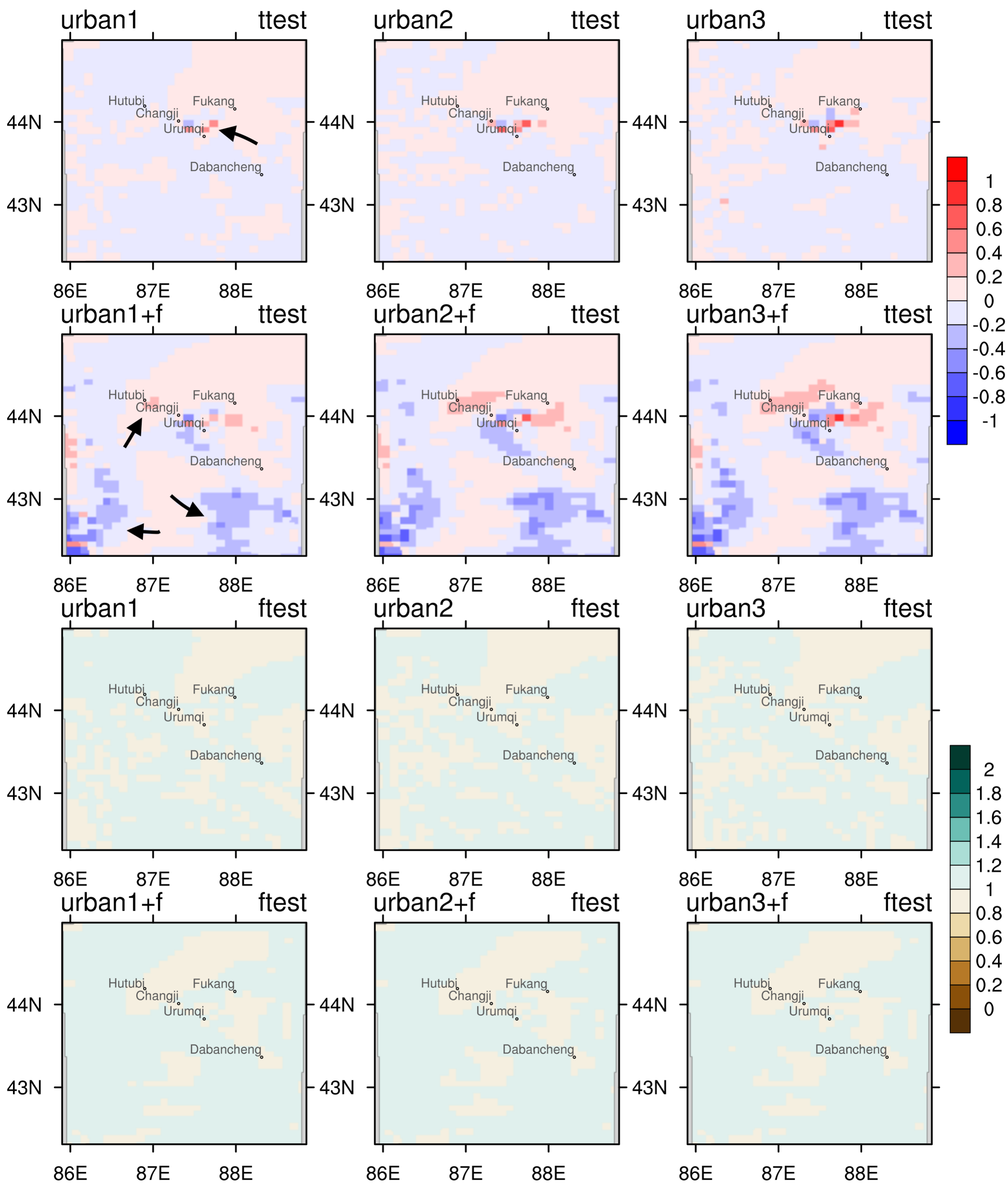

Figure 5.9 Temperature sensitivity on urban scenarios

related to the amount of urban expansion ($urban3 > urban2 > urban1$). The warming effect is an expected outcome of converting irrigated croplands into urban built-up areas. The decrease of vegetation cover lowers the cooling effect brought by evapotranspiration, thus reduces latent heat flux and increase sensible heat. In the afforestation scenarios, though the urban introduced warming is still evident, large cooling areas emerge in the southwest and southeast corners of the domain as well as west of Urumqi. In addition, a second warming area emerges in between Changji and Hutubi city. The complex temperature pattern introduce by afforestation is hard to explain though. It could indicate an oversensitive local climate or merely a model artifact. Nevertheless, neither the warmings nor the coolings are significant statistically, due to their relatively small magnitude (within $\pm 1°C$) compared to overall temperature variability. The F-test is neither significant nor showing any interesting patterns.

For precipitation (figure 5.10), urban expansions have very little impact on its average amount. Most places, including the expanded urban areas, have a difference to the base scenario within $\pm 0.0002 mm/h$, which translates to within $\pm 1.75 mm$ annually. The afforestation scenarios show stronger impacts, with the west edge of the domain being dryer and the south slope of Tianshan Mountains a little wetter, but neither is statistically significant. The F-test suggests great variations in the temporal pattern of precipitation despite little difference in overall precipitation amount. For the basic urban change scenarios, there are two patches of significant areas, the center-north, and the southeast. Most of the significant places are showing shades of green, indicating more intense but less frequent precipitation. A couple of brown areas (more even precipitation) to the northeast of Urumqi persist in all scenarios. The afforestation scenarios are showing deeper green patches above Urumqi urban area, more than twice of the original standard deviation, and their intensity and spatial extents increase as the degree of urban expansion increases. The patterns for other areas are difficult to read or relate to urban scenarios.

For wind speed (figure 5.11), the basic urban scenarios are showing a clear pattern of significantly decreased and less variable wind speed in the core urban area. The more the urban expansion, the larger the impact. This is also an expected result of urban expansion since build-

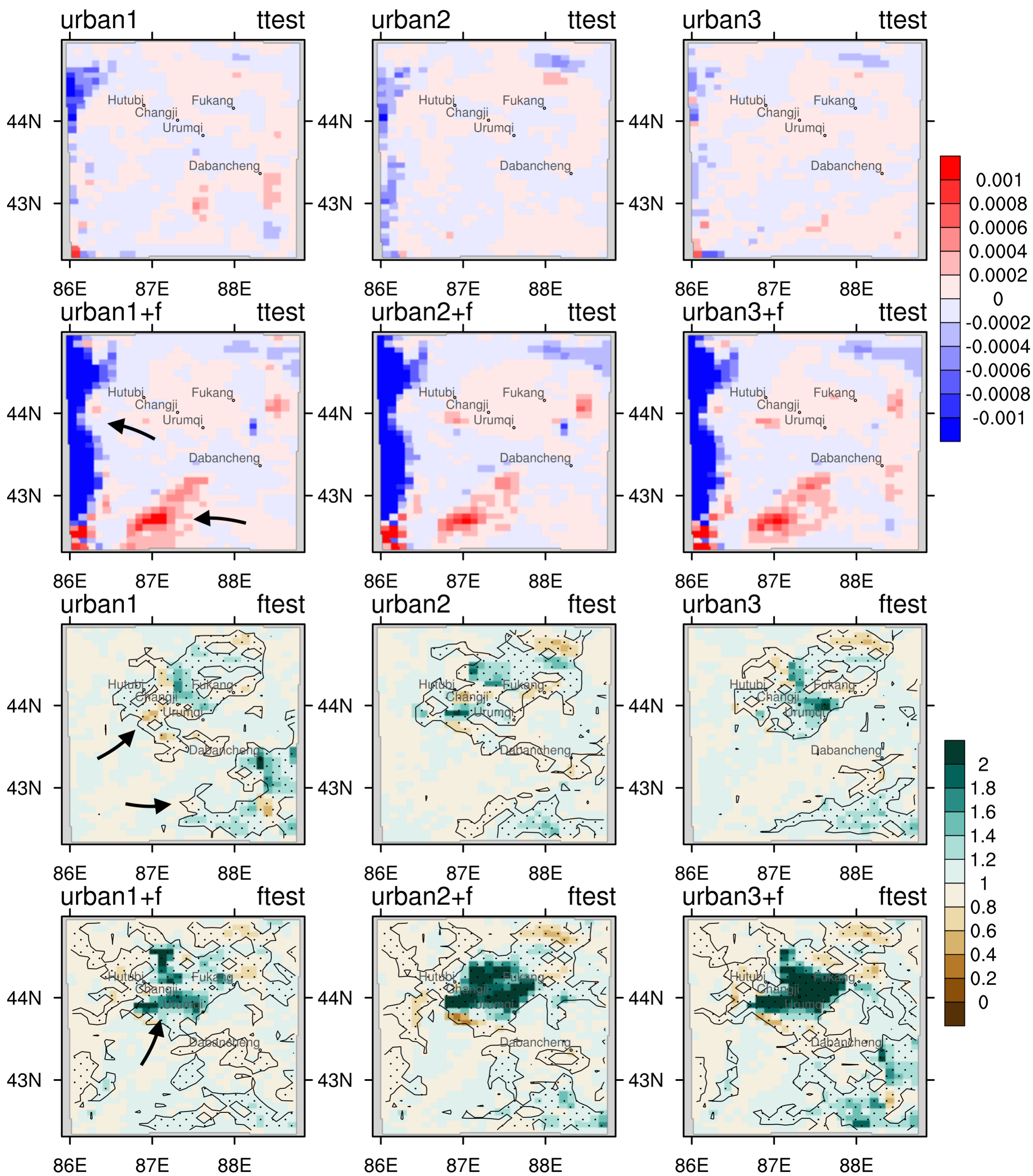

Figure 5.10 Precipitation sensitivity on urban scenarios

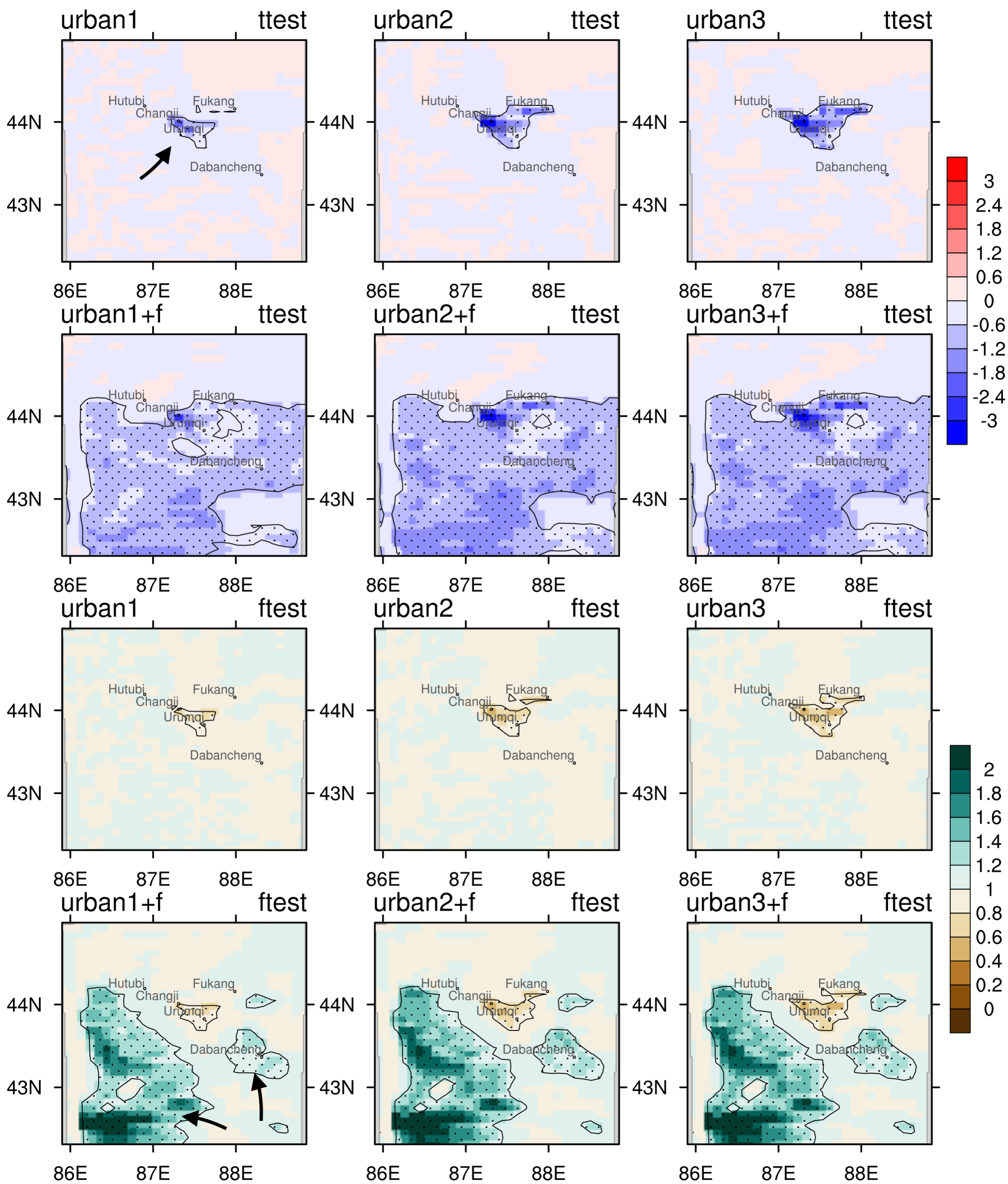

Figure 5.11 Wind speed sensitivity on urban scenarios

ings increase surface roughness thus aerodynamic resistance that prevents wind from speeding up. The afforestation scenarios show a dramatic effect on wind speed deceleration. Although trees are supposed to reduce wind speed compared to grasslands or barren lands, the extent of such impact revealed in this experiment does not seem realistic. It suggests significant wind speed decrease occur in roughly one-third of the entire domain, covering most places south of 44 $^{\circ}N$. It also introduces stronger wind speed variation (areas in green) in the southwest Tianshan Mountains and southeast Chaiwopu-Dabancheng valley.

5.4 Impact of land cover uncertainty on regional climate simulations

MODIS land cover type (MCD12Q1) is an annual global land cover product that is often used in RCMs, including the Regional Atmospheric Modeling System (RAMS) and the Weather Research and Forecasting (WRF) model. However, the data quality of MCD12Q1 is rarely adequately considered in RCM modeling works.

Inaccuracies in land cover products arise in every step of data production (Congalton et al., 2014) and are described in different terms (Messina et al., 2008). In this study, the focus was put on "uncertainty" as the degree of data fidelity open to question, instead of "error" as discrepancies between data and reference. Land cover errors are typically recognized via disagreement between MCD12Q1 and other land cover datasets or ground reference (Cohen et al., 2003; Giri et al., 2005; Ran et al., 2010; Fritz et al., 2011). Land cover error propagations are then studied by comparing model outputs from different land cover inputs (Yin et al., 2007; Ge et al., 2009; Gao and Jia, 2013). However, in one hand, the collection of ground reference by foreign institutes is prohibited in Urumqi due to the political environment, which makes it impossible to conduct traditional error assessment. In the other hand, comparing dataset from different dates and classification schemes would introduce additional sources of uncertainty, thus overstate the impact of data quality.

In this section, MCD12Q1 categorical uncertainty will be characterized by the use of the time-series of MCD12Q1 products themselves for Urumqi area, following the approach introduced by Liang and Gong (2010) which assessed MCD12Q1 data quality at global scale. The Binary-

Control model will then be developed to construct alternative land covers based on characterized MCD12Q1 uncertainty. Finally, MCD12Q1 uncertainty propagation through the RAMS model will be examined. The majority of this section has been published in Climate Dynamics (Li et al., 2017).

5.4.1 The MCD12Q1 product

MCD12Q1 is a yearly product available from 2001 to the present. The base algorithm is a C4.5 (Quinlan, 2014) decision-tree and ensemble classifications are estimated using boosting. Classification inputs twelve sets of 32-day average nadir BRDF-adjusted reflectance (Schaaf et al., 2002) for MODIS band 1-7, enhanced vegetation index (Huete et al., 2002) and land surface temperature (Wan et al., 2002) together with their annual minimum, maximum and mean. The high temporal resolution of these datasets made it possible to utilize phenological and other temporally variable information to facilitate classification. Outputs then go through a three-year moving-window stabilization procedure to reduce the amount of spurious inter-annual changes from 30% to 10% (See Friedl et al. (2010) for more details on MCD12Q1 production). However, the producer suggested that this rate is still well above the actual global land cover change rate, leaving a large model output space to data uncertainty. Urban areas were produced separately from other land cover types using MODIS data from 2001-2002 (Schneider et al., 2009), and have not been updated.

Although the overall classification accuracy of the MCD12Q1 product is assessed at 74.8% (Team, 2014), it can be much lower for certain classes or in certain regions. Zeng et al. (2015) reported an overall accuracy of MCD12Q1 Version 5.1 at 64.62% for China, varying between 36.11% and 76.52% in different provinces and between 3.74% (shrublands) and 82.92% (water bodies) in different land cover classes. Confidence assessment maps (McIver and Friedl, 2001) are provided with the products, but they do little to help in understanding the impact of data quality on climate modeling outputs.

To investigate the data uncertaity, the version 5.1 MCD12Q1 products with a spatial resolution of 500 m were acquired from 2001 to 2012 using the IGBP class layer (figure 5.12). A spatial

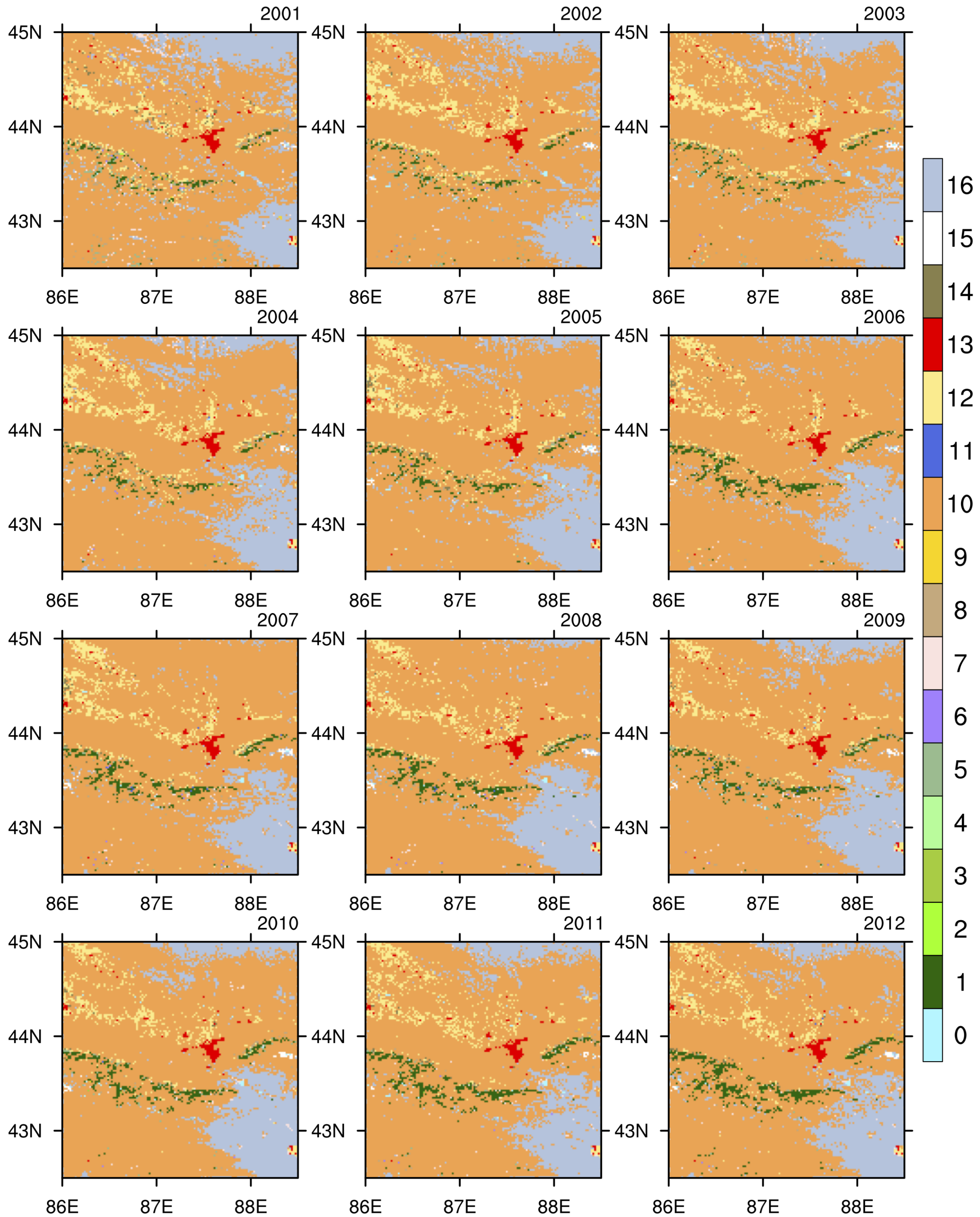

0 - water, 1- evergreen needleleaf forest, 2 - evergreen broadleaf forest, 3 - deciduous needleleaf forest, 4 - deciduous broadleaf forest, 5 - mixed forest, 6 - closed shrublands, 7 - open shrublands, 8 - woody savannas, 9 - savannas, 10 - grasslands, 11 - permanent wetlands, 12 - croplands, 13 - urban and built-up, 14 - cropland/natural vegetation mosaic, 16 - snow and ice, 16 - barren or sparsely vegetated

Figure 5.12 MCD12Q1 2001-2012

subset of 42.5°N-45°N, 86°E-88.5°E, roughly 5.6×104 km^2, was extracted corresponding to the RAMS domain setup in the previous section.

5.4.2 Characterizing uncertainty in MCD12Q1

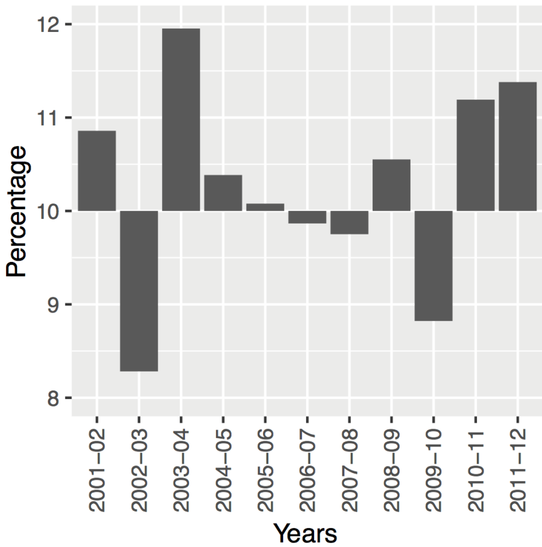

(a) Annual change rate

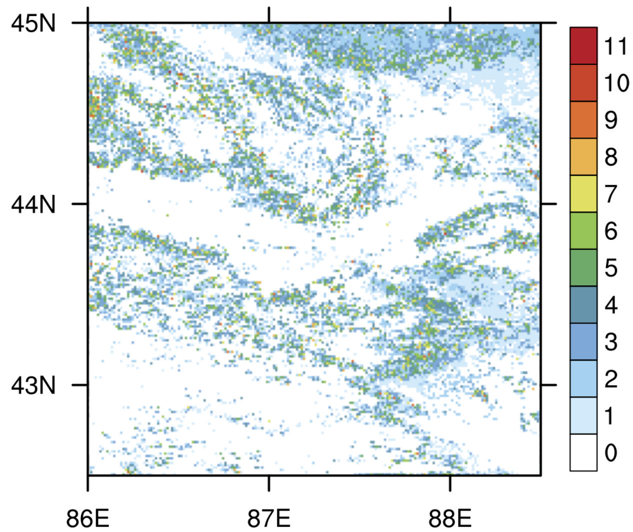

(b) Number of changes (C)

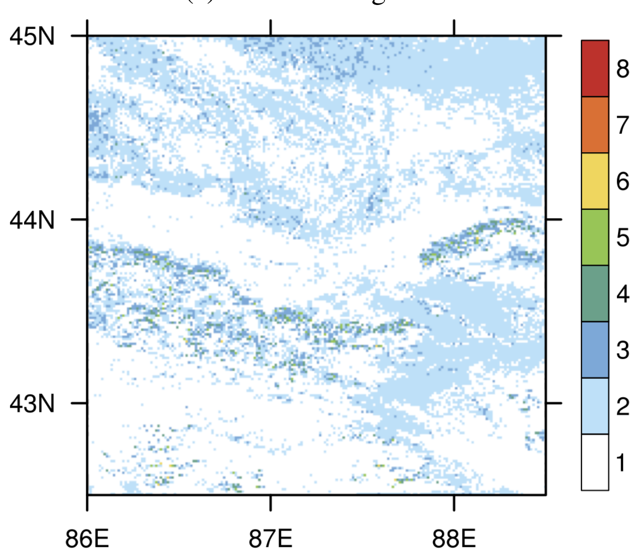

(c) Variety (V)

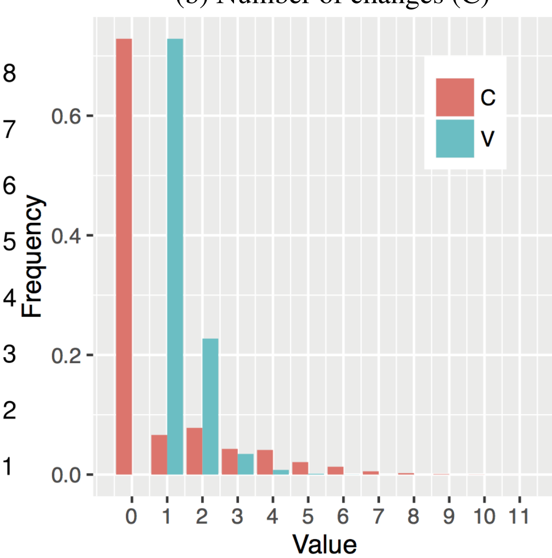

(d) Frequency distribution of C and V

Figure 5.13 Temporal characteristics of MCD12Q1

Following Messina et al. (2008), a distinction is made between error in the underlying data, and uncertainty due to the model itself. In this study, MCD12Q1 model process uncertainty is explored through the use of the time series of MCD12Q1 products themselves. A similar approach to assess the quality of MCD12Q1 at global scale was introduced by Liang and Gong (2010). The approach hypothesizes that locations with highly unstable land cover classes over time are more likely to be suffering from classification process inaccuracy rather than experiencing actual land cover changes. Thus, the uncertainty of land cover data can be quantified from those unstable locations and then modeled to test for its propagation impacts.

- Uncertainty characterization

Within the 12-year MCD12Q1 (as shown in figure 5.12), most years show unrealistically high (above 10%) inter-annual change rates as compared to previous years (figure 5.13a), suggesting that something other than actual land cover change is occurring (Zhang et al., 2007). A change trajectory from 2001 to 2012 is generated for each pixel. Two variables are computed to characterize trajectories: the number of changes (C, figure 5.13b) and the variety (V, figure 5.13c) of types that occupied the pixel. Pixels are further divided into groups based on the distributions of these two variables (figure 5.13d).

Stable pixels ($C \leq 4$) were those consistently classified throughout the period. Unstable ($C > 4$) pixels were further divided into two groups depending on V with a cutoff at 3. For the group with both high C and V, it is difficult to retrieve meaningful categorical uncertainty while the other group (high C low V, figure 5.14) contains pixels flipping among a small set of land cover types. The latter indicates that the automated MCD12Q1 classification model may have difficulty in distinguishing between particular land cover types, especially for this study area or ecotone.

In order to find inter-category uncertainties, the 12-year trajectories of those "flipping" pixels were subdivided into separate changes from one year to the next. Table 5.2 shows the most frequent change directions in the flipping pixel changes. The first four directions account for over 85% of the total changes, and they perfectly cover two pairs of land cover types. For 2011, over 9% of the entire landscape fell into these four spurious directions compared to 2010.

Figure 5.15 shows that the uncertain areas present some spatial structure across the entire landscape, with concentrations in the northern and southeastern parts. Opposite directions tend to be spatially intermingled with each other, which suggest inherent spatial patterns with our discov-

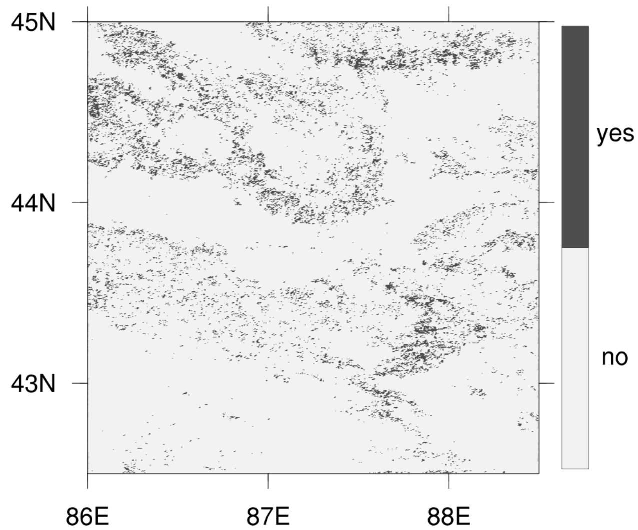

Figure 5.14 Flipping pixels

Table 5.2 Spurious change directions and their frequencies.

Rank	From	To	Overall frequency	2010 to 2011 area (km^2)
1	grasslands	croplands	21.74%	1366.00
2	barren	grasslands	21.66%	1696.75
3	grasslands	barren	21.54%	1064.00
4	croplands	grasslands	20.87%	988.00

ered uncertainty. However, it could be argued that the spurious (or uncertain) inter-annual changes might result from particular farming practice or natural vegetation dynamics, thus not necessarily from data uncertainty.

To lend support to our findings, a set of Landsat 5 TM data were collected for our study area in August of respective years (figure 5.16a), along with those years of 16-day average Enhanced Vegetation Index (EVI) from MOD13A1 Version 6 (Didan, 2015) for 100 random sample locations of each spurious change direction (figure 5.16b). The August TM images were chosen for their low cloud cover and strong vegetation signal. In this semi-arid environment, croplands are heavily dependent on irrigation, therefore, showing vigorous green color in the pseudo-color TM images compared to nearby natural grasslands. No large-scale shifts between grasslands and croplands were found in the TM images, as opposed to the spurious changes detected from MCD12Q1 (see figure 5.15). Not surprisingly, the grasslands/barren uncertainty is much harder to elucidate. The

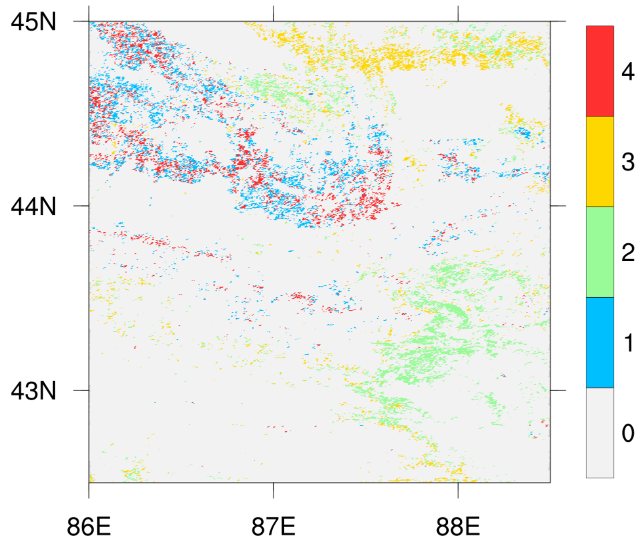

Figure 5.15 Spurious changes from 2010 to 2011

IGBP scheme defines barren as no more than 10% vegetation at any time of the year. It requires a reference dataset of high temporal resolution to distinguish between grasslands and barren. The time series of EVI does not reveal much difference between the year 2010 and 2011 for any sample groups (spurious directions). Year 2011 may have slightly higher averaged EVIs during the growing season but this is the case in all samples. Therefore I consider the identified changes more likely to result from data uncertainty rather than actual land cover changes.

- Uncertainty model

Monte Carlo simulation is a widely applicable approach to study uncertainty propagation in complex nonlinear system modeling (Heuvelink, 1998). The basic idea is to generate a set of statistically equivalent realizations for the uncertain variable and then run the model using those realizations, thus producing a set of model outputs. Uncertainty propagation can be studied based on the distributions of those outputs. The same idea is used to test the MCD12Q1 uncertainty propagation through RAMS (figure 5.17).

Let the two land cover types in an arbitrary spurious direction be A and B. Assume: (1) for a single pixel that changed in a spurious direction as shown in table 1, it has equal probabilities of being A or B; (2) the classification uncertainties between two consecutive years are systematic, which means all pixels that fell into a specific spurious direction were either all A or all B; (3) the

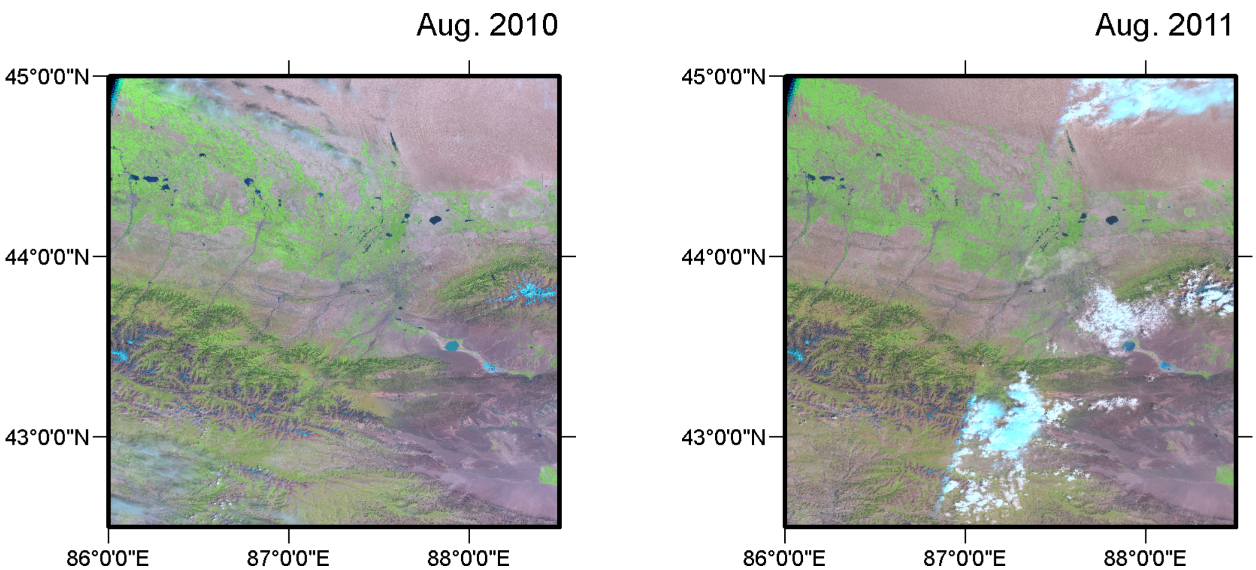

(a) Landsat 5 TM pseudo-color images (5, 4, 3)

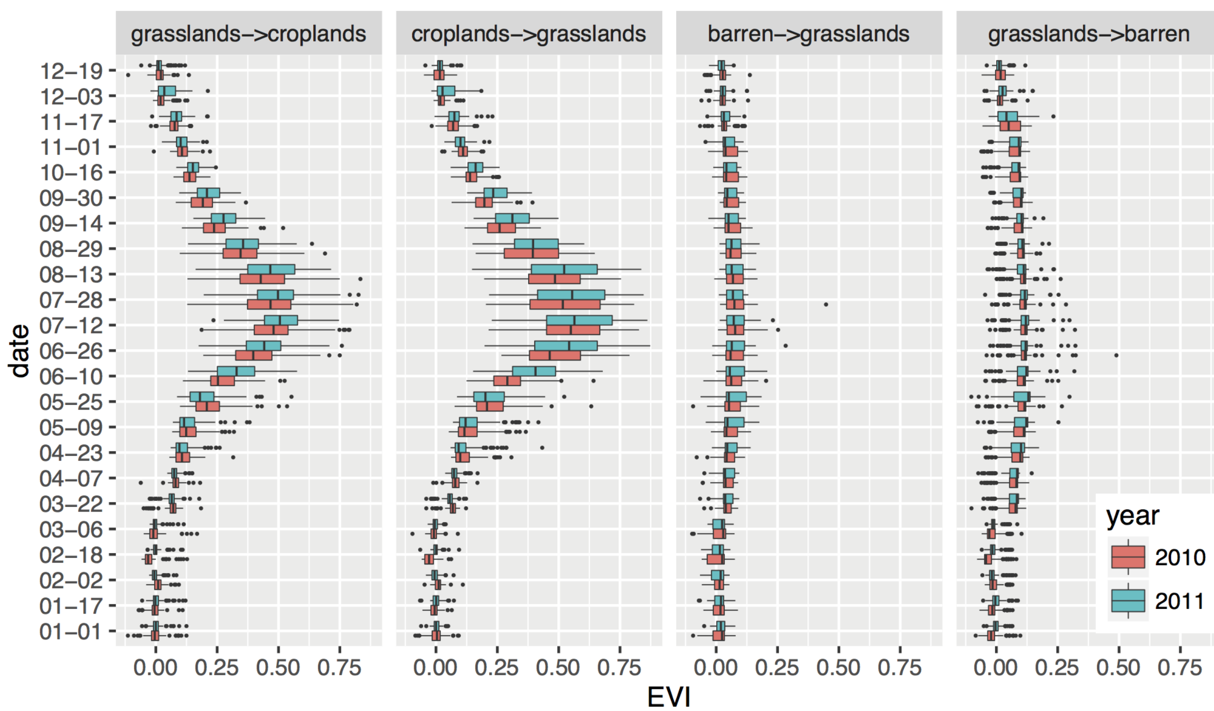

(b) Vegetation phenology at sample locations of each spurious change

Figure 5.16 MCD12Q1 uncertainty references

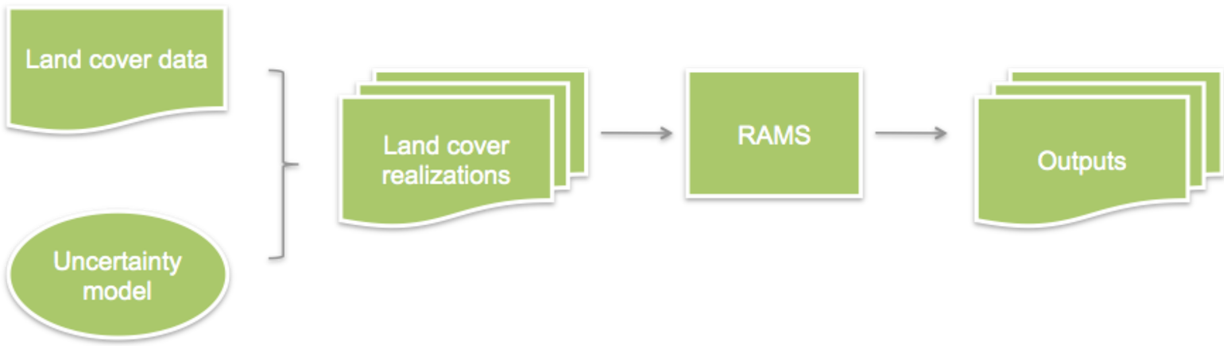

Figure 5.17 Workflow for testing MCD12Q1 uncertainty propagation through RAMS

spurious directions are independent from each other.

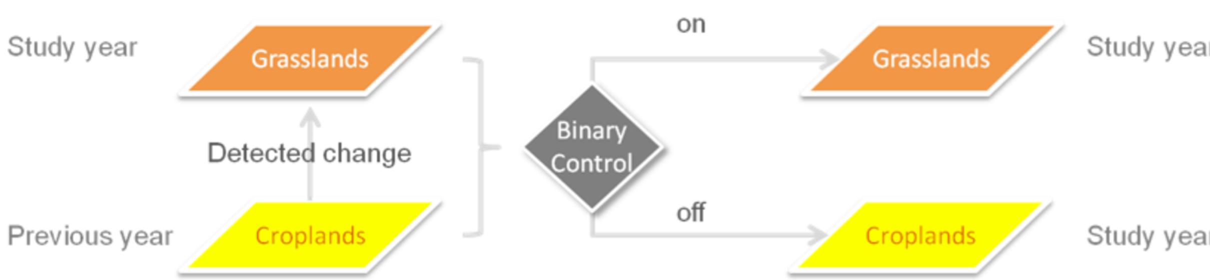

Figure 5.18 An illustration of the Binary Control model

Following the above assumptions, a binary control model (figure 5.18) was developed based on combinations of spurious change directions. A simple "On and Off" rule was used to generate possible land cover realizations within our defined uncertainty space. For example from maps 2010 to 2011, if the direction "croplands to grasslands" is turned "off", all pixels that fell in this direction need to be modified from grasslands to croplands in the 2011 map. Since 4 spurious directions were discovered, the "On and Off" perturbation can be set to all these directions, thus yielding, in total, 16 equally possible land cover realizations (figure 5.19). All will be later passed into RAMS, including the original 2011 land cover (the “all-on” realization) as a reference, and the variations among their outputs will be examined.

5.4.3 Propagation impacts on RAMS simulation results

- Overall uncertainty propagation

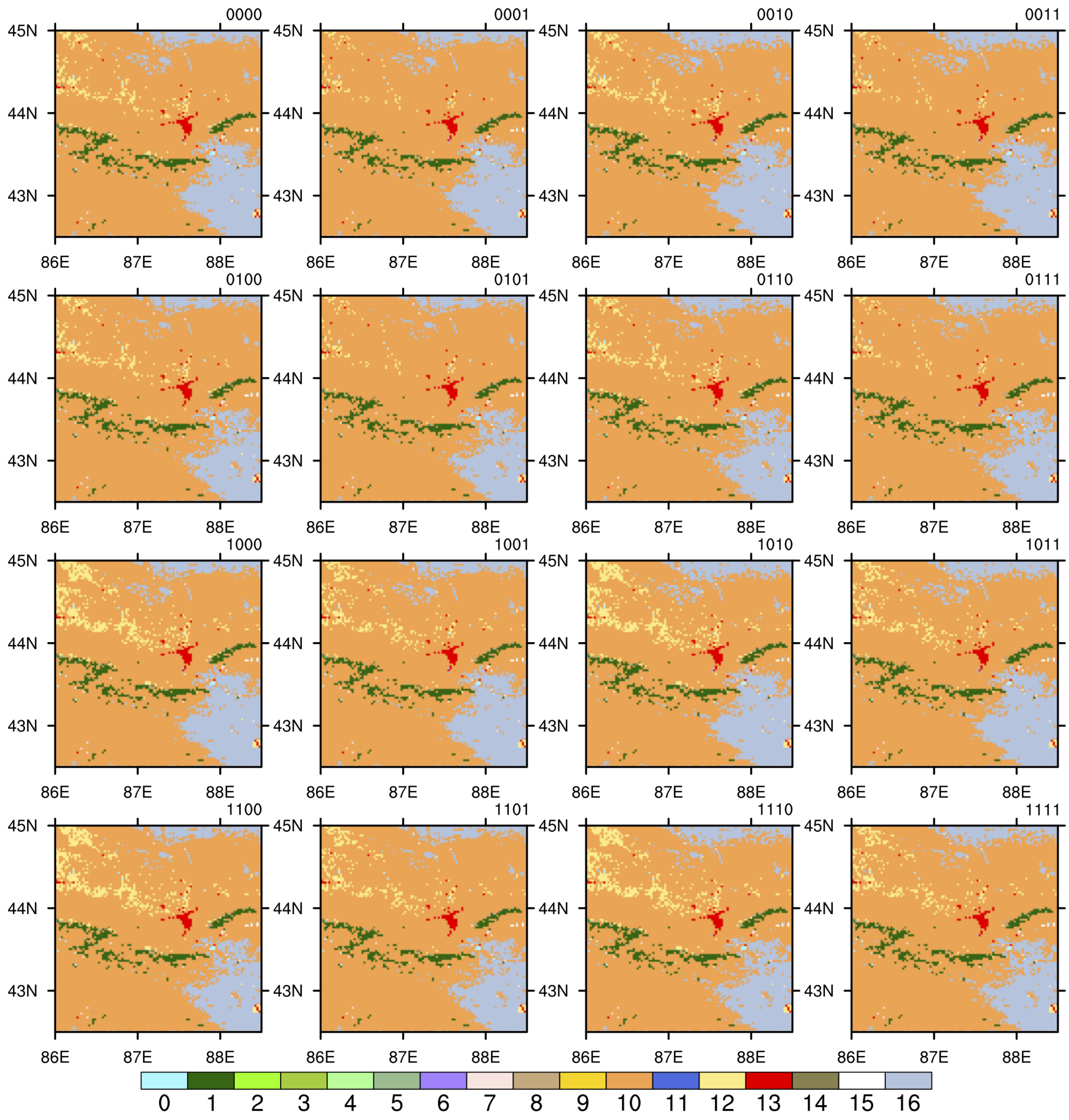

Note: The 4-digit realization ids correspond to the 4 spurious directions in table 5.2, where 0 means "off" and 1 means "on".

Figure 5.19 2011 land cover realizations

First, domain-averaged daily series for selected variables were calculated. As illustrated in figure 5.20, land cover uncertainties affected LHF substantially, with daily ranges among simulations at 4.32 W/m^2 in average, accounting for 14.6% of its overall data range. SHF (2.44 W/m^2, 1.57%), WS (0.08 m/s, 1.24%) responded slightly, while TEMP (0.08°C, 0.67%), HP ($3.29\times10^{-5} mm/h$, 0.65%) and VM ($6.88\times10^{-4} m/s$, 0.33%) revealed little impact. The range of differences appeared to diminish over time.

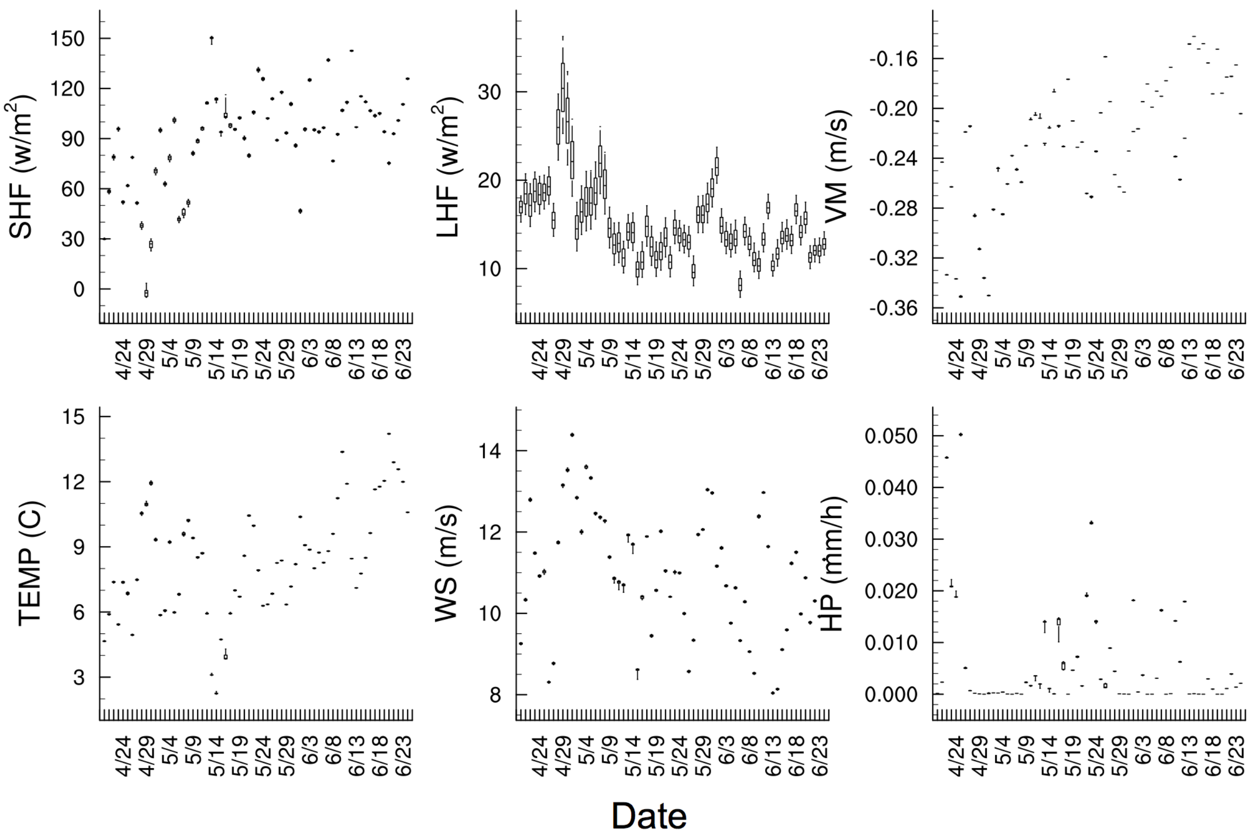

Figure 5.20 Box plots of daily domain averages

The second step was to evaluate the spatial distribution of propagated uncertainty. For the same set of variables, pixel-based data ranges at every time step were calculated and then averaged over the entire analysis period (figure 5.21). Unlike domain-averaged results, substantial differences were found in most variables with great spatial heterogeneity. At roughly 44°N, 87°E, a hot spot was evident in SHF, LHF, TEMP and WS, which corresponds to the areas with high grasslands/croplands uncertainty. The associated northeast down-wind area also manifests impacts in

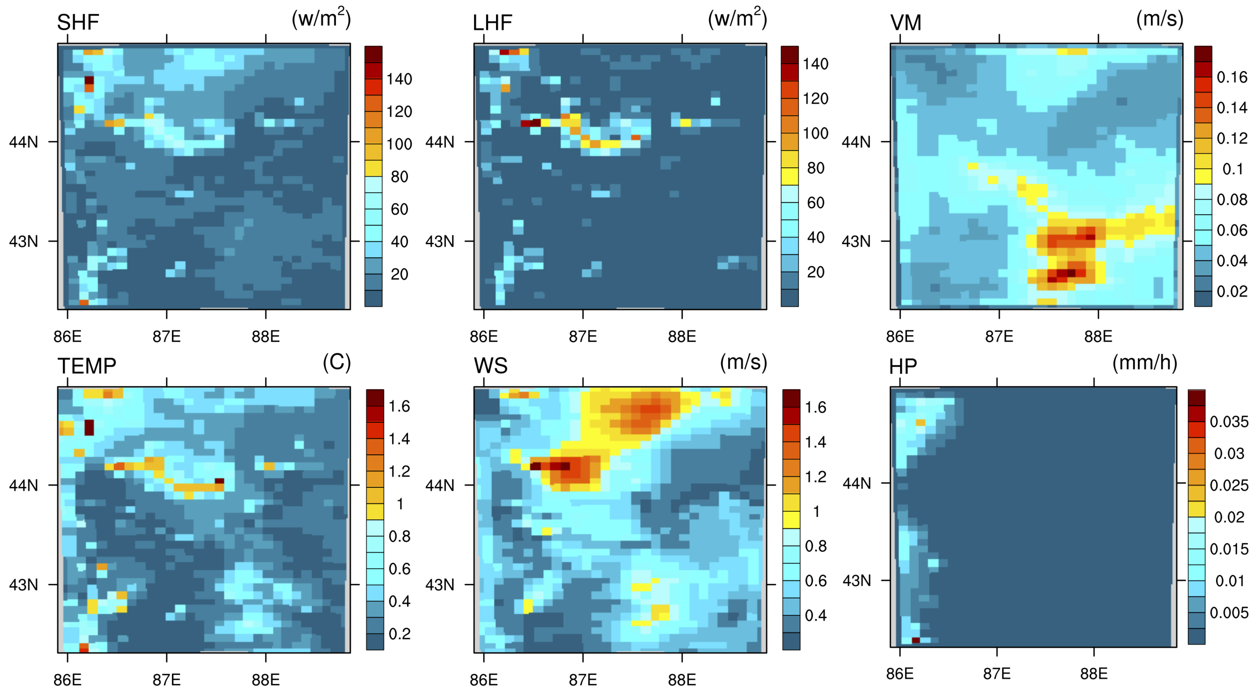

Figure 5.21 Average ranges over the analysis period

SHF, VM and WS, likely demonstrating a spatial propagation effect. Another hot spot (43°N, 87.5°E) emerged with high VM and moderately high TEMP and WS variations. It is collocated in an area with grasslands-barren uncertainty on mountain slopes. As for HP, greater impact was found along the western border where most of the resolved precipitation occurs.

• Comparison among simulations

The effects of particular land cover perturbations were tested by comparing each simulation with the reference, using NCAR Command Language (NCL) 6.2.0. At pixel-level, T-test and F-test, adjusted for temporal autocorrelation, were performed to examine whether the differences between simulation and reference are statistically significant. Figure 5.22 shows the percentage of pixels identified as significantly different from the reference at the 0.05 level in mean or variance. Different means suggest changes in their distribution baseline while different variances suggest changes in the magnitude of their fluctuations. In general, two variables stand out in the significance tests, LHF and HP. For LHF, similar amounts of pixels were identified to have different means or variances, but HP differs only in variances and more pixels were affected compared to other variables. SHF, VM and WS emerged, while TEMP was found not significant in any case.

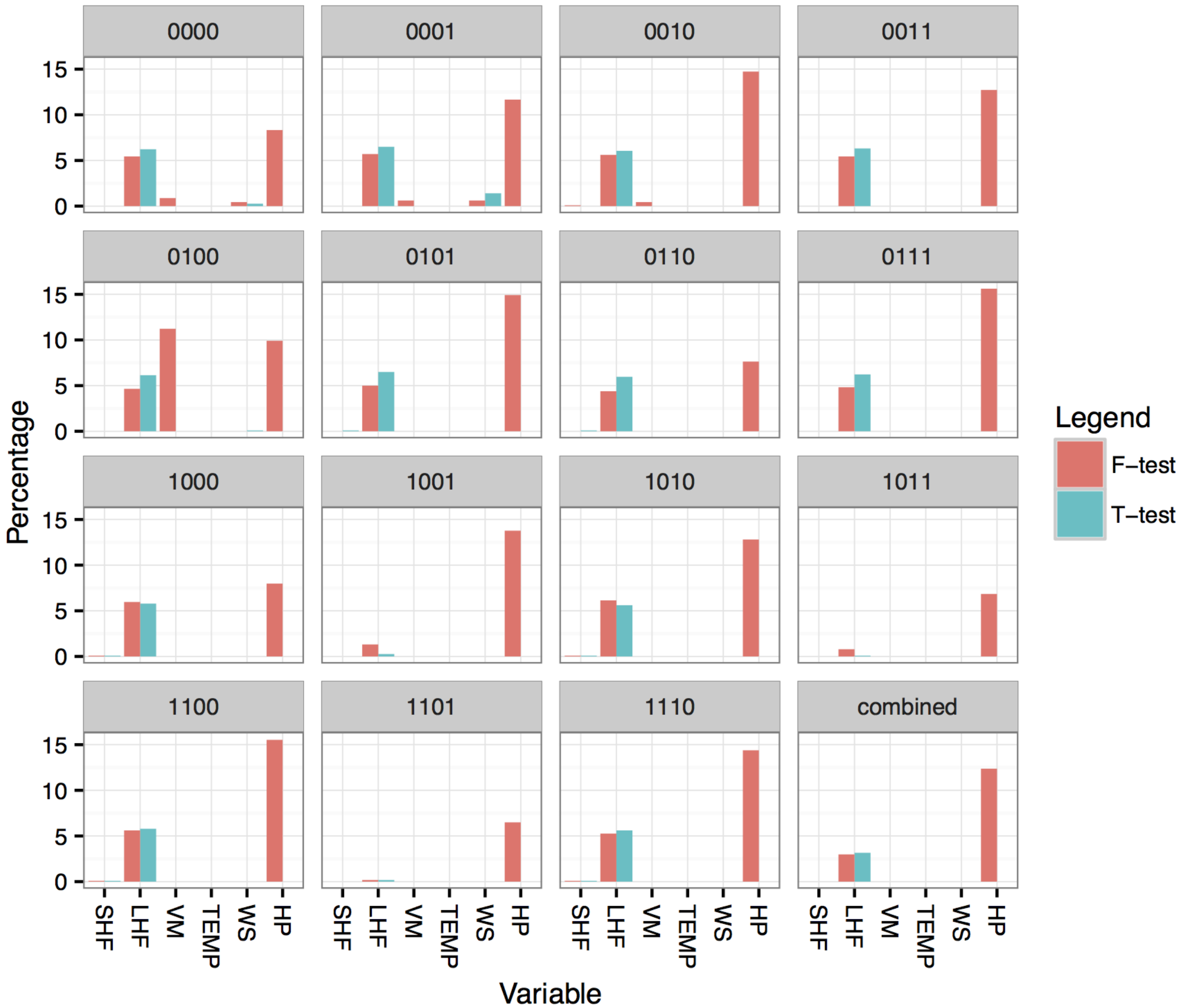

Note: The 4-digit simulation ids correspond to the 4 spurious directions in table 5.2, where 0 means "off" and 1 means "on".

Figure 5.22 Percentage of significant pixels in t-tests and f-tests against reference-run

For simulations with only one direction turned off, manipulations on direction 1 and 4, which are grasslands to/from croplands, had the greatest impacts. Direction 2 and 3, barren to/from grasslands, caused smaller changes. When more directions were altered together, the patterns of significant pixels become complicated. Direction 1 and 4 slightly mitigated each other, and did more so on HP than on LHF, while direction 2 and 3 seems added up on each other. Combinations of three or more directions even resulted in significant pixels in VM and/or WS.

Finally, the combined experiment shows that the aggregated results exhibited different distributions for only LHF and HP, variables that are strongly connected to the presence of water. For LHF, pixels with significantly different means or variances were both around 3%; and for HP, there were no significant differences in mean, but over 12% of the pixels showed significantly different variances. Figure 9 further illustrated the area and magnitude of such differences. The statistical significant pixels for LHF in both t-test (figure 5.23a) and f-test (figure 5.23b) seem connect to locations with high land cover uncertainty. All the significant pixels in figure 5.23b have values over 1, suggesting greater variability comparing to the reference. Variability in precipitation (figure 5.23c) exhibit a more complex pattern.

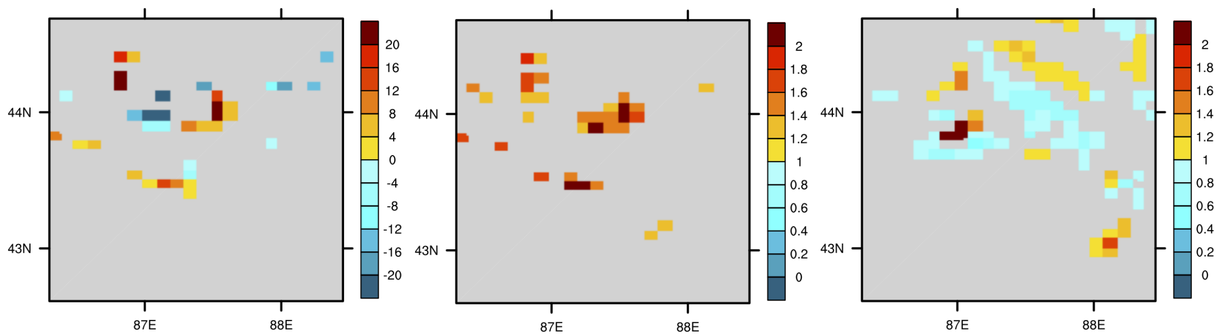

(a) T-test for LHF (b) F-test for LHF (c) F-test for HP

Note: Insignificant pixels were shown in grey. T-test shows the difference in mean comparing to reference in W/m^2, and F-test shows the ratio of standard deviation to that of the reference.

Figure 5.23 Maps of significant pixels from combined experiment

5.4.4 Comparing future climate to the uncertain current

To compare with the hot years selected for future climate simulations, the four warmest years in recent history (1997, 2001, 2006, and 2008, see fig. 5.24), in terms of summer average daily maximum temperature, were selected to represent the current hot years. The NCEP-DOE Reanalysis 2 (Kanamitsu et al., 2002) data for selected years were acquired and used to drive RAMS simulations. Using the same model setup as in section 5.3.2, and only replacing the land cover input with the 12-year modal MCD12Q1, the simulations of current climate were conducted from January 1^{st} of each year to December 31^{st}. Just like in the future simulations, the first two months were discarded as spin-up period, and only outputs from March to November were used in the following analysis.

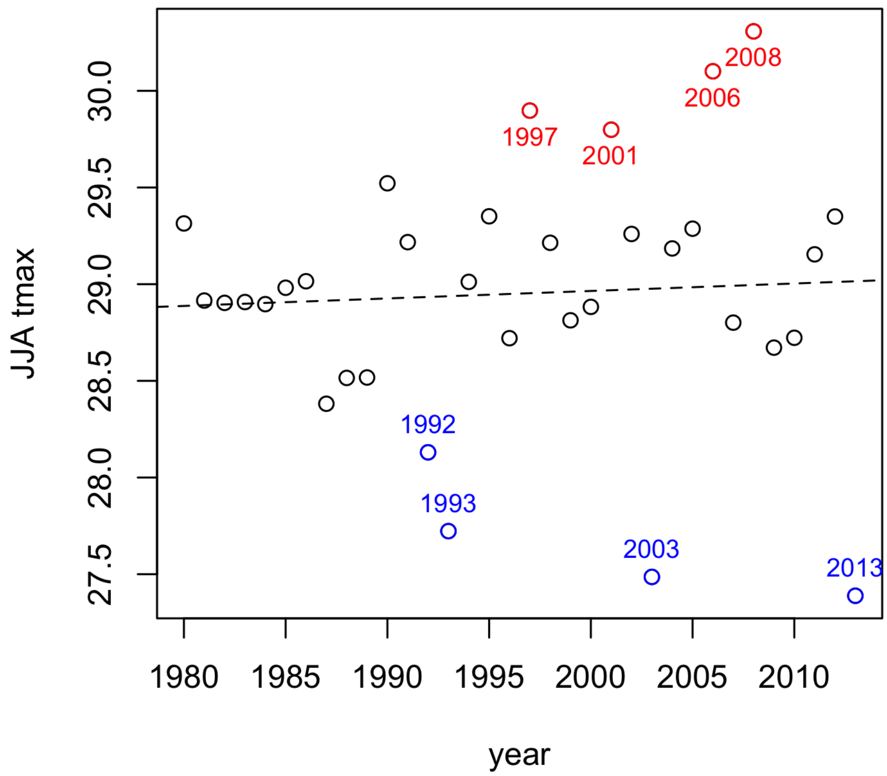

Data source: Global Historical Climatology Network

Figure 5.24 Urumqi historical summer average daily maximum temperature

When comparing the simulation results of future and current climate, four years of data were grouped to form a larger sample. More specifically, and hereafter, the future (2030s) simulation refers to RAMS outputs from the years 2028, 2029, 2031 and 2032, and the current (2010s) refers to the years 1997, 2001, 2006, and 2008. Similar to sections 5.3.3 and 5.4.3, adjusted T-test and F-test were conducted to examine places with statistically different mean or variance. Again, the T-test plots show the difference in mean, and F-test plots show the difference in variance, in the form of $\sigma(future)/\sigma(current)$, and with the dotted pattern indicating the significant areas at 0.05 level. Although the test for land cover uncertainty propagation (section 5.4.3) was performed in a different year and for a much shorter period, its magnitude and spatial extent can be considered in the interpretation of the future-current comparisons.

For temperature (figure 5.25), all scenarios are showing roughly the same pattern. The majority

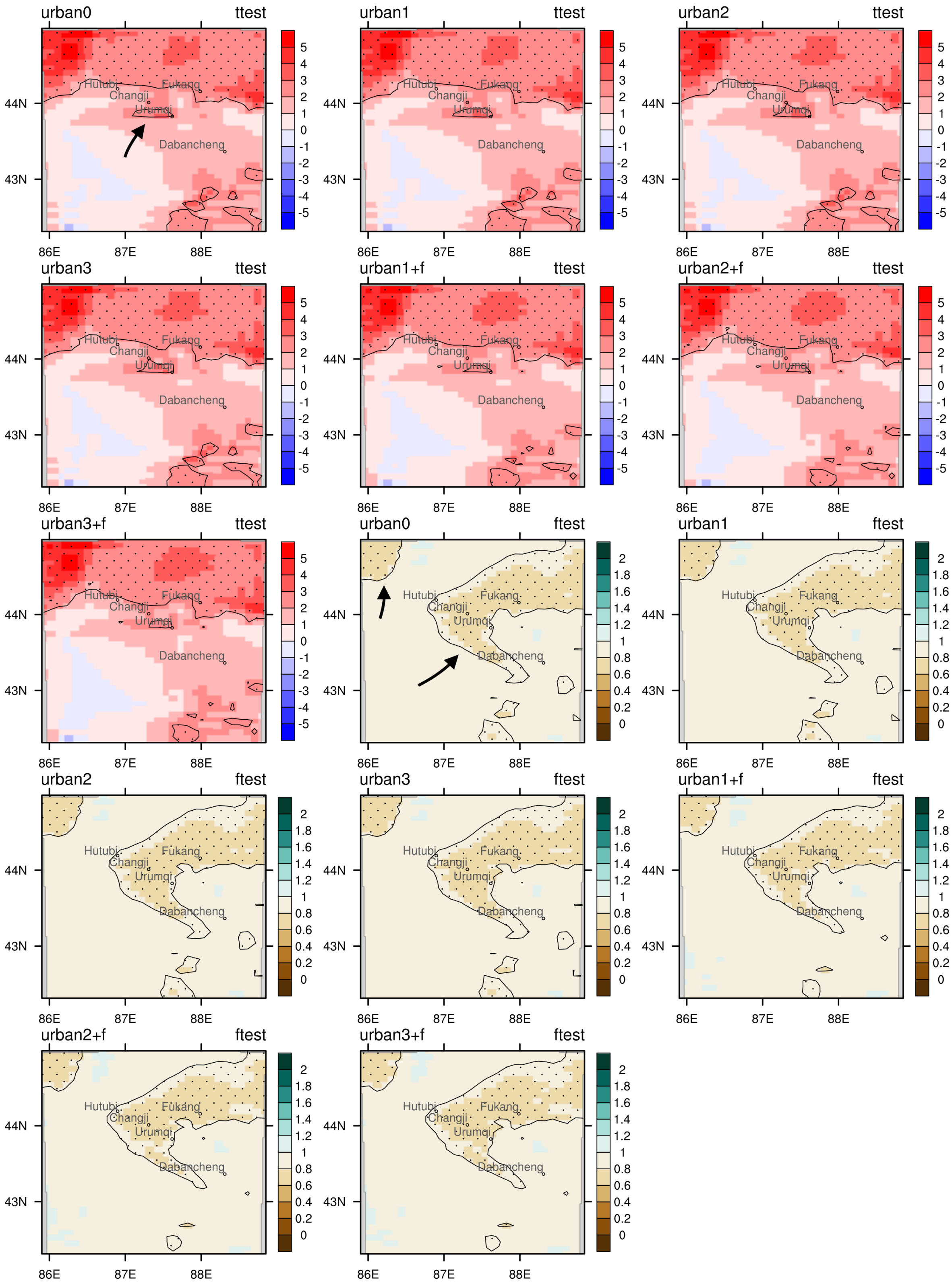

Figure 5.25 Temperature change in 2030

of the domain is getting warmer except for some insignificant cooling on top of the Tianshan Mountains. All the statistically significant areas are getting warmer, including the Dzungaria Basin (+ 2 $\sim$ 5 °C) north of 44 °N and the Turpan Depression (+ 2 $\sim$ 4 °C) in the southeast corner of the simulation domain. A small area between the cities of Urumqi and Changji is also becoming significantly warmer (+ 2 $\sim$ 4 °C). This location is where most of the recent and predicted urban expansions take place, and its extent seems to grow slightly as urban expansion gets increasingly aggressive (urban 3 > urban 2 > urban 1). While in the afforestation scenarios, this area is smaller and not as warm (+ 2 $\sim$ 3 °C) as in the basic urban scenarios, and does not change in response to the more aggressive scenarios. The F-tests suggest an overall decrease in temperature variation. Two areas are highlighted, including the northwest corner and an L-shaped area, starting from the northeast corner and turning southeast to the Chaiwopu-Dabancheng Valley. Both areas are predicted to have a significant decline (over 20%) in the standard deviation of hourly temperature. They cover the major urban agglomerations and substantial amount of croplands in this area. The land cover uncertainty was not significant for temperature, so it does not affect the interpretations here.

For precipitation (figure 5.26), differences among urban change and afforestation scenarios are minimal. Most of the area has an insignificant change in the average amount of precipitation. The west border of the domain, however, has more than $0.05 mm/h$ or $438 mm/y$ of precipitation loss in most places and up to $0.03 mm/h$ or $263 mm/y$ gain in one pixel near the northwest corner. The magnitude of these differences is in the same order of the average precipitation in these areas, which may not be realistic. Another significant area covers places south of the peaks of Tianshan Mountains, which is normally the rain shadow area. This area is predicted to have as much as $0.02 mm/h$ or $175 mm/y$ more precipitation. The F-test shows a dramatic difference in precipitation variation almost everywhere. The wetter places will have precipitation varying more than twice as before while the drier places will lose up to 20% to 100% of the precipitation variability. The land cover uncertainty in precipitation, though statistically significant in F-test, is substantially weaker compared to the amount of differences here. It is also evident that precipitation varies substantially

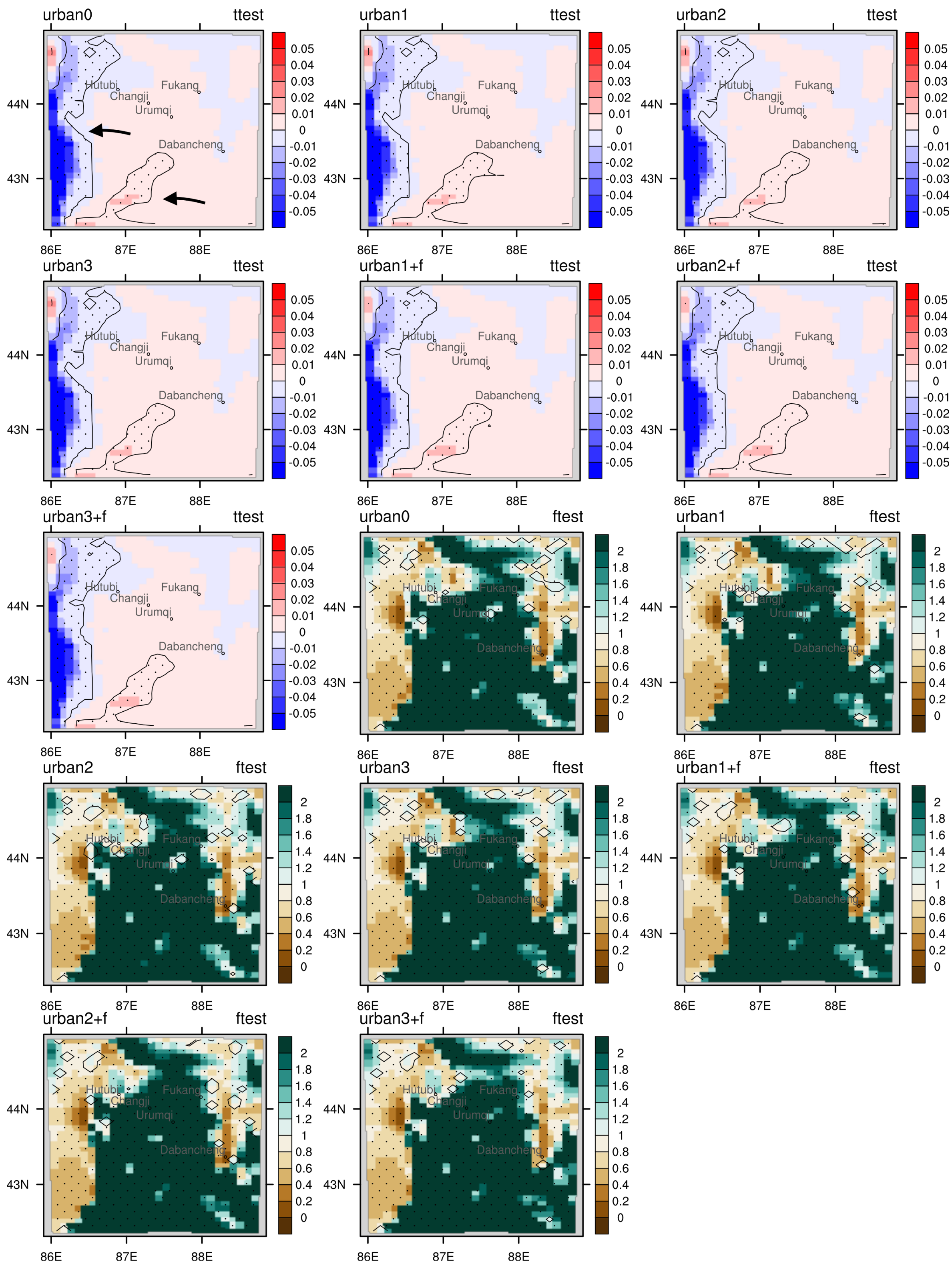

Figure 5.26 Precipitation change in 2030

at the western edge in the earlier tests, suggesting a lack of predictability rather than real climate change.

For wind speed (figure 5.27, urban expansion and afforestation introduce substantial differences. In the baseline scenario (urban0), wind is significantly stronger in three-quarters of the domain, including Urumqi urban area. In the basic urban expansion scenarios, wind becomes significantly slower in a narrow stripe spanning from Changji to north Urumqi and then to Fukang and another area in the Chaiwopu-Dabancheng valley southeast of Urumqi. As urban expansion getting aggressive, these two areas continue to intensify (from $-2m/s$ to $-5m/s$), grow in size, and eventually become connected. In the afforestation scenarios, wind further weakens in the southwest mountain areas. F-test suggests, in general, a less varying wind despite the increase in wind speed. The mountain areas, both the southwest and the east, have more varied wind speed, especially in the afforestation scenarios. Land cover uncertainty is ignored since it was not significant for wind speed.

5.5 Discussion and conclusions

In this chapter, a hot near future (2030) regional climate was simulated in the RAMS model, fed by NASA-GISS-E2-H GCM outputs of year 2028, 2029, 2031 and 2032, and with varying land cover inputs. The simulated future climate was compared among urban change and afforestation scenarios as well as simulations for the current hot years (1997, 2001, 2006, and 2008). The propagation impact of the input land cover data (MCD12Q1) uncertainty was examined, which in this case was mostly insignificant either by itself or compared to the difference between simulated future and current climate conditions. Below are summaries of the findings in this chapter.

- Temperature

Climate simulation results suggest an overarchingly warming trend in the study area in the 2030s. Most area is expected to gain at least 2 °C in average temperature. At the same time, temperature variation is predicted to decline significantly. Urban expansion is found to contribute to the additional warming where new urban expansion concentrates, and afforestation seemingly

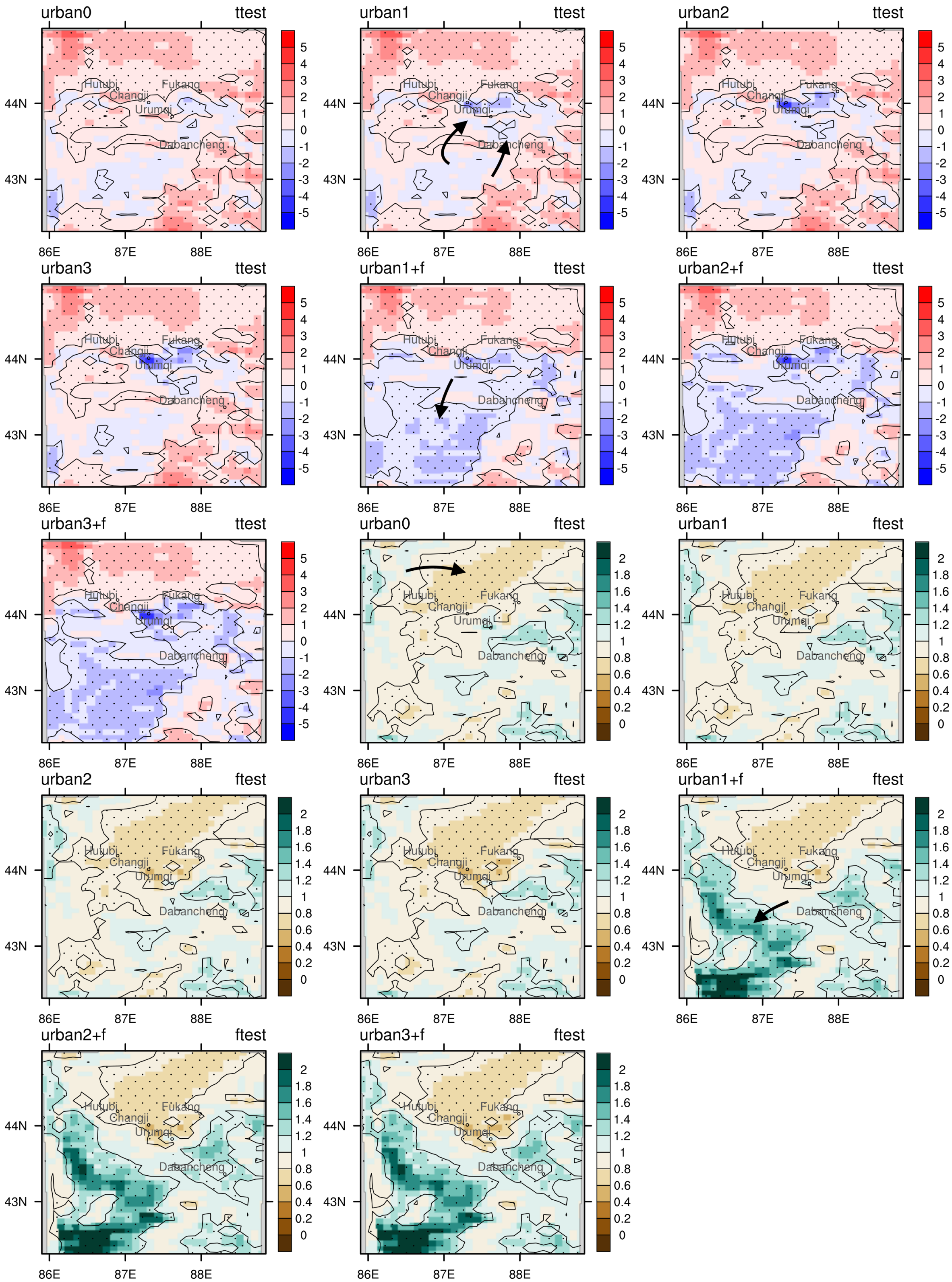

Figure 5.27 Wind speed change in 2030

reduces such effect. The impact of land cover data uncertainty is negligible.

- Precipitation

Precipitation change is dramatic but unrealistic. With most areas getting slightly wetter, the west side of the domain has significant precipitation changes in the order of hundreds of millimeters per year, equivalent to the total annual precipitation in this area. It is more likely that the simulations failed to produce realistic precipitation patterns, considering the overall precipitation variability in the western border from the more controlled experiments (aka. sensitivity tests for land cover uncertainty and urban scenarios).

- Wind speed

Wind is generally getting stronger and less variable in the 2030s. Urbanization significantly reduces wind speed in urban areas by as much as $5m/s$ in the most aggressive scenario. Afforestation further brings down the wind speed but to an unrealistic extent that reduces more than $0.6m/s$ almost everywhere south of 44 °N.

In general, the regional climate simulations are showing interesting spatial patterns within the global climate change context. Many of them are related to the urban change and afforestation scenarios, though some could be a manifestation of poor model performance. The land cover uncertainties were minor compared to the simulated climate change. However, it does not necessarily mean a good quality of input land cover data. It could also be possible that they have huge bias despite little variance within the time-series. The particular impacts of changing climate conditions, either from global forcing or local disturbance, need to be re-examined in the context of specific themes of urban sustainability, which is the focus of the next chapter.

CHAPTER 6

URUMQI'S SUSTAINABILITY UNDER FUTURE CLIMATE CHANGE

6.1 Introduction

Urumqi is facing an increasing threat from its limited water availability. On the supply side, Urumqi is fed only by a couple of short rivers (and their groundwater systems) that run from the top of Tianshan Mountains to salt lakes at dessert fringe. On the demand side, Urumqi needs to support over three million people and its water-intensive coal-petrol industries. This area also features extensive planting of some water-hogging crops, for example, cotton and alfalfa. In addition to Urumqi's own water shortage, over-consumption of water resources in this endorheic system will lead to drying-up of the terminal lakes. The case of the Aral Sea (Micklin, 2007) and the nearby Ebinur Lake (Liu et al., 2011a) may provide some insights on the environmental disasters associated with this problem.

In this chapter, several sustainability-related topics are explored which are within the scope of the Human-Land-Atmospheric system and particularly crucial to the Urumqi area. Each of the following sections was developed by comparing the future (2030s) conditions for that specific issue with the base year (2010s), supported by the simulated urban change and climate change results in addition to the theme-related local statistics and literature. Most of the following work is exploratory, in the sense of illustrating the analytic frameworks of the problems and potential usage of the simulation results.

6.2 Water supply and demand

6.2.1 Overview

According to Li and Tursun (2001), Urumqi's long-term average renewable water resources (annual flow of rivers and groundwater) are $11.48 \times 10^8 m^3/year$, around 40% of its total precipitation, including surface and groundwater from six drainage areas: Urumqi River ($4.74 \times 10^8 m^3$), Baiyang River ($2.88 \times 10^8 m^3$), Toutun River ($1.68 \times 10^8 m^3$), Chaiwopu lake ($1.45 \times 10^8 m^3$), and Alagou River($0.72 \times 10^8 m^3$). Urumqi's water consumption, on the other hand, has risen from $4.59 \times 10^8 m^3$ in 1995 to $10.89 \times 10^8 m^3$ in 2010 (Tang et al., 2013), quickly approaching the limit of its average water availability. According to the Statistics Bureau of Xinjiang Uygur Autonomous Region (2012), Urumqi's available water resource in 2011 was $9.85 \times 10^8 m^3$, but the total consumption was $10.68 \times 10^8 m^3$. The agricultural sector used 58.52% of the water, the manufacturing sector 21.72%, the service sector 1.87%, household-use 13.86%, and environmental protection[1] 4.03%.

Urumqi's renewable water resources primarily come from precipitation and glacier/snow melting, which compensate each other in hot/cold and wet/dry years (Li and Tursun, 2001). Recent climate change has reported having a significant impact on the availability of water resources. The Urumqi river, accounting for more than 40% of Urumqi's water resources, has an increased runoff at 2.2% /10a in the past 50 years (Lan et al., 2011). The primary factors are the increased precipitation and temperature in the mountain areas (Han et al., 2005; Lan et al., 2011; Saydi et al., 2015). Precipitation directly recharged surface and groundwater, which is the main reason for the increased runoff. The elevated temperature accelerated snow and glacier melting (Sun et al., 2013), which slightly and temporarily added to river flow but in the long-run will deplete the overall freshwater reservoir and weaken their ability to adjust intra- and inter-annual runoff balance.

Urumqi's water consumption has surpassed its annual water resource several times in the recent years. The need for securing its water supply is urgent. Besides overdrawing groundwater and transporting water from remote rivers, Urumqi also looks for ways to increase water-use efficiency. Table 6.1 presented data collected from multiple sources regarding Urumqi's water-use efficiency, compared with the national average and some global and national leading cases. In general, Urumqi consumes less water per capita and per 10k CNY of GDP than Chinese cities in average. The agriculture water use efficiency is relatively high, but the manufacturing water reuse rate and water leakage rate in municipal distribution networks are behind the national average.

[1] Water used in environmental protection includes landscaping water and water supplementing rivers, lakes, and wetlands.

Table 6.1 Water use efficiency

Indicies	Urumqi	National	Leading cases
Total renewable water resources ($m^3/perc$)	339[1]	454[3]	220.7 (Israel)[4]
Household daily water consumption ($L/perc$)	143.68[2]	170.94[2]	–
Productivity ($m^3/10kCNY$)	64[1]	129[3]	15.8 (Beijing)[5]
Manufacturing water reuse rate	70%[1]	85.7%[2]	94.07 (Tianjin)[2]
Agriculture water-use efficiency	0.62[1]	0.51[3]	0.773 (Israel)[6] 0.709 (Beijing)[7]
Municipal water loss	17.9%[1]	13.01[2]%	2.2% (Tokyo)[8] 7.82% (Denmark)[9]

Data sources: 1. He et al. (2014), 2. Ministry of Housing and Urban-Rural Development (2012), 3. Ministry of Water Resources People's Republic of China (2011), 4. FAO (2016), 5. Beijing Municipal Bureau of Statistics (2016), 6. Israeli Water Authority (2011), 7. Wei (2016), 8. Bureau of Waterworks, Tokyo Metropolitan Government (2014), and 9. Danish water and wastewater association (2016)

Nevertheless, when compared with national and global leading examples, Urumqi has potential to improve its water-saving practices.

Based on the expectation of climate change and urban development in the near future, both the supply and demand sides of water resources will fluctuate. The question here is how to assess them under the coupled Human-Land-Atmosphere system.

6.2.2 Climate change and water availability

As mentioned previously, precipitation and temperature are the primary determinants of Urumqi's annual renewable water resources. Cumulative precipitation (eq. 6.1) and Positive Degree Day (PDD, eq. 6.2) were calculated from the 2030 and 2010 climate simulations and their differences were examined by season and by location. The winter season (DJF) was not included because the first two months were discarded in model spin-up. Given the fact that winter is not the main season for snow-melting and its precipitation is much smaller compared to summer, the final result will not be affected much. The calculation also excludes the outmost five pixels of the simulation domain due to the strong edge effect discovered in Chapter 5. The differences among urban change scenarios are negligible in this case, so only the average results are presented.

$$C_{prcp} = \sum_{t=1}^{T} HP_t \tag{6.1}$$

Where HP_t is the hourly precipitation at time t

$$DD = \sum_{t=1}^{T} \frac{D_t}{n}$$
$$D_t = \begin{cases} TEMP_t - th, & \text{if } TEMP_t \geq th \\ 0, & \text{otherwise} \end{cases} \tag{6.2}$$

Where:

n is the number of time-steps in one day

$TEMP_t$ is the temperature in time t

th is the temperature threshold, in this case 0°C

Local precipitation is the ultimate source of various forms of renewable water in this area. Most of the precipitation occurs in the mountainous regions and summer months. As shown in figure 6.1, precipitation will decrease slightly in spring (MAM) and fall (SON), but increase in an average of 5 mm for the summer (JJA). The mountain (>1500m) and high mountain (>3000m) areas will receive 10 mm more. If 40% (Li and Tursun, 2001) of it becomes usable, the entire domain is expecting $3.16 \times 10^6 m^3$ more available water in the three seasons. $3.71 \times 10^6 m^3$ more water goes to mountain area that is more likely to become river runoff and recharge groundwater in the plain areas.

Temperature affects the melting of glaciers and snow cover. Most seasonal snow cover in lower altitude areas melt into water nevertheless. Only the high mountain area is sensitive to temperature change in a way that would affect annual water availability. As shown in figure 6.2, despite the overall warming trend, the high mountain area is getting cooler in spring ($-0.30°C \cdot d$) and fall ($-1.71°C \cdot d$) and slightly warmer in summer ($0.94°C \cdot d$). The ratio between PDD and glacier melting depth is called Degree Day Factor (DDF), which ranges from $0.98 - 14.3 mm \cdot^{\circ} C^{-1} \cdot d^{-1}$ in this area (Cui et al., 2013). Assuming peak DDF ($14.3 mm \cdot^{\circ} C^{-1} \cdot d^{-1}$) in summer and average

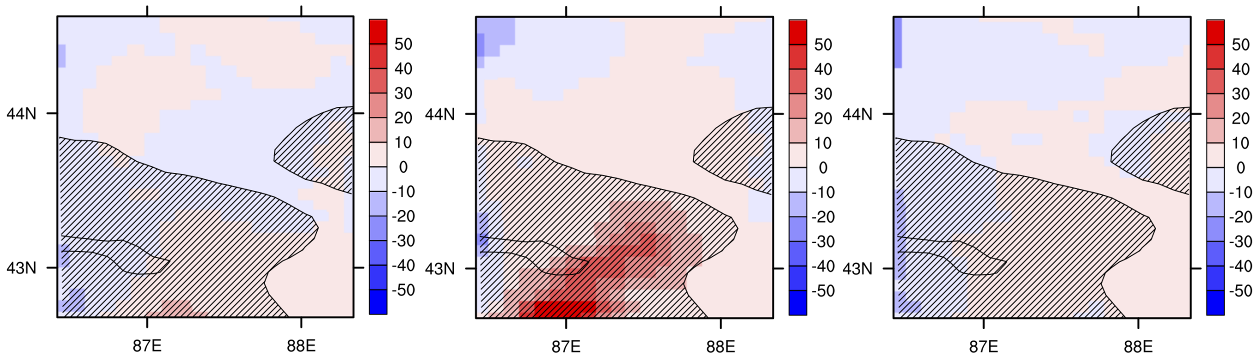

(a) MAM (b) JJA (c) SON

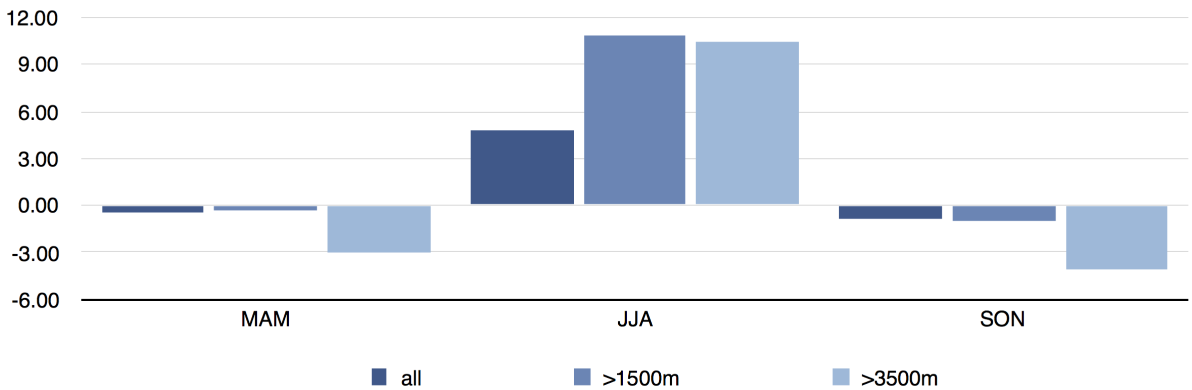

(d) Summary

Figure 6.1 Seasonal changes in cumulative precipitation

DDF ($7.64 mm \cdot ^{\circ}C^{-1} \cdot d^{-1}$) in spring and fall, the melting differences will be 13 mm, -2 mm, and -13 mm, respectively. The overall change is negative for the three seasons combined, indicating less water from glacier and snow melting in the 2030s compared to the 2010s. However, the amount of volume change is negligible given the limited area of glaciers and multi-year snow cover.

To sum up, the overall water balance between the 2030s and 2010s will be no more than $3.71 \times 10^6 m^3$ in this particular simulation, which is merely 0.3% of Urumqi's average annual water resources. The precipitation and snow-melting increase in summer and their decrease in spring and fall will further enlarge the seasonal gap in water availability. In that case, the city will face a greater challenge to redistribute its water equitably throughout the year. It is worth mentioning again that these estimates are tied to the particular simulation from the earlier chapter and many of the changes in temperature and precipitation are not statistically significant.

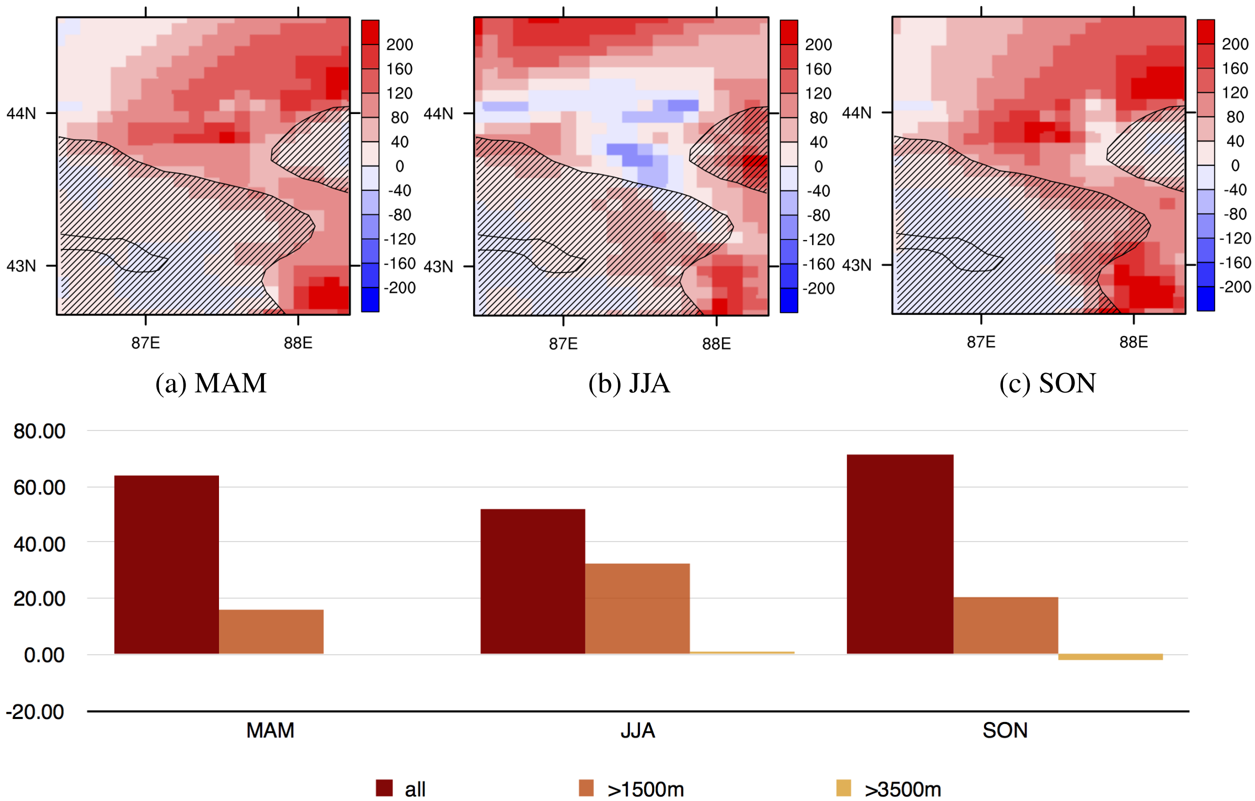

(a) MAM (b) JJA (c) SON

(d) Summary

Figure 6.2 Seasonal changes in Positive Degree Day

6.2.3 Urban development and water demand

In 2030, Urumqi is projected to increase its population by one third, GDP to nearly tripled, and urban area by 20%, 70%, and 120% based on different development scenarios, compared to 2010 (see chapter 4). Estimating future water demand can be simple or complex depending on the assumptions and number of factors taking into consideration. He et al. (2011) projected Urumqi's 2030 water consumption as $13.96 \times 10^8 m^3$ based on socioeconomic projections and published national water-use quota. Tang et al. (2014) used System Dynamics model to simulate the 2030 water usage under scenarios of different development speed and produced estimations ranging widely from 13 to 54 $\times 10^8 m^3$. All estimates have surpassed Urumqi's total water resources but to varying degrees. In this section, I will make several projections using simple methods based on the national quota and water-use efficiency. The purpose is not to produce the most accurate prediction but reasonable estimations that help in understanding the water stress as well as potential solutions.

Table 6.2 Quota based 2030 urban water use estimations ($10^8 m^3$)

	Scenario	Urban area $m^3/(km^2 \times day)$ GB1998	Urban area GB2016	Population $m^3/(perc \times day)$ GB1998	Population GB2016*
Quota		0.6-1.0	0.35-0.6	0.5-0.8	0.3-0.5
Estimates	S1	9.01-15.02	5.26-9.01	8.63-13.81	5.18-8.63
	S2	12.77-21.28	6.38-10.64		
	S3	16.53-27.54	8.26-13.77		

* GB2016 specifies water use for different urban land use. The aggregated quota was derived from applying the proportional change of the population quotas on the GB1998 urban area quota.

In 2016, the Ministry of Housing and Urban-Rural Development published a new Code for Urban Water Supply Engineering Planning (GB 50282-2016, GB2016 hereafter) to replace an older version (GB 50282-1998, GB1998 hereafter) that was frequently used in urban planning to estimate future urban water consumption. This code recommends water use quotas based on urban areas or total population. Table 6.2 listed various urban water estimates based on quotas from different years. Before looking into those numbers, it is important to know that these estimates are only for urban, not including agricultural use. If taking the 2011 agricultural water consumption, 6.25 $\times 10^8 m^3$, out from the long-term average of 11.48 $\times 10^8 m^3$ total water resources, the maximum water allowance for urban use, including manufacturing use, is 5.23 $\times 10^8 m^3$. GB1998 produces estimates from 8.63 $\times 10^8 m^3$ to 27.54 $\times 10^8 m^3$, well beyond the water availability. Only the most strict quotas in GB2016 produce estimates around the city's capacity, and just for the most conservative urban expansion scenario. Generally speaking, Urumqi must follow the most strict GB2016 quotas to contain its water consumption within its water availability, and it needs to do even better if it is seeking to expand its area more than the 20% scenario. To achieve such goal, Urumqi needs to make substantial efforts to improve its water-use efficiency.

Based on the 2011 water consumption data, table 6.3 tweaks several efficiency-related indices thus provide both future estimates and the potential water-saving benefit from improving water-use efficiency. Agriculture has the biggest share in today's water consumption. Assuming the net

Table 6.3 Efficiency based 2030 water use estimations ($10^8 m^3$)

Sectors	Water use 2011		Water use 2030 Current	Improved	Advanced
		Agriculture water-use efficiency	62%	70%	77%
Agriculture	6.25	Estimates	6.25	5.54	5.03
		Water consumption m^3 per 10k CNY GDP	30.56	20	8.34
Manufacture	2.32	Estimates	5.01	3.28	1.37
		Water consumption m^3 per 10k CNY GDP	2.2	–	–
Service	0.20	Estimates	0.43	–	–
		Daily water consumption $L/perc$	143.68	140	130
Household	1.48	Estimates	2.48	2.42	2.24
Environment	0.43		0.43	–	–
Total	**10.83**		**14.61**	**12.10**	**9.51**
Municipal		Leakage rate	17.9%	7.8%	2.2%
water leak	0.58	Water-saving	–	0.33	0.51

water use in the agricultural sector remains the same[2], improving water-use efficiency from 62% to 70% and 77% will save 11% and 20% of agricultural water, respectively. Manufacturing water use is the second biggest portion which is expected to grow considerably in the future. If there is no improvement in efficiency, manufacture will use 116% more water than 2011. Improving water consumption to 20 and 8.34 m^3 per 10k CNY GDP will change the balance to +41% and -41%, respectively. Household water use is directly related to population growth and has the smallest elasticity. Keeping the 143.68 L daily consumption level requires 1 $\times 10^8 m^3$ more water for the additional population. The 140 and 130 L scenario will save 2% and 10% respectively compared with no improvement. Assuming the environmental use stays the same, and the tertiary sector remains its low water demand, meaning only 0.23 $\times 10^8 m^3$ more water from these two sectors. Moreover, improving the leakage rate in the water-distribution network to 7.8% and 2.2% will save 0.33 $\times 10^8 m^3$ and 0.51 $\times 10^8 m^3$ respectively.

In summary, if keeping today's water use habits, Urumqi's annual water consumption is estimated to reach 14.61 $\times 10^8 m^3$ in the year 2030. If improving water-use efficiency, the annual water consumption may be limited to 12.10 or even 9.51 $\times 10^8 m^3$ if today's most advanced water-saving practices can be adopted. The biggest water-saving potentials lie in the primary and secondary

[2]The loss of agricultural land to urban expansion was not considered because (1) its relatively small area and (2) the governmental regulation that requires restoring the same amount of cropland.

sectors and municipal water-distribution infrastructure. Together they would save 2.68 $\times 10^8 m^3$ annually, which is more than enough to support the additional 1 $\times 10^8 m^3$ household water demand.

6.2.4 Summary

Urumqi is an oasis city facing tremendous water stress. Its annual water consumption is approaching its long-term average of renewable water resources and is expected to increase as the population and economy continue to grow. Urumqi already has no resilience to inter-annual water variability. In the case of a dryer than normal year, Urumqi will face immediate water shortage. Regional climate simulation provides a basis for estimating future water supply through precipitation and temperature projections. The particular simulation results in this study suggest slightly increased precipitation and possibly decreased snow-melting in the 2030s, which in total would increase $3.71 \times 10^6 m^3$ for Urumqi's annual water availability. Neither the urban change nor the afforestation scenarios have significant impacts on this estimate.

On the other hand, even the most strict national water use quota cannot guarantee Urumqi's water security in 2030. The estimated urban water consumption ranges from 5.18 to 27.54 $\times 10^8 m^3$ depending on urban expansion scenarios and different quotas. The water consumption is projected to be $3.13 \times 10^8 m^3$ more than its average water availability if keeping today's water use efficiency. It is equivalent to 3/4 of the Urumqi River or 1/25 of the total mountain glaciers in this area if considering water import and glacier exploitation as solutions to Urumqi's water problem. In the case of adopting the state-of-art water-saving practices, the overall water consumption can potentially be reduced by $5.61 \times 10^8 m^3$, even less than the current water use, despite a one-third increase in population and nearly tripled GDP. It does depend on any uncertain technological innovations, but the success stories in more developed areas around the world, e.g., Israel, Tokyo, Beijing. Substantial capital investments are inevitably required, but in the long run, they may justify themselves considering the alternative costs on the unstainable solutions. However, the financial feasibility of any water-saving project is beyond the scope of this study.

6.3 Agriculture productivity

6.3.1 Overview

Population growth and economic development generally require more agricultural production. Agriculture is an integral part of sustainable urban development. It provides food and raw materials for urban consumption and is under constant stress from urban growth (competition for land, pollution). In the Urumqi area, most recent and prospective urban expansions occurred or will occur on agriculture lands, according to historical data and future simulations. The future urban change simulations for the three scenarios result in 90, 247, and 372 km^2 agriculture lands lost respectively. Although the governmental regulation requires cropland restoration somewhere else, the makeup lands are often of less quality. On the other hand, future climate change, together with land cover change, will alter the agroclimatic/agrometeorological environment of this area, impacting agricultural suitability and productivity in various ways.

Urumqi has limited agriculture land within its administrative boundary, but the neighboring Changji region is a major agricultural base in North Tianshan area and is closely connected and under the impact of Urumqi urban area. Therefore, Changji is included as part of the greater Urumqi area (Wu-Chang) in this case. According to Statistics Bureau of Xinjiang Uygur Autonomous Region (2015), Urumqi and Changji have a total of 6090 km^2 sown area, with 50% for grains, 22% for cotton, 9% for vegetables, 7% for oilseeds, and 12% for others. The main grain crop here is wheat and corn. Another 191.5 km^2 is devoted to fruit orchards, of which 53% for grapes and 14.3% for apples.

Agriculture lands in Urumqi area (see figure 4.11 for reference) lie primarily on alluvial plains north of Tianshan Mountains. They surround cities and towns and span from mountain foothills to the edge of the desert. Most of them are below the elevation of 1000 m. Another agricultural agglomeration is to the south and southwest of Urumqi, in the Chaiwopu-Dabancheng Valley, with the elevation between 1000m and 1500m. In the following of this section, these two areas will be referred as the plain and valley agriculture areas, respectively.

The general agroclimatic environment here can be described as short growing season, low and (spatially and temporally) uneven heat and precipitation, high diurnal temperature variation, and ample sunshine hours (Pu and Zhang, 2011). The major weather-related hazards include drought, cold waves, late/early frosts, and high winds (Liu, 2011). All these conditions may change due to future climate change and urban expansion. In the following of this section, I will explore future agroclimatic resources and agrometeorological risks based on climate simulation results.

6.3.2 Agroclimatic resources

Agroclimate describes the relationship between crop adaptation and climate. Solar radiation, heat, and rainfall are the major factors that determine the type of crops to grow and their potential yield and quality. In areas with advanced irrigation coverage, such as Urumqi, precipitation matters only indirectly through surface and groundwater systems and overall water budget. Heat is, therefore, the dominant uncontrolled variable and is also projected to change significantly in the future.

Four indices were selected to depict Urumqi's agroclimatic environment, including the length of Growing Season (LGS, day), Growing Degree Day (GDD, $^{\circ}C \cdot day$), maximum summer temperature (TMAX, $^{\circ}C$), and average Daily Temperature Range (DTR $^{\circ}C$). LGS is defined as the longest freeze-free (temperature > $0^{\circ}C$) period that permits normal plant growth. A short LGS is often a major limitation for local crop selection. The GDD is the cumulative degree days with a temperature base of $10^{\circ}C$. GDD is a good indicator for many aspects of crop development, e.g., suitability, growing-stage and even pest life cycles. TMAX is the temperature extreme that affects crop suitability, especially for cotton, a staple crop in this area. DTR, or diurnal temperature variation, is the difference between the maximum and minimum temperature of the same day. Larger DTR leads to better nutrition and dry matter accumulation for many crops. All these indices were calculated for the RAMS regional climate simulation results for both the base (2010s) and future (2030s) years (discussed in section 5.4.4). Again, only March to November were included in the calculations. The lack of winter months will not cause big problems here because they are usually outside the growing season.

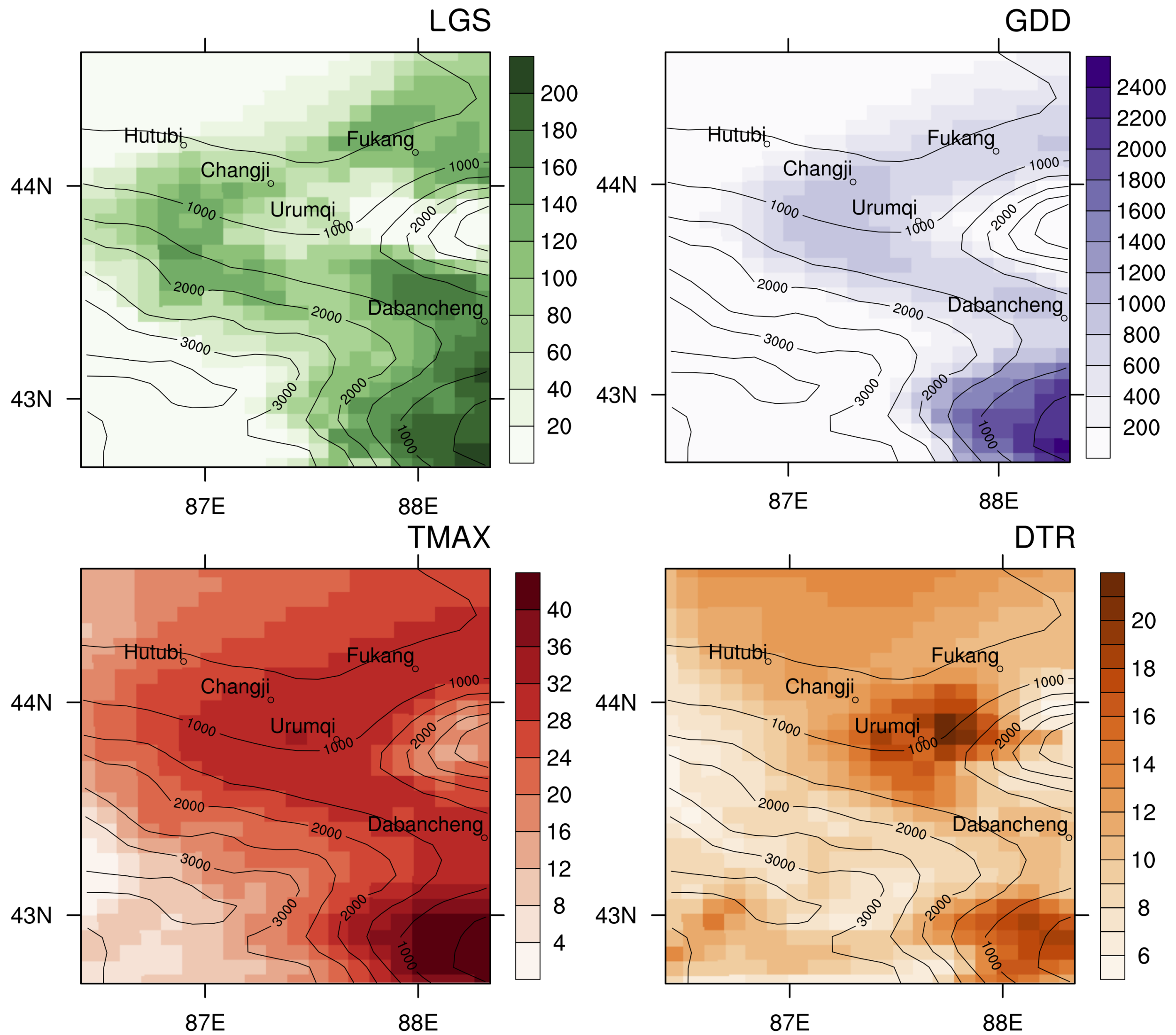

Figure 6.3 Agroclimatic resources 2010

The base year results show increasing heat resource from north to south and from mountain to valley and plain (figure 6.3). It is worth mentioning that LGS, GDD, and TMAX all seem underestimated compared to Urumqi's historical records. According to (Pu and Zhang, 2011), the average LGS, GDD, and TMAX at northern alluvial plains are 140-170d, 2400-3200$^{\circ}C$, and 33-37$^{\circ}C$, respectively. The northwest corner is most problematic for the simulated climate with LGS less than 20d, GDD less than 200$^{\circ}C$, and TMAX smaller than 20$^{\circ}C$. The DTR seems somewhat close to what was reported in the literature (12$^{\circ}C$).

Estimated changes in the four indices of different scenarios were calculated by subtracting

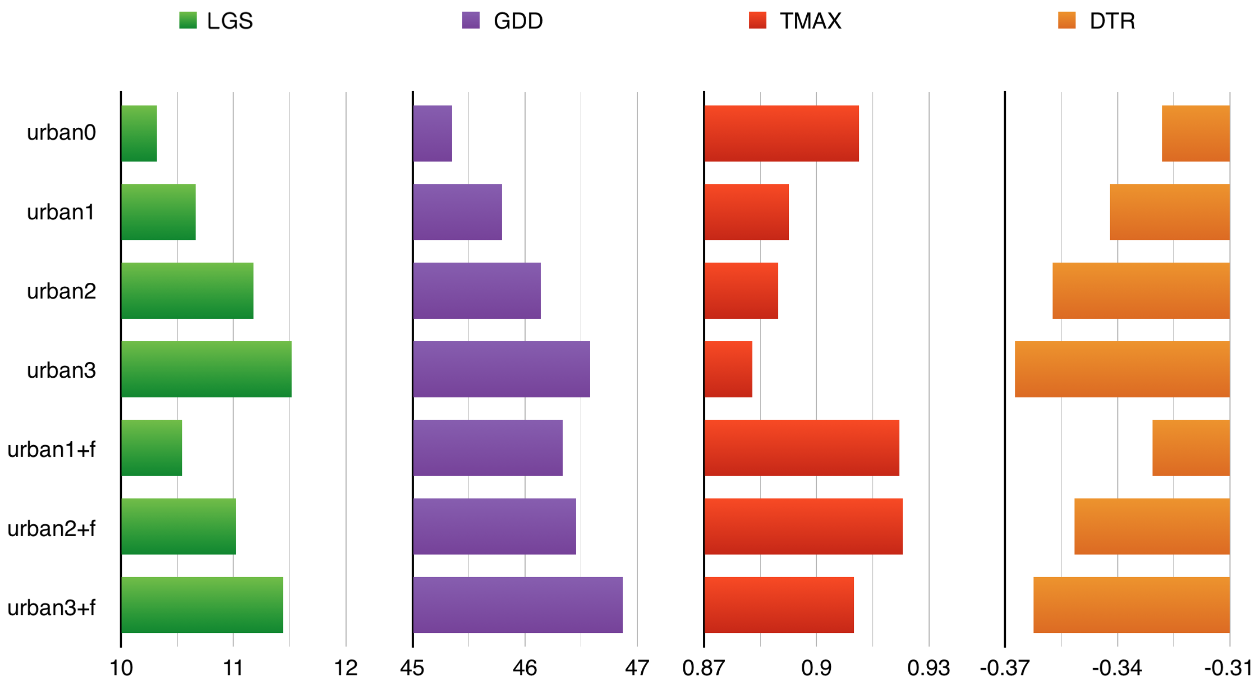

Figure 6.4 Changes in agroclimatic resources by scenario

the base year value from simulated future values. Both the base and future year are a collection of multiple years, so the average annual values were presented. The average changes across the domain were summarized by scenario (figure 6.4). Overall, LGS, GDD, and TMAX are estimated to increase while it is the opposite for DTR. Urbanization impacts positively on LGS and GDD, but negatively on TMAX and DTR. Afforestation mitigates the impact of urbanization on LGS and DTR but aggravates it on GDD and TMAX. The spatial variation of these variables only differ slightly among scenarios, so just the urban2 scenarios were further examined.

As shown in figure 6.5, the alluvial plains to the north get longer LGS and increased GDD, except for a narrow band following 44 °N and ends near Fukang. The valley agricultural area to the south receives shorter LGS and less GDD despite the overall warming trend. It seems like urban expansion increases heat in situ but causes cooling in its downwind nearby places. TMAX rises at most locations, but drops a little in a large triangular area covering Hutubi, Changji, Urumqi, and almost reach Dabancheng. DTR mostly shrinks except areas near the western border. The place with the greatest drop in DTR sits in the city of Urumqi.

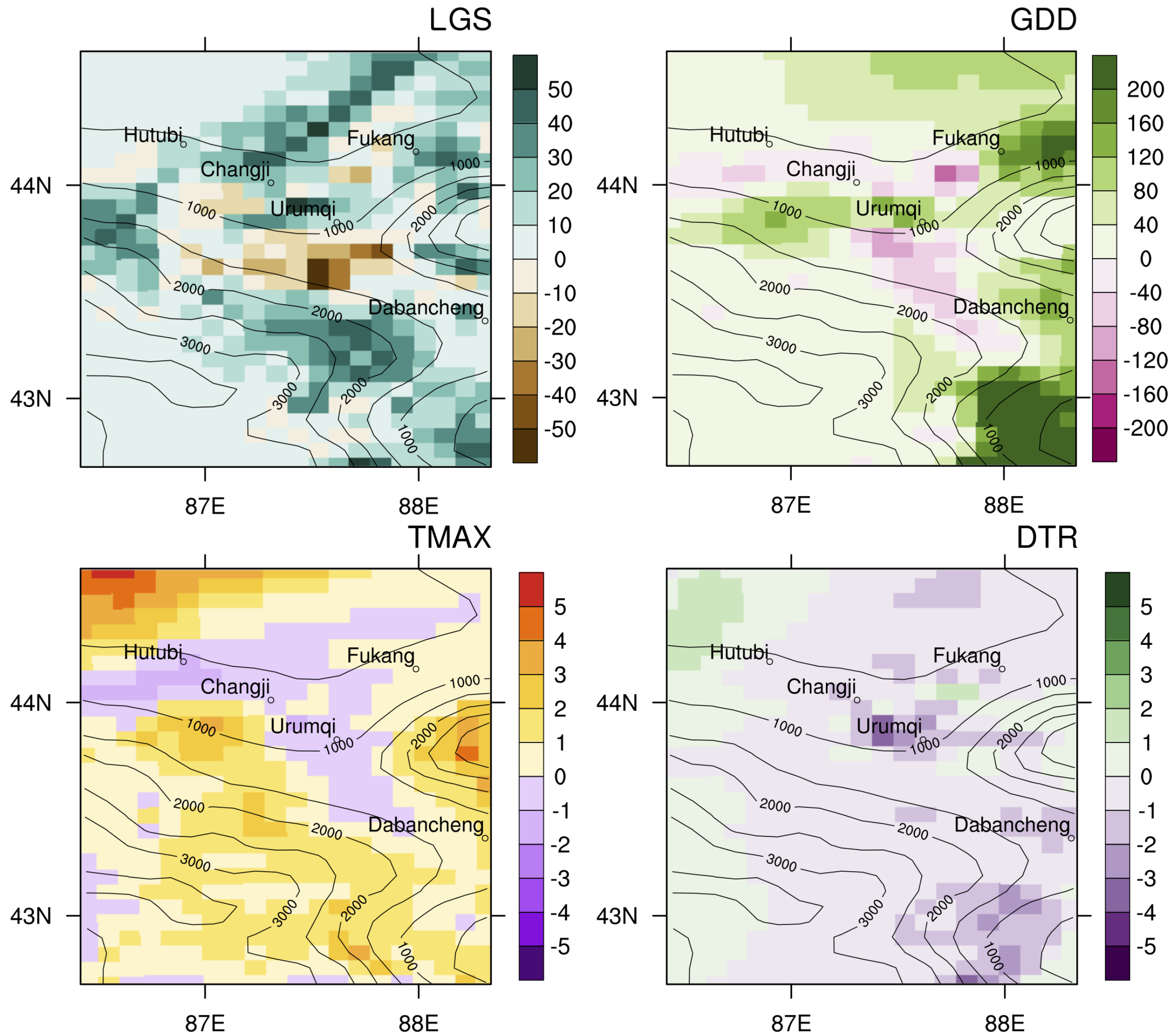

Figure 6.5 Changes in agroclimatic resources: scenario urban2

6.3.3 Agrometeorological risks

Agrometeorological risks usually associate with some weather events that could be detrimental to crop growth. Some of the events are extreme and harmful by themselves, e.g., drought, cold wave, and high wind; some are normal but dangerous when happening in unusual times, e.g., late spring frost and early fall frost. Just like in the previous section, the impact of precipitation becomes complicated as a result of intensive irrigation coverage. Only the temperature and wind speed based indices were examined in the following.

Four indices were selected to illustrate agrometeorological risks in Urumqi area (figure 6.6).

Cold Wave (CW) is the number of times with temperature dropping greater than $8°C$ within 24 hours or $10°C$ within 48 hours and with the minimum temperature below $4°C$. Plants may suffer cold injuries during cold waves, with or without temperature dropping to freezing, leading to poor growth, loss of harvest or even plant death. High Wind (HW) counts the number of days with maximum wind speed above $17m/s$. High winds could damage tall plants, field structures, and also aggravate the impact of cold, heat and drought. Last Frost (LF) is the last date that has a minimum temperature below $0°C$ before the longest freeze-free period (growing season). If the last frost comes later than usual, it will damage the low cold-hardiness crops that have been planted following old schedules. First Frost (FF), in the opposite, is the first date that temperature drops below $0°C$, marking the end of growing season. An earlier first frost may catch the farmers unprepared and their harvest loss due to freeze injury. LF and FF were presented as the number of days after March 1st, and both were set to 0 for places with year-round freezing.

Estimated changes in the four indices of different scenarios were calculated by subtracting the base year value from simulated future values. The average changes across the domain were summarized by scenario (figure 6.7). Both CW and HW are estimated to increase their frequencies in 2030 for basic urbanization scenarios. Urban expansion seems to slow down the increase. Afforestation further increases CW but decreases HW to be even lower than 2010. LF and FF are brought forward/backward respectively as warmer climate expand the growing season. Urban expansion further extends the growing season. Afforestation does not affect the length much but seems to move the entire growing season a little later.

Results for the urban2 scenario is examined in detail as all have similar spatial patterns. For CW, the plain area between 500m and 1000m generally gets fewer events of cold waves. The area lower than 500m and the valley area are expecting more of them. Most agriculture areas are getting slightly more HW. The area between Changji and Hutubi is a little complicated, with decreasing HW in lower places and significant increase around the elevation of 1000m. Dabancheng is getting considerably more HW as well. Late LF may strike the valley area. Early FF will impact a large area including the 1000-1500m valley area and the 500-1000m plain area. The drastic

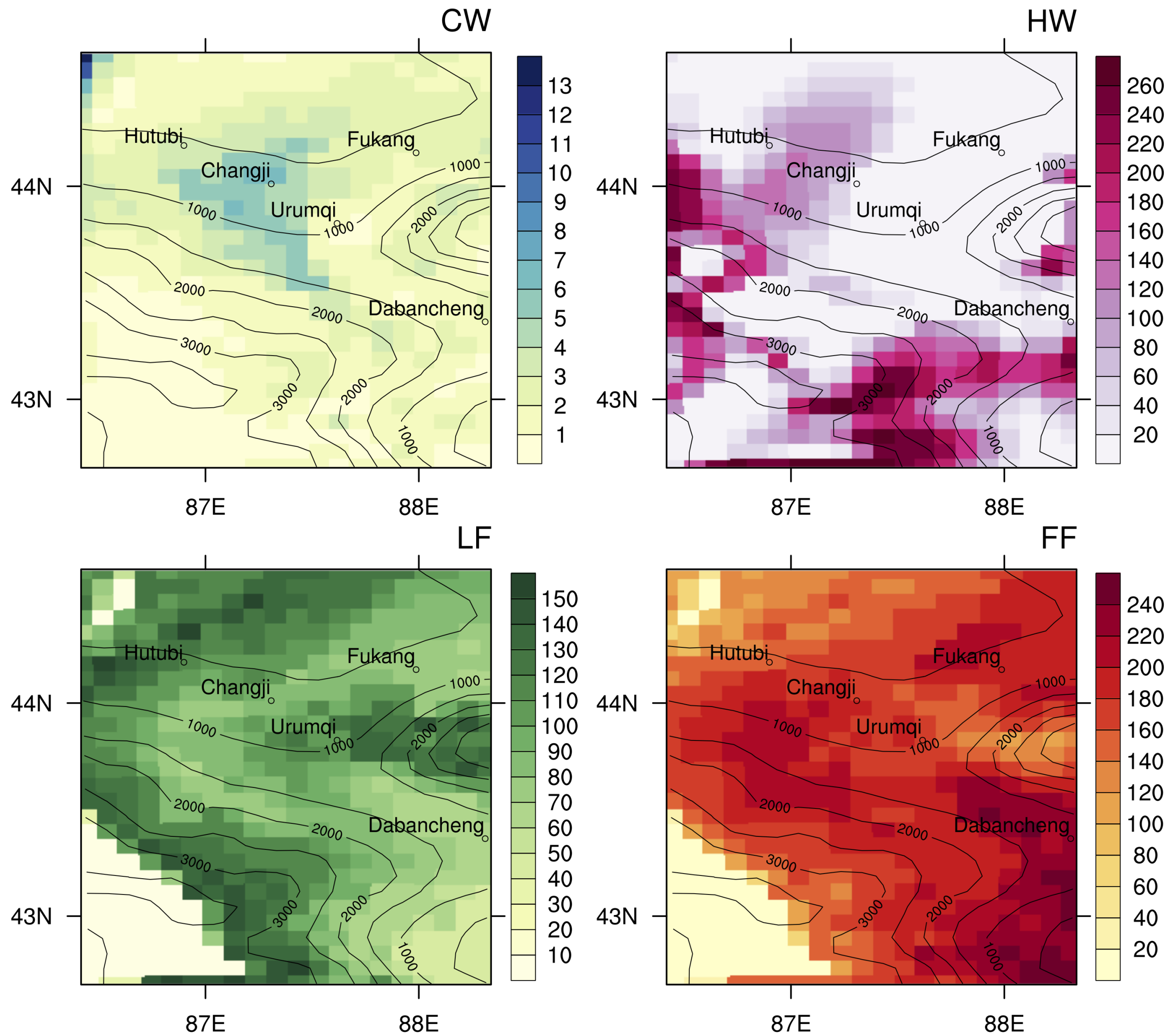

Figure 6.6 Agrometeorological risks 2010

changes in the northwest corner are, however, less important because the simulated growing season is extremely short (see figure 6.3).

6.3.4 Summary

Four variables were calculated to illustrate the spatial pattern of agroclimatic resources, including the length of growing season, growing degree days, maximum temperature, and daily temperature range. Another four variables were calculated to show local agrometeorological risks, including cold waves, high winds, last frost, and first frost. A rough comparison with historical record

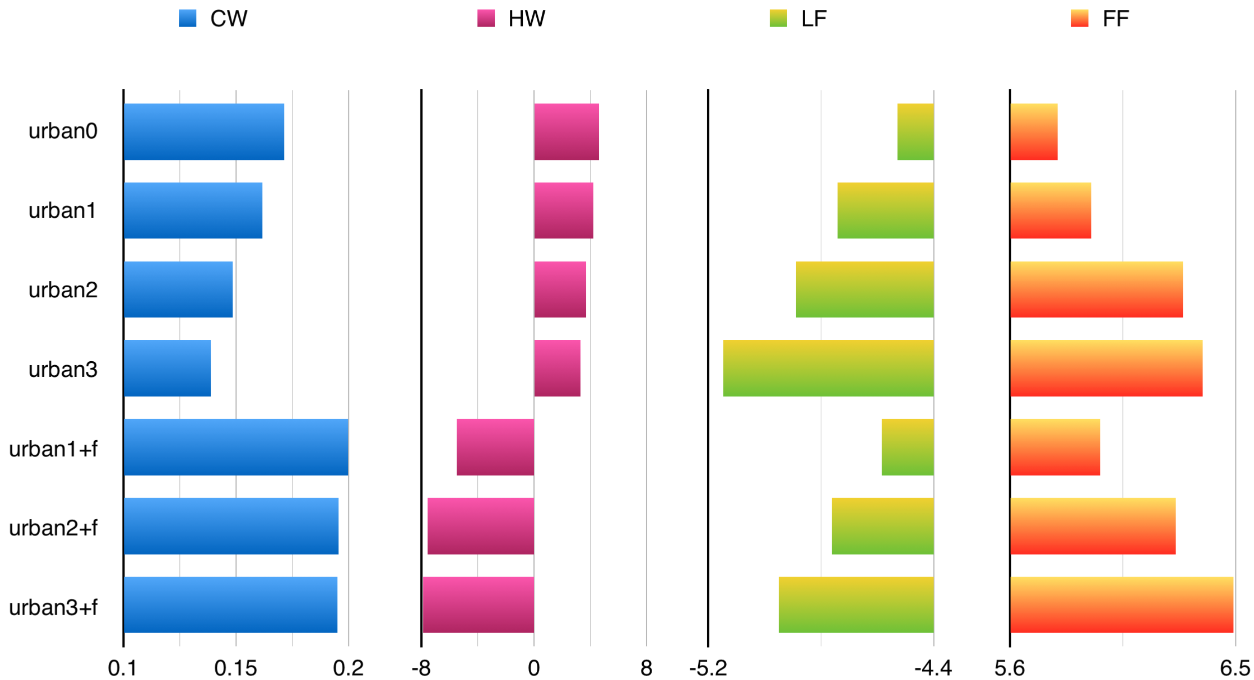

Figure 6.7 Changes in Agrometeorological risks by scenario

revealed substantial underestimation of heat resources. The future-current comparisons of those variables unraveled complex patterns that could impact different agriculture production areas differently. The comparisons among urban and afforestation scenarios are potentially informative when assessing the impact of specific scenarios on agriculture productivity and vulnerability.

6.4 Discussion and conclusions

Two sustainability-related topics were discussed in this chapter. Water availability may be the single most natural constraint on Urumqi's future development, while agriculture is probably the sector that future climate change will impact most.

For water, regional climate simulations supported the estimation of future water resource availability. On the consumption side, even following the most strict water-use quota cannot prevent Urumqi from water deficiency. If no significant improvement is to be made on water-use efficiency, there will be a water deficiency at $3.13 \times 10^8 m^3$ per year, around 30% of Urumqi's current annual renewable water. Fortunately, if adopting the best water-saving practices available today in the field of, e.g., irrigation, industry water reuse and leakage prevention in municipal water network,

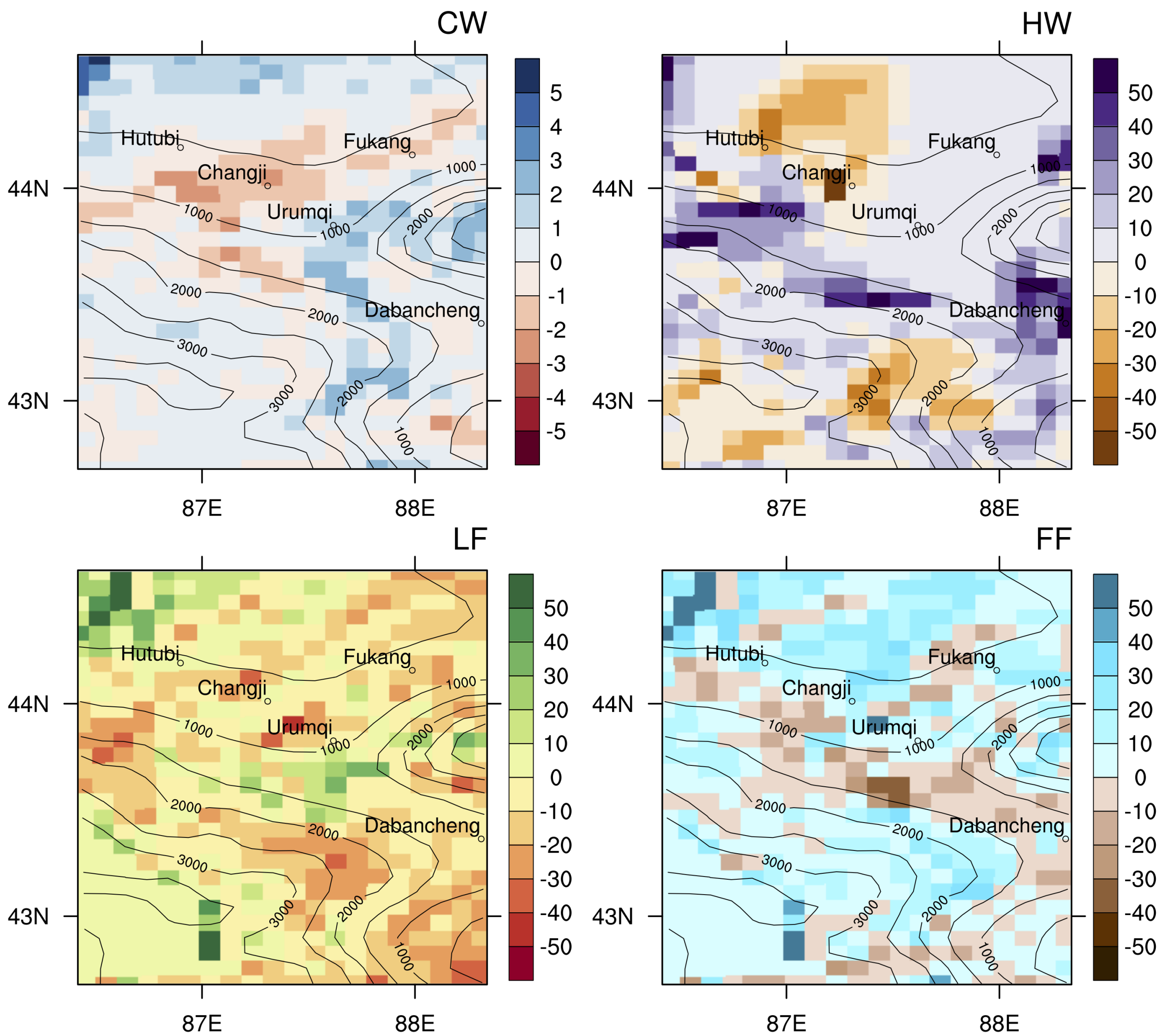

Figure 6.8 Changes in Agrometeorological risks: scenario urban2

the water usage can be contained within sustainable levels.

Agriculture in Urumqi area will lose some land to urban expansion but could potentially benefit from a warmer climate through increased heat resources. Both agroclimatic resources and agrometeorological risks were evaluated using the temperature and wind speed outputs from regional climate simulations. Complex patterns of those variables emerge in response to both the warming trend and different urban and afforestation scenarios. Although the results may not be directly usable due to their substantial discrepancies with the historical records, they suggest the need for future research to investigate climate change impact for different agriculture areas.

Many more themes are potential candidates to discuss within the Human-Land-Atmospheric framework. For example, the weaker wind brought by the urban expansion will lead to poorer air quality in the city. It may also impact energy generation at the famous wind farms in the Chaiwopu-Dabancheng valley. Temperature changes, especially in the hottest and coldest months will alter water consumption, energy use, and air quality consequently. Different urban change scenarios, with substantial variations in population density, are inherently different in potential traffic preferences, which in turn affect energy consumption and air quality.

CHAPTER 7

GENERAL DISCUSSION AND CONCLUSIONS

7.1 Summary and conclusions

The ultimate purpose of this study was to explore Urumqi's sustainability under the impact of both urban expansion strategies and climate change. Different urban development strategies should yield distinct urban expansion trajectories regarding total area and spatial pattern. Those urban change scenarios potentially affect how global climate change manifests at regional and local scales. Both urban change and climate change may increase Urumqi's vulnerability to climate change and diminish prospects for sustainable development.

To explore potential outcomes, a coupled Human-Land-Atmospheric modeling framework was used to unravel the consequences of the human decision on urban expansion and then on local climate. It combines statistical models for population, GDP, and urban area predictions, the Dyna-CLUE model which simulates land use change spatially and dynamically based on locational suitability and competition between different land uses, and the RAMS model which dynamically downscales general circulation according to local land surface conditions. The outputs of this modeling framework, i.e., urban and climate patterns in 2030 corresponding to different development strategies, were used to support preliminary investigations on sustainability-related issues, e.g., the city's water security and agricultural productivity.

Historically, Urumqi is high in urbanization rate, i.e., urban population percentage, but low in urban land use intensity, in terms of population and GDP densities in urban areas. Three different scenarios were developed based on various predictions to represent different urban use intensities in 2030. All predictions were based on a population of 3.25 million and GDP of 365.23 billion CNY, as predicted by the time-series models.

The conservative scenario leads to an urban land intensity similar to other major Chinese cities. It yields a 20% increase in urban land area from 2010 to 2030. In this scenario, predicted by the

Dyna-CLUE model, the urban area will expand from the northern fringe of Urumqi city and along the transportation axis between Urumqi and Changji city. The planning scenario respects the published land use/urban planning documents. In this scenario, the urban land area will increase 70%. All urban and industrial establishments to the north of Tianshan Mountain will grow significantly, including northern Urumqi, Changji, Wujiaqu, Ganquanpu, and Fukang. The West Mount area also starts to see some new urban developments. The aggressive scenario represents the business-as-usual, which maintains low urban land use intensity and will require a 120% increase in the urban area to accommodate growing population and economy. In this scenario, two new urban clusters, Urumqi-Changji and Ganquanpu-Fukang, are formed from previously disconnected urban patches. Also, Urumqi's aggressive afforestation plan was extracted from local planning maps to evaluate its effect on top of urbanization scenarios. As a result, six different urban expansion scenarios were produced. Three of them are the above listed and three with added afforestation.

It is also worth mentioning that a new index, the multi-resolution adjusted-kappa, was developed to support calibration and validation effort for land use change simulation using the Dyna-CLUE model. The new index compares simulated land use pattern with reference focusing on the changed area and match on general patterns. Six different model setups were proposed and tested using this new index. The best match was at 0.67 in the calibration phase (1990-2000) and 0.62 in the validation phase (2000-2010).

The six scenarios, together with the baseline 2010 urban land map, were passed into RAMS to test the sensitivity of future climate change. The non-urban areas were filled by modal land cover type from MCD12Q1 2001-2012. The global forcing uses the NASA-GISS-E2H model, and the years 2028, 2029, 2031, and 2032 from RCP 4.5 were selected to present a hot 2030 climate. However, the RAMS simulation results suggest that urban change scenarios introduced no statistically significant impact on temperature. The differences in the average precipitation were not significant either, but some areas were significant in terms of variance change, including the core urban area which was predicted to have more intense but less frequent precipitation. The wind speed is found to be significantly lower and with less variance at urban area. The afforestation introduced stronger and more extensive wind speed decrease, which may be unrealistic, and increased wind speed variation in mountain areas. In general, the magnitude and spatial extent of those difference are positively related to the degree of urban expansion.

Before looking at climate change, the uncertainty propagation effect from land cover input to RAMS was evaluated for the MCD12Q1 product. It was found that nearly 10% of the pixels in the simulation domain may be incorrectly classified due to categorical uncertainty in grassland-cropland and grassland-barren types. A binary control model was developed to generate alternative land cover maps from the categorical uncertainty. The sensitivity of climate simulation to those uncertainties was tested in RAMS. The experiment suggests a significant impact on latent heat flux primarily due to the different settings in soil moisture for cropland and grassland. No significant effect was found for temperature and wind speed, but the precipitation variance was slightly affected by land cover data uncertainty.

To assess the climate change, the four recent hottest years (1997, 2001, 2006, 2008) were chosen to represent a current hot climate and simulated using the same parameterization as in the future simulations. The collection of future and present hot years were then compared statistically to reveal changes. Temperature, precipitation and wind speed were all found significantly different in both mean and variance. The magnitude of those changes was well above the uncertainty introduced by land cover inputs. In general, most of the area was found to become hotter but with smaller temperature variance. The overall precipitation is predicted not to change much, but most of the area will experience more intense but less frequent rainfalls. The wind speed will increase in most places except urban areas. However, some of the results are not realistic, especially for precipitation.

Finally, two sustainability-related topics were explored. Water resource availability is the primary natural constrain for Urumqi and agricultural productivity as the most affected sector under climate change. It was illustrated that the coupled Human-Land-Atmospheric modeling framework could be used to help evaluate future water supply/demand, agroclimatic resources, and agrometeorological risks.

7.2 Research limitations

Although the possible uses of the proposed modeling framework are presented, the specific projections from this study may not satisfy the need of real-world decision-making. The limitation lies in both the breadth and depth of this research, as sustainability assessment of a city requires a comprehensive understanding of nearly every aspect of city functioning. This study delved into a few sub-systems, i.e., population, economy, land use, climate, water, and agriculture, in relatively simple ways, the synergy of which is still not sufficient to present the big picture of Urumqi's sustainability under future climate change. Listed below are some specific limitations.

• Simple land-atmosphere interaction

The insignificant impact of the dramatically different urban expansion scenarios on local climate is possibly a side effect of the inadequate representation of the urban land-atmosphere interaction. Urban land was simply treated as a uniform artificial cover on the land surface. It differs from other land covers only in physical conditions, such as radiative reflectance, evapotranspiration, and surface height, etc.. The intensive human activity and associated waste heat emission are completely ignored, and may be a significant contributor to urban heat islands (Li and Zhao, 2012).

• Insufficient simulation accuracy

The urban land change simulations achieved no better than 70% accuracy even in the calibration phase. It was not a huge concern due to the coarse resolution used in regional climate simulations (8*km* in RAMS vs. 120*m* in Dyna-CLUE). However, if the predicted urban land use pattern is used in evaluating other sustainability-related issues, for example, transportation and infrastructure, the current model accuracy may become a consideration. The quality of regional climate simulation directly impacted the intended sustainability assessment. Realistic evaluations on water resource availability and agroclimatic conditions could not be achieved due to the substantial underestimation of temperature and precipitation. Moreover, the tested land cover uncertainties represent only a small portion of the potential uncertainties inherent in the modeling framework. The high computational burden of regional climate simulations discourages more extensive uncertainty investigations.

• Unaccounted uncertainties

The uncertainty impact of MODIS land cover products on RAMS simulations were investigated in this study. However, it presents only a limited portion of the uncertainty within the modeling framework. Every modeling component and their interactions could suffer from uncertainty pitfalls. Especially for the regional climate simulations, there are plenty of other model inputs that could suffer great uncertainty, such as topography. The particular GCM used in this study is only one of the dozens of widely different GCMs included in the IPCC reports and may or may not be representative. Ideally, more GCMs need to be incorporated to construct probability based future estimations and more extensive and accurate observations will be needed to calibrate and reduce model biases. However, the computational burden of regional climate simulations will become a major obstacle for extensive uncertainty investigations.

• Inadequate social dimension

As mentioned in section 3.2.2, the Uygur-Han ethnic contention can be a major obstacle for Urumqi to function and thrive. Unfortunately, the HLA system analysis in this study contributed nothing to the understanding of or the solution to this problem. It is hard to imagine easing the historically and culturally rooted conflict using solely urban planning measures. Besides, the livelihood of other ethnic groups need to be considered given that the macro economic development policies may interfere with their traditional lifestyles. In one word, the potential inter-group imbalance of opportunities and different vulnerabilities under climate change and various urban development strategies should not be overlooked.

Despite the various shortcomings, the coupled HLA system modeling efforts presented a constructive step towards the more comprehensive and scientifically founded sustainability assessment for alternative urban development decisions.

7.3 Prospects

The major contribution of this study is the design and implementation of the coupled HLA modeling framework. It fills the gap of the decision-support process for addressing various HLA related sustainability concerns at the local level. The HLA modeling framework and its supported systematic approach are generalizable. It can be readily adapted to a different study area where the climate consequences of urban development strategies are of interest. The analysis workflow presented in this study may provide direct guidance for places with similar environment and problems, such as many other semi-arid cities in northwest China and Central Asia. However, it is more likely that the location specifics of a new study area will require a different set of factors to drive process models and a different set of model outputs to address particular sustainability concerns.

Attempting to thoroughly assess urban sustainability within the coupled HLA system through single-person effort is worthwhile but likely not ideal. The breadth and depth of sustainability science questions would be better served by a multi-disciplinary research team. The challenge of co-operation often lies in, as in any interdisciplinary research, the communication among experts with different expertise, research scopes, and terminologies. Nevertheless, the effort of this study presented potential benefits as well as pitfalls when integrating all the different models to investigate urban system dynamics and sustainability.

Under a teamwork setting, more models can be integrated into the framework to assess a larger set of sustainability-related issues and in greater depth. For example, air quality simulations can be integrated to assess the impact of urban and climate change on Urumqi's toxic winter air. Transportation models can improve land use change prediction and evaluate changing traffic patterns under different urban expansion paths. Hydrological models are capable of predict soil moisture, surface runoff, and groundwater balance, as well as water pollution which reduces already inadequate water supply. With well-organized modeling frameworks and some successful case applications, the coupled HLA modeling framework and associated sustainability evaluation method will be applicable in any city if general uncertainty and location specifics are well considered.

More interested parties need to get involved to make the modeling work policy-relevant. Local government and planning departments should play a leading role in initiating and sponsoring interdisciplinary sustainability assessments using coupled HLA modeling frameworks. Such assessments can be incorporated into the effort of developing periodic socio-economic, land use, and urban master plans. The involvement of local communities will ensure successful identification of local vulnerabilities and promote social equity through public-participation in the policy-making process.

BIBLIOGRAPHY

BIBLIOGRAPHY

Alberti, M. (1996). Measuring urban sustainability. *Environmental impact assessment review*, 16(4-6):381–424.

Aldrich, R. C. (1975). Detecting disturbances in a forest environment.[erts land use surveys].

Anas, A. and Liu, Y. (2007). A regional economy, land use, and transportation model (relu-tran©): formulation, algorithm design, and testing. *Journal of Regional Science*, 47(3):415–455.

Anderson, T. R. and Egeland, J. A. (1961). Spatial aspects of social area analysis. *American Sociological Review*, pages 392–398.

Barbier, E. B. (1987). The concept of sustainable economic development. *Environmental conservation*, 14(02):101–110.

Barry, S. and Elith, J. (2006). Error and uncertainty in habitat models. *Journal of Applied Ecology*, 43(3):413–423.

Batty, M. (2007). *Cities and complexity: understanding cities with cellular automata, agent-based models, and fractals*. The MIT press.

Bauer, M. E., Cipra, J. E., Anuta, P. E., and Etheridge, J. B. (1979). Identification and area estimation of agricultural crops by computer classification of landsat mss data. *Remote Sensing of Environment*, 8(1):77–92.

Beijing Municipal Bureau of Statistics (2016). 2016 nian bei jing shi neng hao shui hao tong ji gong bao [beijing energy and water consumption bulletin 2016]. http://www.bjstats.gov.cn/zxfb/201707/t20170726_379161.html. Accessed: 2017-07-28.

Beven, K. (2007). Towards integrated environmental models of everywhere: uncertainty, data and modelling as a learning process. *Hydrology and Earth System Sciences Discussions*, 11(1):460–467.

Böhringer, C. and Jochem, P. E. (2007). Measuring the immeasurable—a survey of sustainability indices. *Ecological economics*, 63(1):1–8.

Bonan, G. B., Oleson, K. W., Vertenstein, M., Levis, S., Zeng, X., Dai, Y., Dickinson, R. E., and Yang, Z.-L. (2002). The land surface climatology of the community land model coupled to the ncar community climate model. *Journal of climate*, 15(22):3123–3149.

Borak, J., Lambin, E., and Strahler, A. (2000). The use of temporal metrics for land cover change detection at coarse spatial scales. *International Journal of Remote Sensing*, 21(6-7):1415–1432.

Box, G. E. and Jenkins, G. M. (1976). *Time series analysis: forecasting and control, revised ed.* Holden-Day.

Brink, A. B. and Eva, H. D. (2009). Monitoring 25 years of land cover change dynamics in africa: A sample based remote sensing approach. *Applied Geography*, 29(4):501–512.

Brovkin, V., Boysen, L., Arora, V., Boisier, J., Cadule, P., Chini, L., Claussen, M., Friedlingstein, P., Gayler, V., Van Den Hurk, B., et al. (2013). Effect of anthropogenic land-use and land-cover changes on climate and land carbon storage in cmip5 projections for the twenty-first century. *Journal of Climate*, 26(18):6859–6881.

Brundtland, G. H. and Khalid, M. (1987). Our common future. *New York*.

Bulkeley, H. and Kern, K. (2006). Local government and the governing of climate change in germany and the uk. *Urban studies*, 43(12):2237–2259.

Bureau of Waterworks, Tokyo Metropolitan Government (2014). Prevention of water leakage in tokyo. https://www.waterprofessionals.metro.tokyo.jp/pdf/PreventionOfWaterLeakage.pdf. Accessed: 2017-07-28.

Callicott, J. B. and Mumford, K. (1997). Ecological sustainability as a conservation concept. *Conservation biology*, 11(1):32–40.

Campbell, S. (1996). Green cities, growing cities, just cities?: Urban planning and the contradictions of sustainable development. *Journal of the American Planning Association*, 62(3):296–312.

Campolongo, F., Cariboni, J., and Saltelli, A. (2007). An effective screening design for sensitivity analysis of large models. *Environmental modelling & software*, 22(10):1509–1518.

Chai, Z., Umut, H., Gou, X.-h., and Luo, S.-z. (2008). Xin jiang chai wo pu shui yuan di di xia shui chao cai yin fa de huan jing wen ti [environmental problems caused by excessive exploitation of groundwater at chaiwopu source in xinjiang]. *Shui tu bao chi yan jiu [Research of Water and Soil Conservation]*, 15(5):132–135.

Chang, C. and Zhu, J. (2012). Wu lu mu qi shi cheng shi lin ye jian she xian zhuang ji dui ce [status and countermeasures of urban forestry development in urumqi]. *Zhong guo cheng shi lin ye [Journal of Chinese Urban Forestry]*, 10(4):17–19.

Chatfield, C. (2006). Model uncertainty. *Encyclopedia of Environmetrics*.

Chen, C. and Cotton, W. R. (1983). A one-dimensional simulation of the stratocumulus-capped mixed layer. *Boundary-Layer Meteorology*, 25(3):289–321.

Chen, F. and Dudhia, J. (2001). Coupling an advanced land surface–hydrology model with the penn state–ncar mm5 modeling system. part i: Model implementation and sensitivity. *Monthly Weather Review*, 129(4):569–585.

Chen, F., Kusaka, H., Bornstein, R., Ching, J., Grimmond, C., Grossman-Clarke, S., Loridan, T., Manning, K. W., Martilli, A., Miao, S., et al. (2011). The integrated wrf/urban modelling system: development, evaluation, and applications to urban environmental problems. *International Journal of Climatology*, 31(2):273–288.

Chen, J. (2007). Rapid urbanization in China: A real challenge to soil protection and food security. *CATENA*, 69(1):1–15.

China National Environmental Monitoring Centre (2016). 2016 nian 23 yue ji di yi ji du 74 cheng shi kong qi zhi liang bao gao [air quality report for 74 major cities, march and first quarter 2016]. http://www.mep.gov.cn/hjzl/dqhj/cskqzlzkyb/201605/P020160526421402833225.pdf. Accessed: 2017-06-27.

Christensen, J. H. (1997). The danish eulerian hemispheric model—a three-dimensional air pollution model used for the arctic. *Atmospheric Environment*, 31(24):4169–4191.

Clements, M. and Hendry, D. (1998). *Forecasting economic time series*. Cambridge University Press.

Cohen, B. (2006). Urbanization in developing countries: Current trends, future projections, and key challenges for sustainability. *Technology in society*, 28(1):63–80.

Cohen, W. B., Maiersperger, T. K., Yang, Z., Gower, S. T., Turner, D. P., Ritts, W. D., Berterretche, M., and Running, S. W. (2003). Comparisons of land cover and lai estimates derived from etm+ and modis for four sites in north america: A quality assessment of 2000/2001 provisional modis products. *Remote Sensing of Environment*, 88(3):233–255.

Collier, C. (2006). The impact of urban areas on weather. *Quarterly Journal of the Royal Meteorological Society*, 132(614):1–25.

Congalton, R. G., Gu, J., Yadav, K., Thenkabail, P., and Ozdogan, M. (2014). Global land cover mapping: A review and uncertainty analysis. *Remote Sensing*, 6(12):12070–12093.

Costanza, R. (1989). Model goodness of fit: a multiple resolution procedure. *Ecological modelling*, 47(3-4):199–215.

Cotton, W. R., Pielke Sr, R., Walko, R., Liston, G., Tremback, C., Jiang, H., McAnelly, R., Harrington, J., Nicholls, M., Carrio, G., et al. (2003). Rams 2001: Current status and future directions. *Meteorology and Atmospheric Physics*, 82(1):5–29.

Cox, P. M., Pearson, D., Booth, B. B., Friedlingstein, P., Huntingford, C., Jones, C. D., and Luke, C. M. (2013). Sensitivity of tropical carbon to climate change constrained by carbon dioxide variability. *Nature*, 494(7437):341.

Cramer, W., Bondeau, A., Woodward, F. I., Prentice, I. C., Betts, R. A., Brovkin, V., Cox, P. M., Fisher, V., Foley, J. A., Friend, A. D., et al. (2001). Global response of terrestrial ecosystem structure and function to co2 and climate change: results from six dynamic global vegetation models. *Global change biology*, 7(4):357–373.

Cui, Y., Ye, B., Wang, J., and Liu, Y. (2013). Influence of degree-day factor variation on the mass balance of glacier no. 1 at the headwaters of ürümqi river, china. *Journal of Earth Science*, 24(6):1008–1022.

Cuo, L., Lettenmaier, D. P., Alberti, M., and Richey, J. E. (2009). Effects of a century of land cover and climate change on the hydrology of the puget sound basin. *Hydrological Processes*, 23(6):907–933.

Danish water and wastewater association (2016). Water in figures. http://www.e-pages.dk/danva/200/html5/. Accessed: 2017-07-28.

Davoudi, S., Shaw, K., Haider, L. J., Quinlan, A. E., Peterson, G. D., Wilkinson, C., Fünfgeld, H., McEvoy, D., Porter, L., and Davoudi, S. (2012). Resilience: a bridging concept or a dead end?"reframing" resilience: challenges for planning theory and practice interacting traps: resilience assessment of a pasture management system in northern afghanistan urban resilience: what does it mean in planning practice? resilience as a useful concept for climate change adaptation? the politics of resilience for planning: a cautionary note: edited by simin davoudi and libby porter. *Planning theory & practice*, 13(2):299–333.

DeFries, R. and Eshleman, K. N. (2004). Land-use change and hydrologic processes: a major focus for the future. *Hydrological processes*, 18(11):2183–2186.

DeFries, R., Field, C., Fung, I., Collatz, G., and Bounoua, L. (1999). Combining satellite data and biogeochemical models to estimate global effects of human-induced land cover change on carbon emissions and primary productivity. *Global Biogeochemical Cycles*, 13(3):803–815.

Di Sabatino, S., Buccolieri, R., Pulvirenti, B., and Britter, R. (2007). Simulations of pollutant dispersion within idealised urban-type geometries with cfd and integral models. *Atmospheric Environment*, 41(37):8316–8329.

Didan, K. (2015). MOD13A1 MODIS/Terra Vegetation Indices 16-Day L3 Global 500m SIN Grid V006. NASA EOSDIS Land Processes DAAC. https://doi.org/10.5067/MODIS/MOD13A1.006.

Dong, W. and Zhang, X. (2011). Urumqi. *Cities*, 28(1):115–125.

Doran, P. T. and Zimmerman, M. K. (2009). Examining the Scientific Consensus on Climate Change. *Eos, Transactions American Geophysical Union*, 90(3):22.

Dorian, J. P., Wigdortz, B., and Gladney, D. (1997). Central asia and xinjiang, china: emerging energy, economic and ethnic relations. *Central Asian Survey*, 16(4):461–486.

Du, H., Zhang, X., and Wang, B. (2006). Co-adaptation between modern oasis urbanization and water resources exploitation: A case of urumqi. *Chinese Science Bulletin*, 51(1):189–195.

Eliasson, I. (2000). The use of climate knowledge in urban planning. *Landscape and urban planning*, 48(1):31–44.

FAO (2016). Aquastat database. http://www.fao.org/nr/water/aquastat/data/query/index.html?lang=en. Accessed: 2016-11-30.

Feng, J. and Su, L. (2016). Cheng shi gui hua yu tu di li yong gui hua hu dong guan xi yan jin ji zhi ji rong he ce lue – ji yu xing wei zhu ti bo yi fen xi [evolving mechanisms and fusion strategies of relationships between urban planning and land use planning, based on behavior subject game mechanism. *Di yu yan jiu yu kai fa [Areal research and development]*, 35(6):134–139.

Field, C. B., Barros, V. R., Mach, K., and Mastrandrea, M. (2014). *Climate change 2014: impacts, adaptation, and vulnerability*, volume 1. Cambridge University Press Cambridge and New York.

Fisher, P., Comber, A. J., and Wadsworth, R. (2005). Land use and land cover: contradiction or complement. *Re-presenting GIS*, pages 85–98.

Foley, J. A., DeFries, R., Asner, G. P., Barford, C., Bonan, G., Carpenter, S. R., Chapin, F. S., Coe, M. T., Daily, G. C., Gibbs, H. K., et al. (2005). Global consequences of land use. *science*, 309(5734):570–574.

Friedl, M. A., Sulla-Menashe, D., Tan, B., Schneider, A., Ramankutty, N., Sibley, A., and Huang, X. (2010). Modis collection 5 global land cover: Algorithm refinements and characterization of new datasets. *Remote sensing of Environment*, 114(1):168–182.

Friedlingstein, P., Cox, P., Betts, R., Bopp, L., von Bloh, W., Brovkin, V., Cadule, P., Doney, S., Eby, M., Fung, I., et al. (2006). Climate–carbon cycle feedback analysis: results from the c4mip model intercomparison. *Journal of climate*, 19(14):3337–3353.

Fritz, S., See, L., McCallum, I., Schill, C., Obersteiner, M., Van der Velde, M., Boettcher, H., Havlík, P., and Achard, F. (2011). Highlighting continued uncertainty in global land cover maps for the user community. *Environmental Research Letters*, 6(4):044005.

Fulton, E. A., Smith, A. D., and Johnson, C. R. (2003). Effect of complexity on marine ecosystem models. *Marine Ecology Progress Series*, 253:1–16.

Fulton, E. A., Smith, A. D., Smith, D. C., and van Putten, I. E. (2011). Human behaviour: the key source of uncertainty in fisheries management. *Fish and Fisheries*, 12(1):2–17.

Füssel, H.-M. (2007). Adaptation planning for climate change: concepts, assessment approaches, and key lessons. *Sustainability science*, 2(2):265–275.

Gao, H. and Jia, G. (2013). Assessing disagreement and tolerance of misclassification of satellite-derived land cover products used in wrf model applications. *Advances in Atmospheric Sciences*, 30(1):125–141.

Gates, W. L. (1992). Amip: The atmospheric model intercomparison project. *Bulletin of the American Meteorological Society*, 73(12):1962–1970.

Ge, J., Torbick, N., and Qi, J. (2009). Biophysical evaluation of land-cover products for land–climate modeling. *Earth Interactions*, 13(6):1–16.

Gent, P. R., Danabasoglu, G., Donner, L. J., Holland, M. M., Hunke, E. C., Jayne, S. R., Lawrence, D. M., Neale, R. B., Rasch, P. J., Vertenstein, M., et al. (2011). The community climate system model version 4. *Journal of Climate*, 24(19):4973–4991.

Giorgetta, M. A., Jungclaus, J., Reick, C. H., Legutke, S., Bader, J., Böttinger, M., Brovkin, V., Crueger, T., Esch, M., Fieg, K., et al. (2013). Climate and carbon cycle changes from 1850 to 2100 in mpi-esm simulations for the coupled model intercomparison project phase 5. *Journal of Advances in Modeling Earth Systems*, 5(3):572–597.

Giorgi, F. and Mearns, L. O. (1991). Approaches to the simulation of regional climate change: A review. *Reviews of Geophysics*, 29(2):191.

Giri, C., Zhu, Z., and Reed, B. (2005). A comparative analysis of the global land cover 2000 and modis land cover data sets. *Remote sensing of environment*, 94(1):123–132.

Hamby, D. (1994). A review of techniques for parameter sensitivity analysis of environmental models. *Environmental monitoring and assessment*, 32(2):135–154.

Hamin, E. M. and Gurran, N. (2009). Urban form and climate change: Balancing adaptation and mitigation in the us and australia. *Habitat international*, 33(3):238–245.

Han, C. and Chen, X. (2005). Wu lu mu qi zao qi ren lei huo dong yu cheng shi xing tai yan bian [early human activities in urumqi and city form evolution]. *Zhong guo li shi di li lun cong [Journal of Chinese Historical Geography]*, 20(2):41–47.

Han, T., Ye, B., Ding, Y., and Jiao, K. (2005). Wu lu mu qi he liu yu jing liu zeng jia de shi shi fen xi [increasing runoff in the urumqi river basin since 1980s]. *Bing chuan dong tu [Journal of Glaciology and Geocryology]*, 5.

Hansen, J., Sato, M., Kharecha, P., Beerling, D., Berner, R., Masson-Delmotte, V., Pagani, M., Raymo, M., Royer, D. L., and Zachos, J. C. (2008). Target atmospheric co2: Where should humanity aim? *arXiv preprint arXiv:0804.1126*.

Hansen, M. C., Potapov, P. V., Moore, R., Hancher, M., Turubanova, S., Tyukavina, A., Thau, D., Stehman, S., Goetz, S., Loveland, T., et al. (2013). High-resolution global maps of 21st-century forest cover change. *science*, 342(6160):850–853.

Harbor, J. M. (1994). A practical method for estimating the impact of land-use change on surface runoff, groundwater recharge and wetland hydrology. *Journal of the American Planning Association*, 60(1):95–108.

Harris, C. D. and Ullman, E. L. (1945). The nature of cities. *The Annals of the American Academy of Political and Social Science*, 242(1):7–17.

He, Y., Jiang, H., Peng, L., and Qiemu, B. (2014). Ji yu ke chi xu fa zhan de wu lu mu qi shi shui zi yuan gong xu fen xi [research on supply and demand of water resources of urumqi water basin on sustainable development]. *Xin jiang huan jing bao hu[Environment protection of Xinjiang]*, 36(1):10–16.

He, Y., Peng, L., and Geng, S. (2011). Ji yu qu yu jing ji ceng ci de cheng shi xu shui ye ce mo xing yan jiu [urban water demand prediction model based on regional economic basis]. *Shui zi yuan yu shui gong cheng xue bao [Journal of Water Resources & Water Engineering]*, 22(1):83–86.

Heald, C. L. and Spracklen, D. V. (2015). Land use change impacts on air quality and climate. *Chemical reviews*, 115(10):4476–4496.

Hernandez, M., Miller, S. N., Goodrich, D. C., Goff, B. F., Kepner, W. G., Edmonds, C. M., and Jones, K. B. (2000). Modeling runoff response to land cover and rainfall spatial variability in semi-arid watersheds. *Environmental monitoring and assessment*, 64(1):285–298.

Heuvelink, G. B. (1998). *Error propagation in environmental modelling with GIS*. Taylor & Francis.

Hoornweg, D., Sugar, L., and Trejos Gomez, C. L. (2011). Cities and greenhouse gas emissions: moving forward. *Environment and Urbanization*, 23(1):207–227.

Howell, A. (2011). Labor market segmentation in urumqi, xinjiang: Exposing labor market segments and testing the relationship between migration and segmentation. *Growth and change*, 42(2):200–226.

Howell, A. and Fan, C. C. (2011). Migration and inequality in xinjiang: a survey of han and uyghur migrants in urumqi. *Eurasian Geography and Economics*, 52(1):119–139.

Huete, A., Didan, K., Miura, T., Rodriguez, E. P., Gao, X., and Ferreira, L. G. (2002). Overview of the radiometric and biophysical performance of the modis vegetation indices. *Remote sensing of environment*, 83(1):195–213.

Huffman, G. J., Adler, R. F., Bolvin, D. T., and Nelkin, E. J. (2010). The trmm multi-satellite precipitation analysis (tmpa). In *Satellite rainfall applications for surface hydrology*, pages 3–22. Springer.

IPCC (2013). *Climate Change 2013: The Physical Science Basis. Contribution of Working Group I to the Fifth Assessment Report of the Intergovernmental Panel on Climate Change*. Cambridge University Press, Cambridge, United Kingdom and New York, NY, USA.

Israeli Water Authority (2011). The state of israel: National water efficiency report. http://www.water.gov.il/Hebrew/ProfessionalInfoAndData/2012/24-The-State-of-Israel-National-Water-Efficiency-Report.pdf. Accessed: 2017-07-28.

Jacob, D. J. and Winner, D. A. (2009). Effect of climate change on air quality. *Atmospheric environment*, 43(1):51–63.

Jepson Jr, E. J. (2001). Sustainability and planning: Diverse concepts and close associations. *CPL bibliography*, 15(4):499–510.

Jetz, W., Wilcove, D. S., and Dobson, A. P. (2007). Projected impacts of climate and land-use change on the global diversity of birds. *PLoS biology*, 5(6):e157.

Jiang, W. and Gao, W. (2003). Ju zhu kong jian fen yi - wu lu mu qi shi zai fa zhan zhong mian ling de yan jun wen ti [residential segregation-the most serious problem in the development of urumqi]. *Gan han qu zi yuan yu huan jing [Journal of Arid Land Resources and Environment]*, 17(4):43–47.

Jung, M., Henkel, K., Herold, M., and Churkina, G. (2006). Exploiting synergies of global land cover products for carbon cycle modeling. *Remote Sensing of Environment*, 101(4):534–553.

Kain, J. S. and Fritsch, J. M. (1993). Convective parameterization for mesoscale models: The kain-fritsch scheme. In *The representation of cumulus convection in numerical models*, pages 165–170. Springer.

Kalnay, E. and Cai, M. (2003). Impact of urbanization and land-use change on climate. *Nature*, 423(6939):528–31.

Kanamitsu, M., Ebisuzaki, W., Woollen, J., Yang, S.-K., Hnilo, J., Fiorino, M., and Potter, G. (2002). Ncep–doe amip-ii reanalysis (r-2). *Bulletin of the American Meteorological Society*, 83(11):1631–1643.

Kelly, R. A., Jakeman, A. J., Barreteau, O., Borsuk, M. E., ElSawah, S., Hamilton, S. H., Henriksen, H. J., Kuikka, S., Maier, H. R., Rizzoli, A. E., et al. (2013). Selecting among five common modelling approaches for integrated environmental assessment and management. *Environmental modelling & software*, 47:159–181.

Kidd, C. and Levizzani, V. (2011). Status of satellite precipitation retrievals. *Hydrology and Earth System Sciences*, 15(4):1109–1116.

Klemp, J. B. and Wilhelmson, R. B. (1978). The simulation of three-dimensional convective storm dynamics. *Journal of the Atmospheric Sciences*, 35(6):1070–1096.

Klugman, J. (2009). Human development report 2009. overcoming barriers: Human mobility and development.

Lan, Y., Zhong, Y., Wu, S., Shen, Y., Wang, G., La, C., and Song, J. (2011). Tian shan nan bei po dian xing he liu chu shan jing liu dui qi hou bian hua xiang ying de fen xi dui bi [response of mountain runoff to climate change in representative rivers originated from the tianshan mountain]. *Zhong guo sha mo [Journal of Desert Research]*, 31(1):254–260.

Land, K. C. (1986). Methods for national population forecasts: A review. *Journal of the American Statistical Association*, 81(396):888–901.

Laniak, G. F., Olchin, G., Goodall, J., Voinov, A., Hill, M., Glynn, P., Whelan, G., Geller, G., Quinn, N., Blind, M., et al. (2013). Integrated environmental modeling: a vision and roadmap for the future. *Environmental Modelling & Software*, 39:3–23.

Leichenko, R. (2011). Climate change and urban resilience. *Current opinion in environmental sustainability*, 3(3):164–168.

Leitao, A. B. and Ahern, J. (2002). Applying landscape ecological concepts and metrics in sustainable landscape planning. *Landscape and urban planning*, 59(2):65–93.

Li, J., Zhuang, G., Huang, K., Lin, Y., Wang, Q., Guo, Y., Guo, J., Yu, S., Cui, C., and Fu, J. S. (2008). The chemistry of heavy haze over urumqi, central asia. *Journal of atmospheric chemistry*, 61(1):57–72.

Li, X., Messina, J. P., Moore, N. J., Fan, P., and Shortridge, A. M. (2017). Modis land cover uncertainty in regional climate simulations. *Climate Dynamics*, pages 1–13.

Li, X. and Tursun, H. (2001). Wu lu mu qi shi shui zi yuan kai fa li yong xian zhuang wen ti ji dui ce [a study on the present situation problems and countermeasures of sustainable exploiture and utilization of water resources in urumqi]. *Gan han qu yan jiu [Arid Zone Research]*, 18(2):11–18.

Li, X. and Yeh, A. G.-O. (2002). Neural-network-based cellular automata for simulating multiple land use changes using gis. *International Journal of Geographical Information Science*, 16(4):323–343.

Li, Y. and Zhao, X. (2012). An empirical study of the impact of human activity on long-term temperature change in china: A perspective from energy consumption. *Journal of Geophysical Research: Atmospheres*, 117(D17).

Li, Z., Liu, W.-z., Zhang, X.-c., and Zheng, F.-l. (2009). Impacts of land use change and climate variability on hydrology in an agricultural catchment on the loess plateau of china. *Journal of hydrology*, 377(1):35–42.

Li, Z., Wang, W., Zhang, M., Wang, F., and Li, H. (2010). Observed changes in streamflow at the headwaters of the urumqi river, eastern tianshan, central asia. *Hydrological Processes*, 24(2):217–224.

Li, Z.-L., Tang, B.-H., Wu, H., Ren, H., Yan, G., Wan, Z., Trigo, I. F., and Sobrino, J. A. (2013). Satellite-derived land surface temperature: Current status and perspectives. *Remote Sensing of Environment*, 131:14–37.

Liang, L. and Gong, P. (2010). An assessment of modis collection 5 global land cover product for biological conservation studies. In *Geoinformatics, 2010 18th International Conference on*, pages 1–6. Ieee.

Lindenschmidt, K.-E. (2006). The effect of complexity on parameter sensitivity and model uncertainty in river water quality modelling. *Ecological Modelling*, 190(1):72–86.

Liu, D., Abuduwaili, J., Lei, J., Wu, G., and Gui, D. (2011a). Wind erosion of saline playa sediments and its ecological effects in ebinur lake, xinjiang, china. *Environmental Earth Sciences*, 63(2):241–250.

Liu, S. (2011). Qi hou bian hua dui wu lu mu qi shi nong ye qi xiang zai hai de ying xiang ji dui ce [effect of climate change on agrometeorological disasters and countermeasures in urumqi]. *Xian dai nong ye ke ji [Modern Agricultural Sciences and Technology]*, (3):301–302.

Liu, Y. Y., Parinussa, R., Dorigo, W. A., De Jeu, R. A., Wagner, W., Van Dijk, A., McCabe, M. F., and Evans, J. (2011b). Developing an improved soil moisture dataset by blending passive and active microwave satellite-based retrievals. *Hydrology and Earth System Sciences*, 15(2):425.

Lo, J. C.-F., Yang, Z.-L., and Pielke, R. a. (2008). Assessment of three dynamical climate downscaling methods using the Weather Research and Forecasting (WRF) model. *Journal of Geophysical Research*, 113(D9).

Loh, J., Green, R. E., Ricketts, T., Lamoreux, J., Jenkins, M., Kapos, V., and Randers, J. (2005). The living planet index: using species population time series to track trends in biodiversity. *Philosophical Transactions of the Royal Society B: Biological Sciences*, 360(1454):289–295.

Lu, D., Yao, S., Li, G., Liu, H., and Gao, X. (2006). Ji yu wo guo guo qing de cheng zhen hua guo cheng zong he fen xi [comprehensive analysis of the urbanization process based on china's conditions]. *Jing ji di li [Economic Geography]*, 27(6):883–887.

Luo, G., Feng, Y., Zhang, B., and Cheng, W. (2010). Sustainable land-use patterns for arid lands: A case study in the northern slope areas of the tianshan mountains. *Journal of Geographical Sciences*, 20(4):510–524.

Ma, L. and Wu, F. (2005). *Restructuring the Chinese city: changing society, economy and space*. Routledge, New York.

Mackerras, C. (2001). Xinjiang at the turn of the century: the causes of separatism. *Central Asian Survey*, 20(3):289–303.

Maclaren, V. W. (1996). Urban sustainability reporting. *Journal of the American planning association*, 62(2):184–202.

Mahrer, Y. and Pielke, R. A. (1977). A numerical study of the airflow over irregular terrain. *Beiträge zur Physik der Atmosphäre*, 50(1):98–113.

Mamtimin, B. and Meixner, F. X. (2011). Air pollution and meteorological processes in the growing dryland city of urumqi (xinjiang, china). *Science of the Total Environment*, 409(7):1277–1290.

Manning, M. R. (2003). The difficulty of communicating uncertainty. *Climatic Change*, 61(1):9–16.

Martilli, A. (2002). Numerical study of urban impact on boundary layer structure: Sensitivity to wind speed, urban morphology, and rural soil moisture. *Journal of Applied Meteorology*, 41(12):1247–1266.

Mas, J.-F. (1999). Monitoring land-cover changes: a comparison of change detection techniques. *International journal of remote sensing*, 20(1):139–152.

Mather, P. and Tso, B. (2016). *Classification methods for remotely sensed data*. CRC press.

Matott, L. S., Babendreier, J. E., and Purucker, S. T. (2009). Evaluating uncertainty in integrated environmental models: a review of concepts and tools. *Water Resources Research*, 45(6).

Matthews, R. B., Gilbert, N. G., Roach, A., Polhill, J. G., and Gotts, N. M. (2007). Agent-based land-use models: a review of applications. *Landscape Ecology*, 22(10):1447–1459.

Mattikalli, N. M. and Richards, K. S. (1996). Estimation of surface water quality changes in response to land use change: application of the export coefficient model using remote sensing and geographical information system. *Journal of Environmental Management*, 48(3):263–282.

McGranahan, G., Balk, D., and Anderson, B. (2007). The rising tide: assessing the risks of climate change and human settlements in low elevation coastal zones. *Environment and urbanization*, 19(1):17–37.

McIver, D. K. and Friedl, M. A. (2001). Estimating pixel-scale land cover classification confidence using nonparametric machine learning methods. *IEEE Transactions on Geoscience and Remote Sensing*, 39(9):1959–1968.

Meehl, G. A., Boer, G. J., Covey, C., Latif, M., and Stouffer, R. J. (2000). The coupled model intercomparison project (cmip). *Bulletin of the American Meteorological Society*, 81(2):313–318.

Meligrana, J., Ren, W., Zhang, Z., and Anderson, B. (2008). Planning a mega-city's future: An evaluation of shanghai's municipal land-use plan. *Town Planning Review*, 79(2-3):267–293.

Messina, J., Evans, T., Manson, S., Shortridge, A., Deadman, P., and Verburg, P. (2008). Complex systems models and the management of error and uncertainty. *Journal of Land Use Science*, 3(1):11–25.

Micklin, P. (2007). The aral sea disaster. *Annu. Rev. Earth Planet. Sci.*, 35:47–72.

Ministry of Housing and Urban-Rural Development (2012). *China Urban Construction Statistical Yearbook*. China Planning Press.

Ministry of Water Resources People's Republic of China (2011). *China Water Resources Bulletin 2011*. China Water & Power Press.

Mori, K. and Christodoulou, A. (2012). Review of sustainability indices and indicators: Towards a new city sustainability index (csi). *Environmental Impact Assessment Review*, 32(1):94–106.

Neumayer, E. (2003). *Weak versus strong sustainability: exploring the limits of two opposing paradigms*. Edward Elgar Publishing.

Newbold, T., Hudson, L. N., Hill, S. L., Contu, S., Lysenko, I., Senior, R. A., Börger, L., Bennett, D. J., Choimes, A., Collen, B., et al. (2015). Global effects of land use on local terrestrial biodiversity. *Nature*, 520(7545):45–50.

Ng, M. K. and Tang, W.-S. (2004). The Role of Planning in the Development of Shenzhen, China: Rhetoric and Realities. *Eurasian Geography and Economics*, 45(3):190–211.

Niu, G.-Y., Yang, Z.-L., Mitchell, K. E., Chen, F., Ek, M. B., Barlage, M., Kumar, A., Manning, K., Niyogi, D., Rosero, E., et al. (2011). The community noah land surface model with multiparameterization options (noah-mp): 1. model description and evaluation with local-scale measurements. *Journal of Geophysical Research: Atmospheres*, 116(D12).

Njoku, E. G., Jackson, T. J., Lakshmi, V., Chan, T. K., and Nghiem, S. V. (2003). Soil moisture retrieval from amsr-e. *IEEE transactions on Geoscience and remote sensing*, 41(2):215–229.

Noël, B., van de Berg, W., Lhermitte, S., Wouters, B., Machguth, H., Howat, I., Citterio, M., Moholdt, G., Lenaerts, J., and van den Broeke, M. (2017). A tipping point in refreezing accelerates mass loss of greenland's glaciers and ice caps. *Nature Communications*, 8.

Nossent, J., Elsen, P., and Bauwens, W. (2011). Sobol'sensitivity analysis of a complex environmental model. *Environmental Modelling & Software*, 26(12):1515–1525.

Nourry, M. (2008). Measuring sustainable development: Some empirical evidence for france from eight alternative indicators. *Ecological economics*, 67(3):441–456.

Oi, J. C. (1995). The Role of the Local State in China's Transitional Economy. *The China Quarterly*, 144:1132.

Oke, T. R. (1982). The energetic basis of the urban heat island. *Quarterly Journal of the Royal Meteorological Society*, 108(455):1–24.

Oreskes, N. (2004). The scientific consensus on climate change. *Science*, 306(5702):1686–1686.

Pachauri, R. K., Allen, M. R., Barros, V. R., Broome, J., Cramer, W., Christ, R., Church, J. A., Clarke, L., Dahe, Q., Dasgupta, P., et al. (2014). *Climate change 2014: synthesis report. Contribution of Working Groups I, II and III to the fifth assessment report of the Intergovernmental Panel on Climate Change*. IPCC.

Parker, D. C., Manson, S. M., Janssen, M. A., Hoffmann, M. J., and Deadman, P. (2003). Multi-agent systems for the simulation of land-use and land-cover change: A review. *Annals of the association of American Geographers*, 93(2):314–337.

Patz, J. A., Campbell-Lendrum, D., Holloway, T., and Foley, J. A. (2005). Impact of regional climate change on human health. *Nature*, 438(7066):310–317.

Pearce, D. (1988). Economics, equity and sustainable development. *Futures*, 20(6):598–605.

Pielke, R. A., Cotton, W., Walko, R. e. a., Tremback, C. J., Lyons, W. A., Grasso, L., Nicholls, M., Moran, M., Wesley, D., Lee, T., et al. (1992). A comprehensive meteorological modeling system—rams. *Meteorology and Atmospheric Physics*, 49(1):69–91.

Pielke, R. A., Marland, G., Betts, R. A., Chase, T. N., Eastman, J. L., Niles, J. O., Running, S. W., et al. (2002). The influence of land-use change and landscape dynamics on the climate system: relevance to climate-change policy beyond the radiative effect of greenhouse gases. *Philosophical Transactions of the Royal Society of London A: Mathematical, Physical and Engineering Sciences*, 360(1797):1705–1719.

Pitman, a. J. (2003). The evolution of, and revolution in, land surface schemes designed for climate models. *International Journal of Climatology*, 23(5):479–510.

Poschlod, P., Bakker, J., and Kahmen, S. (2005). Changing land use and its impact on biodiversity. *Basic and Applied Ecology*, 6(2):93–98.

Programme), U.-H. U. N. H. S. (2001). Global urban indicators database, version 2. Technical Report www.unhabitat.org.

Pu, Z. and Zhang, S. (2011). Jin 49 nian wu lu mu qi di qu nong ye re liang zi yuan shi kong bian hua [analysis of spatial-temporal variation of agricultural-heat resources in recent 49 years in urumqi region]. *Gan han di qu nong ye yan jiu [Agricultural Research in the Arid Areas]*, 29(2):243–252.

Qian, Z. (2013). Master plan, plan adjustment and urban development reality under China's market transition: A case study of Nanjing. *Cities*, 30:77–88.

Quinlan, J. R. (2014). *C4. 5: programs for machine learning*. Elsevier.

RAMS (n.d.). A description of RAMS. Retrieved from http://rams.atmos.colostate.edu/rams-description.html. Accessed: 2017-03-16.

Ran, Y., Li, X., and Lu, L. (2010). Evaluation of four remote sensing based land cover products over china. *International Journal of Remote Sensing*, 31(2):391–401.

Rees, W. E. (1992). Ecological footprints and appropriated carrying capacity: what urban economics leaves out. *Environment and urbanization*, 4(2):121–130.

Refsgaard, J. C., van der Sluijs, J. P., Højberg, A. L., and Vanrolleghem, P. A. (2007). Uncertainty in the environmental modelling process–a framework and guidance. *Environmental modelling & software*, 22(11):1543–1556.

The World Bank (2015). World development indicators. Technical Report https://data.worldbank.org/data-catalog/world-development-indicators.

United Nations, Department of Economic and Social Affairs Population Division (2015). World urbanization prospects: the 2014 revision. Technical Report (ST/ESA/SER.A/366).

Ren, G. Y., Chu, Z. Y., Chen, Z. H., and Ren, Y. Y. (2007). Implications of temporal change in urban heat island intensity observed at Beijing and Wuhan stations. *Geophysical Research Letters*, 34(5).

Renard, B., Kavetski, D., Kuczera, G., Thyer, M., and Franks, S. W. (2010). Understanding predictive uncertainty in hydrologic modeling: The challenge of identifying input and structural errors. *Water Resources Research*, 46(5).

Revi, A. (2008). Climate change risk: an adaptation and mitigation agenda for indian cities. *Environment and Urbanization*, 20(1):207–229.

Reynolds, R. W., Smith, T. M., Liu, C., Chelton, D. B., Casey, K. S., and Schlax, M. G. (2007). Daily high-resolution-blended analyses for sea surface temperature. *Journal of Climate*, 20(22):5473–5496.

Ridley, J., Gregory, J. M., Huybrechts, P., and Lowe, J. (2010). Thresholds for irreversible decline of the greenland ice sheet. *Climate Dynamics*, 35(6):1049–1057.

Rotmans, J. and van Asselt, M. B. (2001). Uncertainty management in integrated assessment modeling: towards a pluralistic approach. *Environmental monitoring and assessment*, 69(2):101–130.

Rounsevell, M., Reginster, I., Araújo, M. B., Carter, T., Dendoncker, N., Ewert, F., House, J., Kankaanpää, S., Leemans, R., Metzger, M., et al. (2006). A coherent set of future land use change scenarios for europe. *Agriculture, Ecosystems & Environment*, 114(1):57–68.

Saydi, M., Re, Z., and Abudu, S. (2015). 1957-2009 nian wu lu mu qi he jing liu yu qi hou bian hua de dui ying guan xi [corresponding relationship between the runoff and climate change in the upper urumqi river basin during thr period from 1957 - 2009]. *Shui Tu Bao Chi Yan Jiu [Research of Soil and Water Conservation]*, 22(5):289–293.

Schaaf, C. B., Gao, F., Strahler, A. H., Lucht, W., Li, X., Tsang, T., Strugnell, N. C., Zhang, X., Jin, Y., Muller, J.-P., et al. (2002). First operational brdf, albedo nadir reflectance products from modis. *Remote sensing of Environment*, 83(1):135–148.

Schmidhuber, J. and Tubiello, F. N. (2007). Global food security under climate change. *Proceedings of the National Academy of Sciences*, 104(50):19703–19708.

Schmidt, G. A., Kelley, M., Nazarenko, L., Ruedy, R., Russell, G. L., Aleinov, I., Bauer, M., Bauer, S. E., Bhat, M. K., Bleck, R., et al. (2014). Configuration and assessment of the giss modele2 contributions to the cmip5 archive. *Journal of Advances in Modeling Earth Systems*, 6(1):141–184.

Schneider, A., Friedl, M. A., and Potere, D. (2009). A new map of global urban extent from modis satellite data. *Environmental Research Letters*, 4(4):044003.

Scoccimarro, E., Gualdi, S., Bellucci, A., Sanna, A., Giuseppe Fogli, P., Manzini, E., Vichi, M., Oddo, P., and Navarra, A. (2011). Effects of tropical cyclones on ocean heat transport in a high-resolution coupled general circulation model. *Journal of Climate*, 24(16):4368–4384.

Serneels, S. and Lambin, E. F. (2001). Proximate causes of land-use change in narok district, kenya: a spatial statistical model. *Agriculture, Ecosystems & Environment*, 85(1):65–81.

Serra, P., Pons, X., and Saurí, D. (2008). Land-cover and land-use change in a mediterranean landscape: a spatial analysis of driving forces integrating biophysical and human factors. *Applied Geography*, 28(3):189–209.

Shan, W. and Chen, G. (2011). The urumqi riots and china's ethnic policy in xinjiang. *East Asian Policy*, 1(3):14–22.

Shen, L.-Y., Ochoa, J. J., Shah, M. N., and Zhang, X. (2011). The application of urban sustainability indicators–a comparison between various practices. *Habitat International*, 35(1):17–29.

Sinclair, R. (1967). Von thünen and urban sprawl. *Annals of the Association of American Geographers*, 57(1):72–87.

Sines, A. (2002). Civilizing the middle kingdom's wild west. *Central Asian Survey*, 21(1):5–18.

Singh, A. (1989). Review article digital change detection techniques using remotely-sensed data. *International journal of remote sensing*, 10(6):989–1003.

Skamarock, W. C., Klemp, J. B., Dudhia, J., Gill, D. O., Barker, D. M., Wang, W., and Powers, J. G. (2005). A description of the advanced research wrf version 2. Technical report, National Center For Atmospheric Research Boulder Co Mesoscale and Microscale Meteorology Div.

Smith, T. M. and Reynolds, R. W. (2005). A global merged land–air–sea surface temperature reconstruction based on historical observations (1880–1997). *Journal of Climate*, 18(12):2021–2036.

Song, W., Chang, Y., Liu, X., Li, K., Gong, Y., He, G., Wang, X., Christie, P., Zheng, M., Dore, A. J., et al. (2015). A multiyear assessment of air quality benefits from china's emerging shale gas revolution: Urumqi as a case study. *Environmental science & technology*, 49(4):2066–2072.

Statistics Bureau of Urumqi (2010). *Urumqi statistical yearbook*. China Statistics Press.

Statistics Bureau of Xinjiang Uygur Autonomous Region (2012). *Xinjiang statistical yearbook*. China Statistics Press.

Statistics Bureau of Xinjiang Uygur Autonomous Region (2015). *Xinjiang statistical yearbook*. China Statistics Press.

Stocker, T. (2014). *Climate change 2013: the physical science basis: Working Group I contribution to the Fifth assessment report of the Intergovernmental Panel on Climate Change*. Cambridge University Press.

Suarez, P., Anderson, W., Mahal, V., and Lakshmanan, T. (2005). Impacts of flooding and climate change on urban transportation: A systemwide performance assessment of the boston metro area. *Transportation Research Part D: transport and environment*, 10(3):231–244.

Sultana, S. (2007). Transportation and land use. *The International Encyclopedia of Geography*.

Sun, B., Yu, X., and Chen, Q. (1998). Wu lu mu qi shi di zhi zai hai gui hua [geological hazard zoning in urumtsi]. *Zhong guo di zhi zai hai yu fang zhi xue bao [THE CHINESE JOURNAL OF GEOLOGICAL HAZARD AND CONTROL]*, page S1.

Sun, M., Li, Z., Yao, X., and Jin, S. (2013). Rapid shrinkage and hydrological response of a typical continental glacier in the arid region of northwest china–taking urumqi glacier no. 1 as an example. *Ecohydrology*, 6(6):909–916.

Tan, M., Li, X., and Lv, C. (2003). Zhong guo cheng shi yong di kuo zhang de qu dong li fen xi [an analysis of driving forces of urban land expansion in china]. *Jing ji di li [Economic geography]*, 23(5):635–639.

Tan, W. and Ma, J. (2003). Cong "wu lu mu qi du shi quan" dao "wu chang du shi qu" – dui wu lu mu qi cheng shi kong jian kuo zhan mo shi de si kao [thinking over the spatial expansion of urumqi]. *City Planning Review*, 12:006.

Tang, H., Xia, F., and Yang, D. (2013). Gan han qu lv zhou cheng shi shui zi yuan kai fa li yong de qian li – yi wu lu mu qi shi wei li [exploitation and utilization potentials of water resources in arid oasis city——a case study in urumqi]. *Gan han qu yan jiu [Arid Zone Research]*, 30(6):973–980.

Tang, H., Xia, F., Yang, D., Huang, F., and Qiao, X. (2014). Gan han qu lv zhou cheng shi fa zhan yu shui zi yuan xu qiu yu jing fen xi – yi wu lu mu qi shi wei li [scenario warning for urban development and water resource demand in the arid oasis city of urumqi]. *Zi yuan ke xue [Resources Science]*, 36(6):1168–1174.

Tanguay, G. A., Rajaonson, J., Lefebvre, J.-F., and Lanoie, P. (2010). Measuring the sustainability of cities: An analysis of the use of local indicators. *Ecological Indicators*, 10(2):407–418.

Taylor, K. E., Stouffer, R. J., and Meehl, G. A. (2012). An overview of cmip5 and the experiment design. *Bulletin of the American Meteorological Society*, 93(4):485–498.

Team, M. L. C. (2014). Status for: Land Cover/Dynamics (MCD12). Retrieved from https://landval.gsfc.nasa.gov/ProductStatus.php?ProductID=MOD12. Accessed: 2017-03-16.

Tewkesbury, A. P., Comber, A. J., Tate, N. J., Lamb, A., and Fisher, P. F. (2015). A critical synthesis of remotely sensed optical image change detection techniques. *Remote Sensing of Environment*, 160:1–14.

Tian, G., Liu, J., Xie, Y., Yang, Z., Zhuang, D., and Niu, Z. (2005). Analysis of spatio-temporal dynamic pattern and driving forces of urban land in china in 1990s using tm images and gis. *Cities*, 22(6):400–410.

Todd, W. J. (1977). Urban and regional land use change detected by using landsat data. *Journal of Research of the US Geological Survey*, 5(5):529–534.

Tong, S. T. and Chen, W. (2002). Modeling the relationship between land use and surface water quality. *Journal of environmental management*, 66(4):377–393.

Tremback, C., Tripoli, G. J., and Cotton, W. R. (1985). A regional scale atmospheric numerical model including explicit moist physics and a hydrostatic time-split scheme. In *Conference on Numerical Weather Prediction, 7 th, Montreal, Canada*, page 1985.

Tripoli, G. (1982). The colorado state university three-dimensional cloud/mesoscale model-1982 part i: General theoretical framework and sensitivity experiments. *J. Rech. Atmos.*, 16:185–219.

Urumqi Environmental Protection Bureau (2017). Wu lu mu qi shi 2016 nian huan jing zhi liang zhuang kuang gong bao [environment quality report for urumqi 2016]. http://www.wlmqhb.gov.cn/196/215/4057/201706/t20170605_25210.html. Accessed: 2017-06-28.

van Vliet, J., Bregt, A. K., and Hagen-Zanker, A. (2011). Revisiting kappa to account for change in the accuracy assessment of land-use change models. *Ecological modelling*, 222(8):1367–1375.

van Vuuren, D. P., Edmonds, J., Kainuma, M., Riahi, K., Thomson, A., Hibbard, K., Hurtt, G. C., Kram, T., Krey, V., Lamarque, J.-F., Masui, T., Meinshausen, M., Nakicenovic, N., Smith, S. J., and Rose, S. K. (2011). The representative concentration pathways: an overview. *Climatic Change*, 109(1-2):5–31.

Veldkamp, A. and Verburg, P. (2004). Modelling land use change and environmental impact. *Journal of Environmental Management*, 72(1):1–3.

Verburg, P., De Koning, G., Kok, K., Veldkamp, A., and Bouma, J. (1999). A spatial explicit allocation procedure for modelling the pattern of land use change based upon actual land use. *Ecological modelling*, 116(1):45–61.

Verburg, P. H. and Overmars, K. P. (2009). Combining top-down and bottom-up dynamics in land use modeling: exploring the future of abandoned farmlands in europe with the dyna-clue model. *Landscape ecology*, 24(9):1167–1181.

Verburg, P. H., Soepboer, W., Veldkamp, A., Limpiada, R., Espaldon, V., and Mastura, S. S. (2002). Modeling the spatial dynamics of regional land use: the clue-s model. *Environmental management*, 30(3):391–405.

Verburg, P. H., van Berkel, D. B., van Doorn, A. M., van Eupen, M., and van den Heiligenberg, H. A. (2010). Trajectories of land use change in europe: a model-based exploration of rural futures. *Landscape ecology*, 25(2):217–232.

Vörösmarty, C. J., Green, P., Salisbury, J., and Lammers, R. B. (2000). Global water resources: vulnerability from climate change and population growth. *science*, 289(5477):284–288.

Waddell, P. (2002). Urbansim: Modeling urban development for land use, transportation, and environmental planning. *Journal of the American planning association*, 68(3):297–314.

Walko, R. L., Band, L. E., Baron, J., Kittel, T. G., Lammers, R., Lee, T. J., Ojima, D., Pielke Sr, R. A., Taylor, C., Tague, C., et al. (2000). Coupled atmosphere–biophysics–hydrology models for environmental modeling. *Journal of applied meteorology*, 39(6):931–944.

Wan, Z., Zhang, Y., Zhang, Q., and Li, Z.-l. (2002). Validation of the land-surface temperature products retrieved from terra moderate resolution imaging spectroradiometer data. *Remote sensing of Environment*, 83(1):163–180.

Wang, C.-w. and Pu, C.-l. (2011). Xin jiang neng yuan kuang chan zi yuan kai fa li yi gong xiang ji zhi yan jiu [benefit-share machanism on the process of energy mineral resources scploitation in xijiang]. *Jing ji di li [Economic Geography]*, 31(7):1152–1156.

Wei, B., Jiang, F., Li, X., and Mu, S. (2010). Heavy metal induced ecological risk in the city of urumqi, nw china. *Environmental monitoring and assessment*, 160(1):33–45.

Wei, W. (2016). Bei jing shi jian she jie shui xing nong ye cheng xiao yu lu jing yan jiu [achievements and approaches in developing beijing's water-saving agriculture]. *Jing ji yan jiu dao lun [Economic Research Guide]*, (6):19–20.

Weng, Q., Lu, D., and Schubring, J. (2004). Estimation of land surface temperature–vegetation abundance relationship for urban heat island studies. *Remote sensing of Environment*, 89(4):467–483.

Wentz, F. J., Gentemann, C., Smith, D., and Chelton, D. (2000). Satellite measurements of sea surface temperature through clouds. *Science*, 288(5467):847–850.

White, R. and Engelen, G. (1993). Cellular automata and fractal urban form: a cellular modelling approach to the evolution of urban land-use patterns. *Environment and planning A*, 25(8):1175–1199.

Wikipedia (nd.). Terrorism in china. [Online; accessed 2017-10-01].

Wu, F. (2007). Re-orientation of the city plan: Strategic planning and design competition in China. *Geoforum*, 38(2):379–392.

Wu, M., Ren, X., Che, Y., and Yang, K. (2015). A coupled sd and clue-s model for exploring the impact of land use change on ecosystem service value: A case study in baoshan district, shanghai, china. *Environmental management*, 56(2):402–419.

Xia, F., Tang, H., Yang, D., Wang, F., and Zhang, W. (2014). Lv zhou cheng shi shui zi yuan ya li ji qi dui cheng shi fa zhan de ying xiang - yi wu lu mu qi wei li [water resources pressure of oasis city and its impact on urban development]. *Gan han qu di li [Arid Land Geography]*, 37(2):380–387.

Xie, Y. and Costa, F. J. (1993). Urban planning in socialist China. *Cities*, 10(2):103–114.

Yee, H. S. (2003). Ethnic relations in xinjiang: a survey of uygur-han relations in urumqi. *Journal of Contemporary China*, 12(36):431–452.

Yin, D., Nickovic, S., and Sprigg, W. A. (2007). The impact of using different land cover data on wind-blown desert dust modeling results in the southwestern united states. *Atmospheric Environment*, 41(10):2214–2224.

Zeng, T., Zhang, Z., Zhao, X., Wang, X., and Zuo, L. (2015). Evaluation of the 2010 modis collection 5.1 land cover type product over china. *Remote Sensing*, 7(2):1981–2006.

Zhang, H., Yang, D., Shi, J., and Cai, W. (2007). Wu lu mu qi shi tu di li yong bian hua ji qi qu dong ying su fen xi [analysis on land use change and driving forces in urumqi]. *Gan han qu zi yuan yu huan jing [Journal of Arid Land Resources and Environment]*, 21(8):96–100.

Zhang, J. and Wu, F. (2008). Mega-event marketing and urban growth coalitions: A case study of nanjing olympic new town. *Town Planning Review*, 79(2-3):209–226.

Zhang, K. H. and Song, S. (2003). Rural–urban migration and urbanization in China: Evidence from time-series and cross-section analyses. *China Economic Review*, 14(4):386–400.

Zhang, X., Mount, T. D., and Boisvert, R. N. (2004). Industrialization, urbanization and land use in China. *Journal of Chinese Economic and Business Studies*, 2(3):207–224.

Zhang, Z., Abuduwaili, J., and Jiang, F. (2013). Determination of occurrence characteristics of heavy metals in soil and water environments in tianshan mountains, central asia. *Analytical Letters*, 46(13):2122–2131.

Zhu, C. (2013). Cong ya ma li ke shan kan wu lu mu qi huang shan lv hua shu zhong de xuan ze [specie selection for urumqi's afforestation based on experiences in yamalike mountain]. *Xin jiang lin ye [Forestry of Xinjiang]*, (4):38–39.

Zhu, Z. and Woodcock, C. E. (2014). Continuous change detection and classification of land cover using all available landsat data. *Remote sensing of Environment*, 144:152–171.

Zwiers, F. W. and von Storch, H. (1995). Taking serial correlation into account in tests of the mean. *Journal of Climate*, 8(2):336–351.